OPTIMIZATION OF NON-UNIFORM PLANAR ARRAY GEOMETRY FOR
DIRECTION OF ARRIVAL ESTIMATION

A THESIS SUBMITTED TO
THE GRADUATE SCHOOL OF NATURAL AND APPLIED SCIENCES
OF
MIDDLE EAST TECHNICAL UNIVERSITY

BY

TOYGAR BİRİNCİ

IN PARTIAL FULLFILLMENT OF THE REQUIREMENTS
FOR
THE DEGREE OF DOCTOR OF PHILOSOPHY
IN
ELECTRICAL AND ELECTRONICS ENGINEERING

JULY 2006

Approval of the Graduate School of Natural and Applied Sciences.

_____

Prof. Dr. Canan Özgen

Director

I certify that this thesis satisfies all the requirements as a thesis for the degree of Doctor of Philosophy.

_____

Prof. Dr. İsmet Erkmen

Head of Department

This is to certify that we have read this thesis and that in our opinion it is fully adequate, in scope and quality, as a thesis for the degree of Doctor of Philosophy.

_____

Prof. Dr. Yalçın Tanık

Supervisor

Examining Committee Members

Prof. Dr. Mete Severcan   (METU, EE)   _____

Prof. Dr. Yalçın Tanık   (METU, EE)   _____

Prof. Dr. Feza Arıkan   (HU, EE)   _____

Assoc. Prof. Dr. Sencer Koç   (METU, EE)   _____

Asst. Prof. Dr. Arzu Tuncay Koç (METU, EE)   _____

I hereby declare that all information in this document has been obtained and presented in accordance with academic rules and ethical conduct. I also declare that, as required by these rules and conduct, I have fully cited and referenced all material and results that are not original to this work.

Name, Last name   : Toygar Birinci

Signature   :

ABSTRACT

OPTIMIZATION OF NON-UNIFORM PLANAR ARRAY GEOMETRY FOR DIRECTION OF ARRIVAL ESTIMATION

Birinci, Toygar

Ph. D., Department of Electrical and Electronics Engineering
Supervisor : Prof. Dr. Yalçın Tanık

July 2006, 117 pages

In this work, a novel method is proposed to optimize the array geometry for DOA estimation. The method is based on minimization of fine error variances with the constraint that the gross error probability is below a certain threshold. For this purpose, a metric function that reflects the gross and fine error characteristics of the array is offered. Theoretical analyses show that the minimization of this metric function leads to small DOA estimation error variance and small gross error probability. Analyses have been carried out under the assumptions of planar array geometry, isotropic array elements and AWGN. Genetic algorithm is used as an optimization tool and performance simulation is performed by comparing the DOA estimation errors of optimized array to a uniform circular array (UCA). Computer simulations support the theoretical analyses and show that the method proposed leads to significant improvement in array geometry in terms of DOA estimation performance.

ÖZ

GELİŞ YÖNÜ KESTİRİMİ İÇİN DÜZENLİ OLMAYAN DÜZLEMSEL DİZİ GEOMETRİSİ ENİYİLEŞTİRMESİ

Birinci, Toygar

Doktora, Elektrik Elektronik Mühendisliği Bölümü

Tez Yöneticisi : Prof. Dr. Yalçın Tanık

Temmuz 2006, 117 sayfa

Bu çalışmada, geliş yönü kestirimi için, dizi geometrisi eniyleştirilmesi için yeni bir yöntem önerilmiştir. Yöntem, hassas hataların sapmasının, kaba hata ihtimalinin belirli bir eşiğin altında olmasına bağlı olarak azaltılmasını temel almaktadır. Bu amaçla, hem kaba hem de hassas hataların karakteristiklerini yansıtan bir başarım fonksiyonu önerilmiştir. Teorik analizler göstermiştir ki, bu başarım fonksiyonun değerinin azaltılması daha düşük geliş yönü kestirimi hata sapmasına ve daha düşük kaba hata ihtimaline yol açmaktadır. Analizler, düzlemsel dizi geometrisi, eşyönlü dizi elemanları, belirli gelen işaret ve toplanan beyaz Gauss gürültüsü varsayılarak yapılmıştır. Eniyileştirme yöntemi olarak genetik algoritma kullanılmıştır ve düzgün dairesel dizinin geliş açısı kestirim hataları karşılaştırılarak başarım analizi yapılmıştır. Bilgisayar benzeşimleri, kuramsal analizleri desteklemiş ve önerilen yöntemin geliş açısı kestirimi başarımında önemli iyileşmeler sağladığını göstermiştir.

Anahtar Kelimeler : Dizi Geometrisi, Geliş Yönü Kestirimi, Eniyileştirme, Genetik Algoritma, Cramér-Rao Sınırı, Kaba Hata

ACKNOWLEDGEMENTS

I would like to express my gratitude to my supervisor Dr. Yalçın Tanık for his valuable guidance and suggestions. Without his support this thesis would not have been possible. I would also like to thank Dr. Mete Severcan, Dr. Feza Arıkan, Dr. Sencer Koç and Dr. Arzu Tuncay Koç for their comments and contributions.

I am particularly grateful to my dear family for providing me the best possible education and for keeping their faith on me. I would especially like to thank my wife Işıl, without her constant support and love my life would not have been complete.

The last but not least, I am indebted to my friends and colleagues for their constant support and encouragement that kept me going during the hard times.

TABLE OF CONTENTS

x

LIST OF TABLES

LIST OF FIGURES

CHAPTER 1

INTRODUCTION

This thesis is focused on the optimization of the sensor array geometry for direction of arrival estimation. The area of sensor array processing has received considerable amount of interest in the literature during the last few decades. The aim of the sensor array processing is the estimation of the parameters by using the collected data with a set of properly placed sensor elements. In array signal processing literature, main effort has been spent on parameter estimation methods and a good survey on this particular subject can be found in [1] and [2]. However, the performances of the suggested parameter estimation methods are heavily dependent on the geometry of the array elements. Array aperture size, number of array elements and the placement of the sensors play a crucial role on the overall performance of the application, yet there is only a very limited number of papers present on those subjects.

Extending the array aperture (spatial distribution) is the only option if a higher resolution and a better accuracy are needed for an array signal processing estimation application. For most of the applications, uniform arrays are the first choice for their isotropic estimation performance. On the other hand, if the number of array elements is restricted, large uniform arrays are usually avoided for their vulnerability to frequent gross errors. In that case, it is more proper to use non-uniform arrays in order to reduce the rate of gross errors while keeping the spatial extent of the array elements. Hence, the main motivation of this work is to optimize

the localization of array elements in an arbitrarily bounded region to attain a better estimation performance.

1.1 Background

The idea of using non-uniform arrays has been introduced more than four decades ago. One of the earliest works on non-uniform arrays is based on redundancy concepts [3]. Redundancy in array design is provided in order to maximize the resolution of an array for a given number of sensors. Sensor elements are arranged in a fashion that the pairwise differences of the array element integer locations d_i, $i=1,2,...,M$, exhaust the set $\{0, 1, 2,...,N \leq M(M-1)/2\}$ where N represents the array length. The structure of differences is first introduced in [4] which treats the problem in an abstract mathematical manner and then adapted to array geometry problem. However, finding the exact solution for large number of array elements requires intensive computations. Some methods that require less computational load have been offered for suboptimal placement of elements [5], [6]. In [7], different non-uniform linear array structures were compared by considering the probability of outliers and it was shown that using minimum redundant arrays is not the optimal way of direction of arrival estimation.

Some statistical approaches have been used for the array geometry design problem. In [8], the authors presented a D-optimality based design criterion, which is related to the minimization of the covariance matrix of the direction of arrival estimates. Simulations showed that arrays that were formed by using D-optimality criterion had better performances than the uniform arrays and the minimum redundant arrays. Although the method is not directly associated with any specific direction of arrival algorithm, it requires certain reference information about direction of arrivals and the environment.

Estimation accuracy is one of the most critical issues for a good array design and a good estimate on its limit is the Cramer-Rao Bound (CRB). CRB on estimation

accuracy has been widely analyzed and there are many good works available in the literature [9]-[16]. Optimization of the array geometry with the constraint of CRB is one of the options to design an array. In [17], expressions for stochastic CRB and asymptotic root mean square error of MUSIC were used as objective functions and a genetic algorithm was utilized to optimize the array geometry. In [18], average CRB over the possible DOA values was chosen as a performance criterion. However, these measures are not sufficient to optimize a large array since gross errors are not taken into account.

Maintaining accuracy together with an attempt to keep the probability of gross errors small is limited in the literature. In [19], again the CRB was chosen as the criterion and MUSIC simulations of each candidate were performed as an empirical approach for ambiguity measure. Also, some other bounds on DOA estimation have been used in array geometry optimization such as Weiss-Weinstein lower bound (WWLB) which takes gross errors into account and gives more realistic bounds for low SNR regions [20]. The method was applied to linear arrays and the optimization results showed that the performance is not satisfactory and about the same as minimum redundancy arrays. Besides, the use of WWLB brings considerable computational burden. In [21], an intuitive similarity measure is defined between the array steering vectors and the authors relate this measure to the ambiguity probability in a practical, yet incomplete way, by using a binary hypothesis testing procedure which can not be fully adequate to make such an analysis. The resulting procedure is considerably complicated for two dimensional arrays and the authors state that an alternative efficient way of performing the task is still under study. [22] is another work that uses a similar function to measure the similarity between the array steering vectors and simplifies the procedure to some extent and provides some examples by using the linear arrays.

Among all the cited papers, only a few of them; [18], [21] and [22] are stated to be applied to two dimensional arrays. Hence, the optimization of two dimensional

array geometries which is the problem we will attempt to solve, is a subject that has received less attention than it deserves.

In this work, we propose a method to optimize the array geometry by taking both gross errors and fine errors into account in an efficient way. For this purpose, a metric function is proposed to reflect the gross and fine error characteristics of the array that can be used as an optimization constraint. The proposed optimization method has been applied to a circularly bounded planar region with 8 isotropic sensors, and the performance of the optimized array was compared with the UCA by using the MUSIC algorithm [23] as the direction finding method. It should be emphasized that the estimation method and the dimensionality of the array do not pose any restrictions to the proposed method: The method can be used for any number of sensors, and it can be extended to three dimensional arrays, in a trivial fashion.

1.2 Outline

The thesis is organized as follows: In Chapter 2, array manifold representation of two dimensional arrays based on [24] is given and the mathematical models used in this work are presented. In Chapter 3, the probability of gross errors is derived and a concise review of previous results on CRB is presented. In Chapter 4, a metric is proposed for optimization which simultaneously works on CRB for fine errors and probability of gross errors and the optimization procedure is summarized and in Chapter 5 the estimation performance of the optimized array is compared with the UCA and as an example to a real life problem, optimized sensor placement is presented on an aircraft[1].

---

[1] This work has been presented in part in European Signal Processing Conference [25] 2005 in Antalya, Turkey.

CHAPTER 2

ARRAY MANIFOLD REPRESENTATION AND THE SIGNAL MODEL

Antenna arrays are the collection of sensors to observe the spatial and temporal characteristics of the impinging wavefield on the sensors. Field which is observed by the antenna array consists of any combination of a single or multiple signals, noise and interference depending on the application of interest. Since the objective of using an antenna array is to take the sample of the field in a certain space-time domain, the spatial configuration of the sensors is important as well as the spatial and temporal characteristics of the signal received by the array. General array and signal configuration is given in Figure 2-1.

The first issue is the array configuration. The array configuration consists of two parts. The first part is the antenna array pattern of the individual elements. It is usually a function of the specific sensor configuration and the distribution of the other elements. In many cases, for simplicity, it is assumed that the elements have an isotropic pattern, which is uniform in all directions. The antenna patterns are included in the analysis afterwards for application specific purposes. The second part of the array configuration is the array geometry. Array geometry defines the physical locations of the sensors: It can be linear, planar or volumetric. Within each geometry, sensors can be distributed uniformly or non-uniformly.
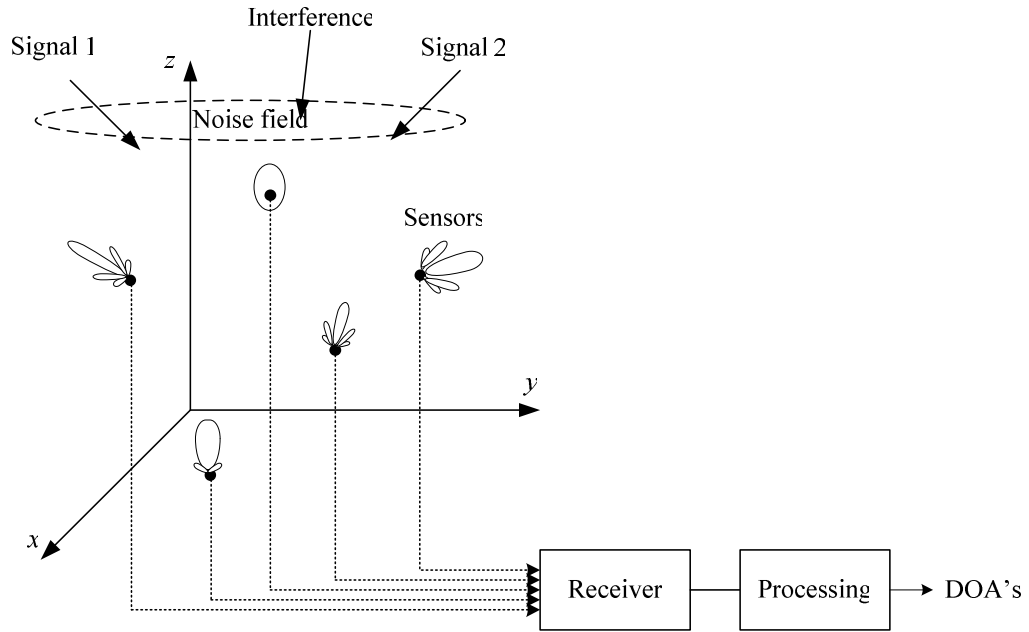
Figure 2-1 General array characteristics

The second issue is the structure of the signal. Signal of interest falls in one of the three categories. First one is the known signals. Second one is the random signals which are the signals whose statistics are known. Third one is the non-random signals which have unknown statistics.

The third issue is the structure of the noise. A noise component is always included that is essentially a white Gaussian noise process, statistically independent from sensor to sensor.

For this particular work, we assumed planar array geometry, known signal and independent additive white Gaussian noise for the analyses. The estimation of the DOA is carried out in the azimuth direction only. Further assumptions are stated in the discussions wherever are necessary.

In this chapter, we focus on the array configuration and give analysis on the array manifold representation and our signal model that is used in further analyses throughout the text.

2.1 Array Manifold Representation of Two Dimensional Arrays

Geometry of a generic two dimensional array is given in Figure 2-2.
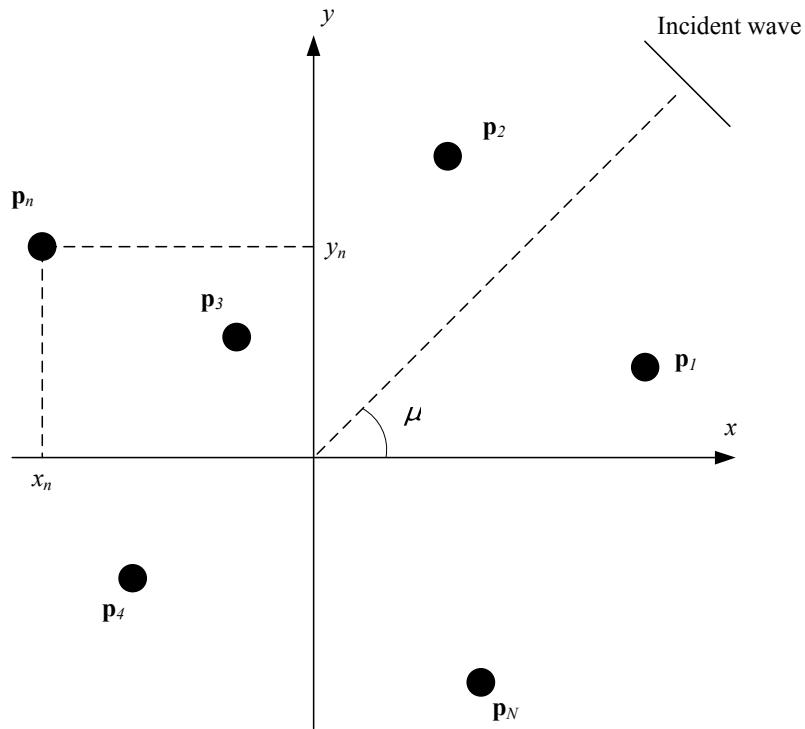
Figure 2-2 Planar array geometry

Locations of the sensors are represented by the position vector **p** in the figure. The sensors are assumed to be isotropic. The azimuth angle of the incoming signal is θ. Array sensors at locations $p_n = [x_n \quad y_n]^T$ receive the incoming signals. Received

signal at each sensor can be expressed as a delayed version of the incoming signal $g(t)$.

$$\mathbf{g}(t,\mathbf{p}) = \begin{bmatrix} g(t-\tau_1) \\ g(t-\tau_2) \\ \vdots \\ g(t-\tau_N) \end{bmatrix} \tag{2-1}$$

where the delays are functions of the array sensor locations and the incidence angle

$$\tau_n = \frac{(-x_n \cos\theta - y_n \sin\theta)}{c}. \tag{2-2}$$

If $g(t)$ is assumed to be a narrowband bandpass signal, it can be represented as,

$$g(t) = \text{Re}\{\tilde{g}(t)e^{j\omega t}\}, \tag{2-3}$$

and the signal at the nth sensor is,

$$\begin{aligned} g_n(t) &= g(t-\tau_n) \\ &= \text{Re}\{\tilde{g}(t-\tau_n)e^{j\omega(t-\tau_n)}\}. \end{aligned} \tag{2-4}$$

The narrowband assumption implies that the delay between the maximum propagation time across the sensors can be approximated by a phase shift;

$$\tilde{g}(t-\tau_n) \cong \tilde{g}(t). \tag{2-5}$$

Using (2-5) in (2-4);

$$g_n(t) = \text{Re}\{\tilde{g}(t)e^{-j\omega\tau_n}e^{j\omega t}\}. \tag{2-6}$$

Prior to time domain processing, a quadrature demodulation of the sensor outputs is performed. The quadrature demodulation process is shown in Figure 2-3. The lowpass filter in the figure has a bandwidth of B.

8

$\cos \omega t$

LPF

$g_q(t)$

$g_n(t, \mathbf{p}_n)$

LPF

$g_i(t)$

$\sin \omega t$
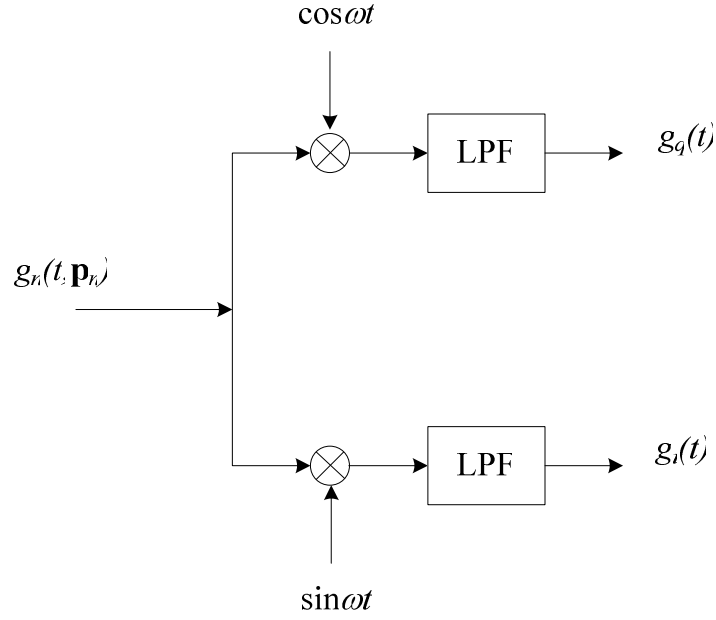
Figure 2-3 Quadrature demodulation

Therefore, the complex envelope of $g_n(t)$ will be

$$\tilde{g}_n(t) = \tilde{g}(t)e^{-j\omega\tau_n} \tag{2-7}$$

and

$$\tilde{\mathbf{g}}(t) = \begin{bmatrix} e^{j\frac{\omega}{c}(x_1\cos\theta + y_1\sin\theta)} \\ e^{j\frac{\omega}{c}(x_2\cos\theta + y_2\sin\theta)} \\ \vdots \\ e^{j\frac{\omega}{c}(x_N\cos\theta + y_N\sin\theta)} \end{bmatrix} \tilde{g}(t). \tag{2-8}$$

As a result, for any arbitrary N-element planar array, the array steering vector is given by

9

$$\mathbf{A}(\theta) = \begin{bmatrix} e^{j\frac{\omega}{c}(x_1 \cos\theta + y_1 \sin\theta)} \\ e^{j\frac{\omega}{c}(x_2 \cos\theta + y_2 \sin\theta)} \\ \vdots \\ e^{j\frac{\omega}{c}(x_N \cos\theta + y_N \sin\theta)} \end{bmatrix}. \tag{2-9}$$

The N dimensional vector $\mathbf{A}(\theta)$ is usually referred to as the steering vector and it represents the array response to an incident wave from direction of arrival θ.

2.2 Signal Model

The received signal vector of the array is

$$\begin{bmatrix} x_1(t) \\ x_2(t) \\ \vdots \\ x_N(t) \end{bmatrix} = \begin{bmatrix} g(t-\tau_1) \\ g(t-\tau_2) \\ \vdots \\ g(t-\tau_N) \end{bmatrix} + \begin{bmatrix} n_1(t) \\ n_2(t) \\ \vdots \\ n_N(t) \end{bmatrix}. \tag{2-10}$$

After bandpass filtering, coherent demodulation and Nyquist rate sampling, the model can be reduced to the following and is usually referred to as the narrowband time domain snapshot model:

$$\mathbf{x}(k) = \mathbf{A}(\theta)g(k) + \mathbf{n}(k) \qquad k = 1,2,\ldots,K. \tag{2-11}$$

The above model for a single signal can be extended to the case of M signals using superposition:

$$\mathbf{x}(k) = \sum_{m=1}^{M} \mathbf{A}(\theta_m)g_m(k) + \mathbf{n}(k) = \mathbf{A}(\theta)\mathbf{g}(k) + \mathbf{n}(k), \tag{2-12}$$

where

10

$$\mathbf{A}(\boldsymbol{\theta}) = \begin{bmatrix} \mathbf{A}(\theta_1) & \mathbf{A}(\theta_2) & \cdots & \mathbf{A}(\theta_M) \end{bmatrix} \qquad \mathbf{g}(k) = \begin{bmatrix} g_1(k) \\ g_2(k) \\ \vdots \\ g_M(k) \end{bmatrix}. \qquad (2\text{-}13)$$

There are two commonly used temporal models for *g(t)* available in the literature. First one is the stochastic model or usually referred to as unconditional model. For this case *g(t)* is modeled as the realization of a stationary, zero mean Gaussian stochastic process that the parameters such as covariance matrix is to be determined. The second one is the deterministic model that each sample of *g(t)* is regarded as a nonrandom parameter to be estimated. These assumptions do not exclude the possibility that the samples of *g(t)* are the samples from a random process since the distributional results are conditioned on the samples of *g(t)*. Thus, the model is referred to as the conditional model in most of the cases. Throughout the text the conditional model will be used.

The noise is assumed to be a zero mean, complex, Gaussian random process that is both spatially and temporally uncorrelated and circularly symmetric:

$$\begin{aligned} E\{\mathbf{n}(k)\} &= \mathbf{0} \\ E\{\mathbf{n}(k)\mathbf{n}^H(l)\} &= \sigma^2 \mathbf{I}\delta_{kl} \\ E\{\mathbf{n}(k)\mathbf{n}^T(l)\} &= \mathbf{0} \end{aligned} \qquad (2\text{-}14)$$

Note that σ^2 is the noise sample power in the receivers of bandwidth *B* and equals *2N₀B*.

CHAPTER 3

PROBABILITY OF GROSS ERRORS AND THE

CRAMER RAO BOUND

In the first part of this chapter, we are going to derive the probability of gross errors in direction of arrival estimation for an array of sensors. Array geometry optimization process aims to minimize the probability of gross errors. For this purpose, we have attempted to find the probability of gross error and commented on the behavior of the function.

It will be helpful to state the terminology we will be using throughout this chapter, in order to increase the readability of the text. We will be talking about two kinds of probabilities when we deal with the subject. The first one is *the individual pairwise gross error probability*. This stands for deciding a specific wrong incidence angle instead of the correct one. This wrongly estimated angle should not reside in the same lobe with the correct incidence angle by definition. Otherwise the erroneous estimate is interpreted to be a fine error. Since there may be infinitely many candidates of these wrong estimates, the total probability of gross errors for a given incidence angle is not the same as these individual pairwise gross error probabilities. Hence the second probability that we will be talking about is *the total probability of gross errors*.

Seeking the probability of gross errors has received limited attention in the literature. In [21] gross error probability is derived by using the simple binary

hypothesis testing. Probability of gross error was calculated as the probability of deciding a wrong DOA instead of the correct one. This approach may be practical to find a close form expression for the probability but will be incomplete since there will be definitely more than one (infinitely many) candidates of wrong decisions. Hence, the analysis in [21] may be used as the intuitive and practical approach to the probability of gross errors which may give satisfactory results to some extent but obtaining the exact probability of gross error requires a more substantial effort. In [26], an upper bound was proposed as the measure of the probability of gross errors. This upper bound was obtained by using a union bound on the individual pairwise error probabilities and how the individual pairwise error probabilities were found will be explained in this chapter. In order to find the probability of gross errors, some ideas are borrowed from the cited paper however the suggested method presented in this thesis makes it possible to have a close approximation rather than an upper bound in expense of some computational power. In that sense, derivation of probability of gross errors presented in this thesis can be considered as original. Nevertheless, individual pairwise error probabilities provide the sufficient information for us to validate our metric function which will be proposed later in this thesis.

In the second part, we have derived the CRB on the estimation of direction of incidence. For a better array performance, the next step is to minimize the fine errors. This can be achieved by minimizing the estimation error variance, hence minimizing the CRB. Since our original problem is to correctly place the sensor array elements; in the next chapter we will state the link between the array element locations and the CRB by using the results of this derivation.

Second part has been widely analyzed in the literature and many different kinds of derivations can be found, all lead to the same result. Derivation outlined in this thesis uses the analyses for the general case given in [24] and the derivation in [16] partially.

3.1 Conditional Maximum Likelihood Estimators

For the signal model stated in Section 2.2 and assuming the conditional model for which the source signals are unknown nonrandom signals whose elements are unknown complex baseband samples, $g(k)$ given as

$$\mathbf{g}(k) = \begin{bmatrix} g_1(k) \\ g_2(k) \\ \vdots \\ g_M(k) \end{bmatrix}. \tag{3-1}$$

Assuming that the noise sample power σ^2 is known and there is only one impinging source waveform, the joint probability density of received signal is

$$p(x) = \prod_{k=1}^{K} \frac{1}{|\pi\sigma^2 \mathbf{I}|} \exp\left[-\frac{1}{\sigma^2} |\mathbf{x}(k) - \mathbf{A}(\theta)g(k)|^2 \right]. \tag{3-2}$$

The log likelihood function is

$$L(\theta) = -KN \ln(\pi\sigma^2) - \frac{1}{\sigma^2} \sum_{k=1}^{K} |\mathbf{x}(k) - \mathbf{A}(\theta)g(k)|^2. \tag{3-3}$$

Maximization of (3-3) is equivalent to minimization of

$$L_2(\theta) = \sum_{k=1}^{K} |\mathbf{x}(k) - \mathbf{A}(\theta)g(k)|^2. \tag{3-4}$$

If θ is fixed and minimized over $g(k)$, an estimate of $g(k)$ is found as

$$\begin{aligned} \hat{g}(k) &= \left[\mathbf{A}^H(\theta)\mathbf{A}(\theta) \right]^{-1} \mathbf{A}^H(\theta)\mathbf{x}(k) \\ &= \frac{1}{N} \mathbf{A}^H(\theta)\mathbf{x}(k) \end{aligned}. \tag{3-5}$$

Using (3-5) in (3-4),

$$L_2(\theta) = \sum_{k=1}^{K} \left| \mathbf{x}(k) - \frac{1}{N} \mathbf{A}(\theta)\mathbf{A}^H(\theta)\mathbf{x}(k) \right|^2 . \tag{3-6}$$

Minimizing (3-6) is equivalent to maximizing the following:

$$\begin{aligned}
L_3(\theta) &= \sum_{k=1}^{K} \left| \frac{1}{N} \mathbf{A}(\theta)\mathbf{A}^H(\theta)\mathbf{x}(k) \right|^2 \\
&= \frac{1}{N^2} \sum_{k=1}^{K} \mathbf{x}^*(k)\mathbf{A}(\theta)\underbrace{\mathbf{A}^H(\theta)\mathbf{A}(\theta)}_{N}\mathbf{A}^H(\theta)\mathbf{x}(k)
\end{aligned} \tag{3-7}$$

which simplifies to

$$L_3(\theta) = \frac{1}{N} \sum_{k=1}^{K} \left| \mathbf{A}^H(\theta)\mathbf{x}(k) \right|^2 . \tag{3-8}$$

3.2 Probability of Gross Errors for Single Snapshot

For any θ_m different from the correct incident angle θ_c, gross error occurs only when

$$L_3(\theta_m) > L_3(\theta_c), \tag{3-9}$$

provided that θ_m is in a sidelobe different from the main lobe that θ_c resides.

Assuming a single snapshot, that is $K=1$, individual pairwise probability of gross errors can be calculated for a given θ_m by following the analysis described below.

$$\begin{aligned}
P_{gem} &= P\{\psi_m > \psi_c\} = P\{|r_m|^2 > |r_c|^2\} \\
&= \int_{0}^{\infty} \int_{\psi_c}^{\infty} p(\psi_c, \psi_m) d\psi_m d\psi_c
\end{aligned} \tag{3-10}$$

where

$$\psi_c \overset{\Delta}{=} |r_c|^2 \overset{\Delta}{=} \left| \mathbf{A}^H(\theta_c)\mathbf{x}(k) \right|^2$$

$$\psi_m \overset{\Delta}{=} |r_m|^2 \overset{\Delta}{=} \left| \mathbf{A}^H(\theta_m)\mathbf{x}(k) \right|^2 \qquad (3\text{-}11)$$

and r_m and r_c are given as,

$$
\begin{aligned}
r_c &= \mathbf{A}^H(\theta_c)\mathbf{A}(\theta_c)g + \mathbf{A}^H(\theta_c)\mathbf{n} \\
&= Ng + \mathbf{A}^H(\theta_c)\mathbf{n} \\
r_m &= \mathbf{A}^H(\theta_m)\mathbf{A}(\theta_c)g + \mathbf{A}^H(\theta_m)\mathbf{n}
\end{aligned}
\qquad (3\text{-}12)
$$

r_c and r_m are gaussian random variables with the following properties:

$$
\begin{aligned}
r_c &= N(Ng, N\sigma^2) \\
r_m &= N(\mathbf{A}_m^H \mathbf{A}_c g, N\sigma^2) \; . \\
\text{Cov}\{r_c, r_m\} &= \mathbf{A}_m^H \mathbf{A}_c \sigma^2
\end{aligned}
\qquad (3\text{-}13)
$$

$\mathbf{A}(\theta_c)$ and $\mathbf{A}(\theta_m)$ are simplified as $\mathbf{A}_c$ and $\mathbf{A}_m$ in (3-13) and from this point on, for simplicity:

$$
\begin{aligned}
\mathbf{A}_c &\overset{\Delta}{=} \mathbf{A}(\theta_c) \\
\mathbf{A}_m &\overset{\Delta}{=} \mathbf{A}(\theta_m)
\end{aligned}
\qquad (3\text{-}14)
$$

The joint probability density in (3-10) can be found by defining,

$$r = [r_{cR}, r_{cI}, r_{mR}, r_{mI}], \qquad (3\text{-}15)$$

where r_{cR} and r_{mR} are the real parts, r_{cI}, r_{mI} are the imaginary parts of r_c and r_m, respectively. The signal g is a complex baseband signal given as

$$g = \alpha e^{j\beta}. \qquad (3\text{-}16)$$

Mean vector of r will be

$$m = \left[N\alpha\cos\beta, N\alpha\sin\beta, \mathbf{A}_m^H \mathbf{A}_c \alpha\cos\beta, \mathbf{A}_m^H \mathbf{A}_c \alpha\sin\beta \right]. \qquad (3\text{-}17)$$

16

The covariance matrix of r will be

$$C = \begin{bmatrix} \lambda & 0 & \rho & 0 \\ 0 & \lambda & 0 & \rho \\ \rho & 0 & \lambda & 0 \\ 0 & \rho & 0 & \lambda \end{bmatrix}, \tag{3-18}$$

where

$$\begin{aligned} \lambda &= \frac{1}{2} N \sigma^2 \\ \rho &= \frac{1}{2} \mathbf{A}_m^H \mathbf{A}_c \sigma^2 \end{aligned} \tag{3-19}$$

r_{cR}, r_{mR}, r_{cI}, r_{mI} are jointly Gaussian random variables and their joint probability density function is given by

$$p(r_{cR}, r_{cI}, r_{mR}, r_{mI}) = \frac{1}{4\pi^2 (\lambda^2 - \rho^2)} \exp\left[-\frac{1}{2}(r-m)^T M(r-m) \right], \tag{3-20}$$

where

$$M = C^{-1} = \frac{1}{\sqrt{|C|}} \begin{bmatrix} \lambda & 0 & -\rho & 0 \\ 0 & \lambda & 0 & -\rho \\ -\rho & 0 & \lambda & 0 \\ 0 & -\rho & 0 & \lambda \end{bmatrix}. \tag{3-21}$$

$$|C| = (\lambda^2 - \rho^2)^2$$

By defining

$$\gamma_c = \sqrt{\psi_c} \qquad \gamma_m = \sqrt{\psi_m}$$

$$r_{cR} = \gamma_c \cos\phi_c \qquad r_{mR} = \gamma_m \cos\phi_m$$

$$r_{cI} = \gamma_c \sin\phi_c \qquad r_{mI} = \gamma_m \sin\phi_m \quad , \tag{3-22}$$

$$\phi_c^{'} = \phi_c - \beta \qquad b = \frac{\left|\mathbf{A}_m^H \mathbf{A}_c\right|}{N}$$

$$\phi_m^{'} = \phi_m - \beta$$

$$p(\gamma_c, \gamma_m) = \frac{\gamma_c \gamma_m e^{\frac{-N\alpha^2}{\sigma^2}}}{\pi^2 N^2 \sigma^4 (1-b^2)}$$

$$\int_0^{2\pi}\int_0^{2\pi} \exp\left[-\frac{\gamma_c^2 + \gamma_m^2 - 2\gamma_c\gamma_m b\cos\left(\phi_c^{'} - \phi_m^{'}\right)}{N\sigma^2(1-b^2)} + \frac{2\alpha\gamma_c\cos\phi_c^{'}}{\sigma^2}\right] d\phi_c^{'} d\phi_m^{'}. \tag{3-23}$$

By integrating and noting that

$$\psi_c = \gamma_c^2 \qquad \psi_m = \gamma_m^2, \tag{3-24}$$

and changing variables;

$$p(\psi_c, \psi_m) = \frac{e^{\frac{-N\alpha^2}{\sigma^2}}}{N^2\sigma^4(1-b^2)} \exp\left[-\frac{\psi_c + \psi_m}{N\sigma^2(1-b^2)}\right]$$

$$I_0\left(\frac{2\sqrt{\psi_c\psi_m}\,b}{N\sigma^2(1-b^2)}\right) I_0\left(\frac{2\alpha\sqrt{\psi_c}}{\sigma^2}\right), \tag{3-25}$$

where I_0 is the modified Bessel function of the first kind. Here, a convenient definition of SNR will be the signal energy over noise spectral density:

18

$$SNR = \sum_{k=1}^{K} \frac{\alpha(k)^2}{\sigma^2} = \frac{1}{\sigma^2} \sum_{k=1}^{K} |g(k)|^2 = \frac{E}{N_0}$$

$$E = \frac{1}{2B} \sum_{k=1}^{K} |g(k)|^2 = \int_{-\infty}^{\infty} |g(t)|^2 dt \qquad . \qquad (3\text{-}26)$$

$$N_0 = \frac{\sigma^2}{2B}$$

By using the joint density function in (3-25), probability of error for a given angle that is the individual pairwise error probability can be calculated by (3-10). Although there is no analytical solution for (3-10), solving it numerically is possible. The results are given in Figure 3-1 for a UCA with an aperture of 2λ and SNR of $0\ dB$ and the incidence angle $\theta{=}0$.

The individual pairwise probability of gross error around $\theta{=}0$ is meaningless since they are not considered as gross errors. At $\theta{=}0$ the integral given in (3-10) is indefinite.

If Figure 3-1 is compared to the MUSIC spectrum of the same array as given in Figure 3-2, it is clearly seen that when the peaks of gross error probability get higher, the MUSIC spectrum of those angles get closer to the value of the correct angle. For $-10\ dB$ SNR, the graphs are shown in Figure 3-3 and Figure 3-4. Similar observations can be made by using these two graphs, besides if we compare Figure 3-3 and Figure 3-1, the angles of the peaks do not change, only the probability of gross errors increase as SNR gets low. This would be an interesting observation and helps us to obtain a method to calculate the overall probability of gross errors by using the individual pairwise gross error probabilities.

Before going into details of obtaining the overall probability of gross errors, an important result should be stated here. The probability of gross error of each individual angle follows the value of

$$b^2 = \frac{\left| A^H(\theta_m) A(\theta_c) \right|^2}{N^2} \qquad . \qquad (3\text{-}27)$$

19

It is not a surprising result since b^2 explicitly resides in (3-25) and can be interpreted as a similarity between the two array steering vectors. The more the similarity between the vectors increase, the more the probability of pairwise gross error increase. This is evident, if we compare the graph of b^2 for incidence angle $\theta=0$ for UCA which is plotted in Figure 3-5 with Figure 3-1 . It will be shown that this result is also valid for multiple snapshots and will play a major role in Chapter 4 when we propose a metric function to measure the array performance.
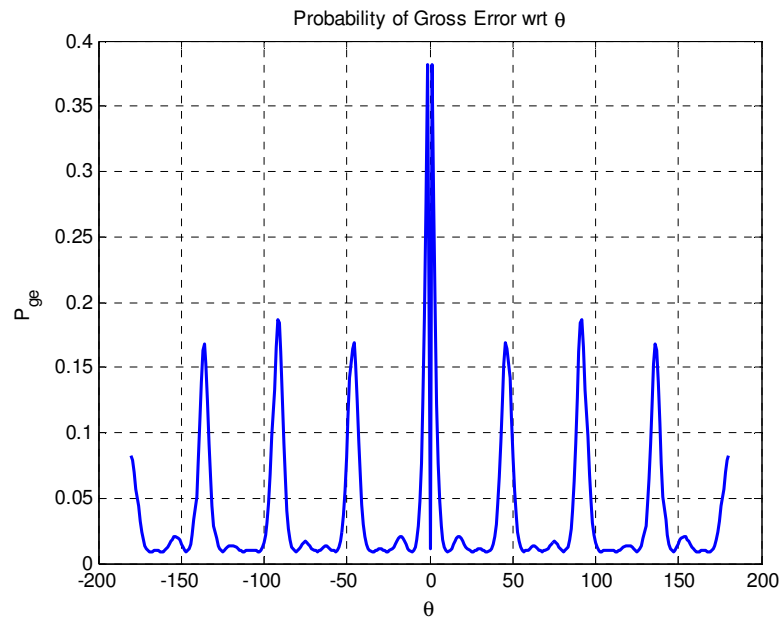
Figure 3-1 Calculated probability of gross errors for the UCA when SNR = *0 dB*
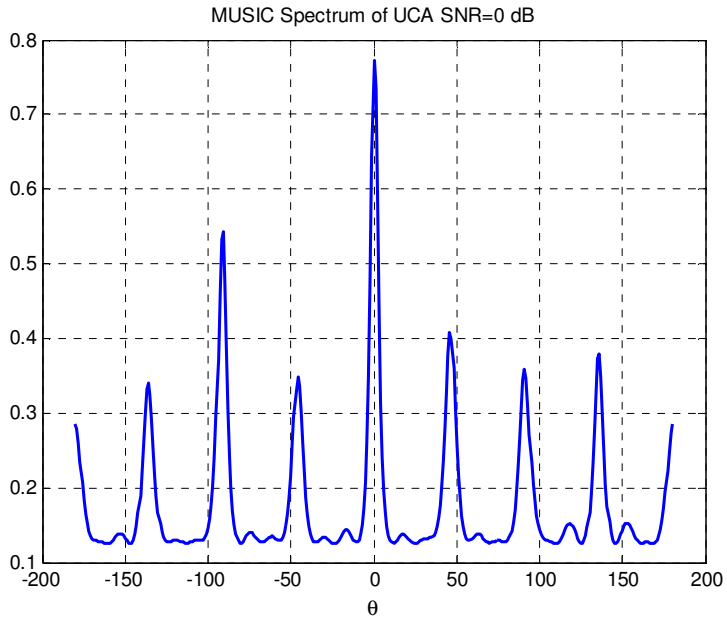
Figure 3-2 MUSIC Spectrum of the UCA when SNR = *0 dB*
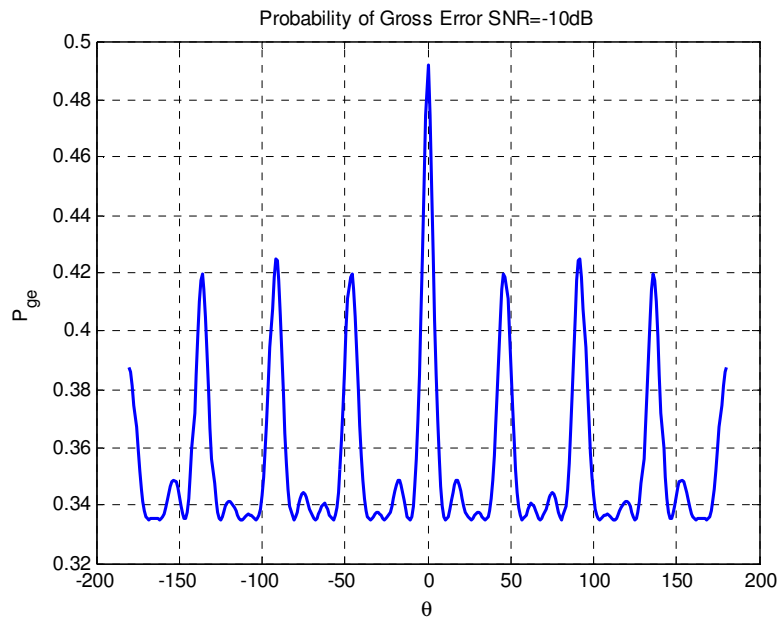
Figure 3-3 Calculated probability of gross error for the UCA when SNR= *-10 dB*
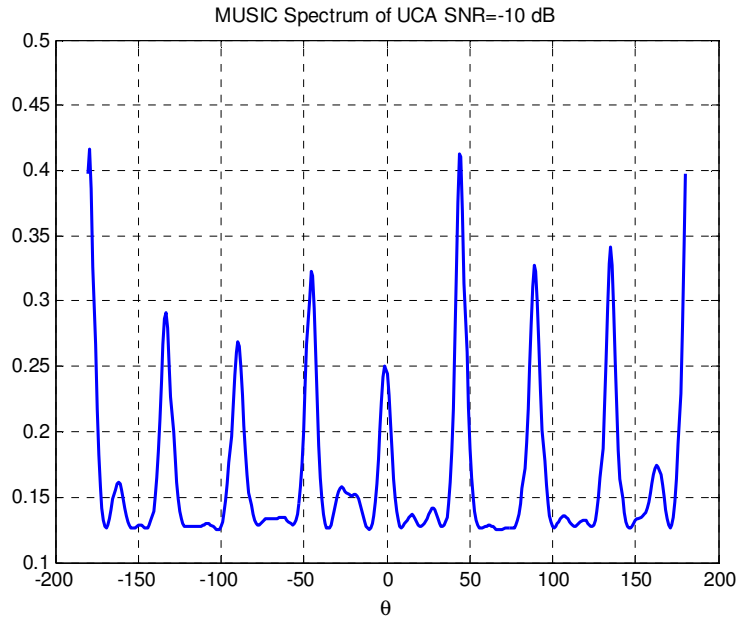
Figure 3-4 MUSIC Spectrum of the UCA when SNR = *-10 dB*
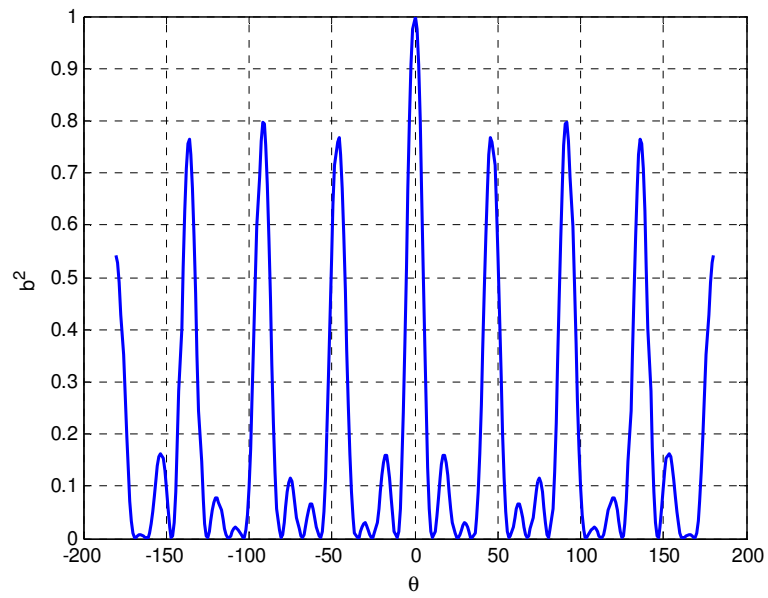
Figure 3-5 Plot of b^2 with respect to θ for the UCA when the incidence angle is *0°*

In order to find the probability of gross error for a given incidence angle, the following approach can be used.

The profile of b^2 sketched in Figure 3-5 can be divided into M different regions as shown in Figure 3-6. Each region contains a peak and therefore M is the total number of peaks in the b^2 plot.
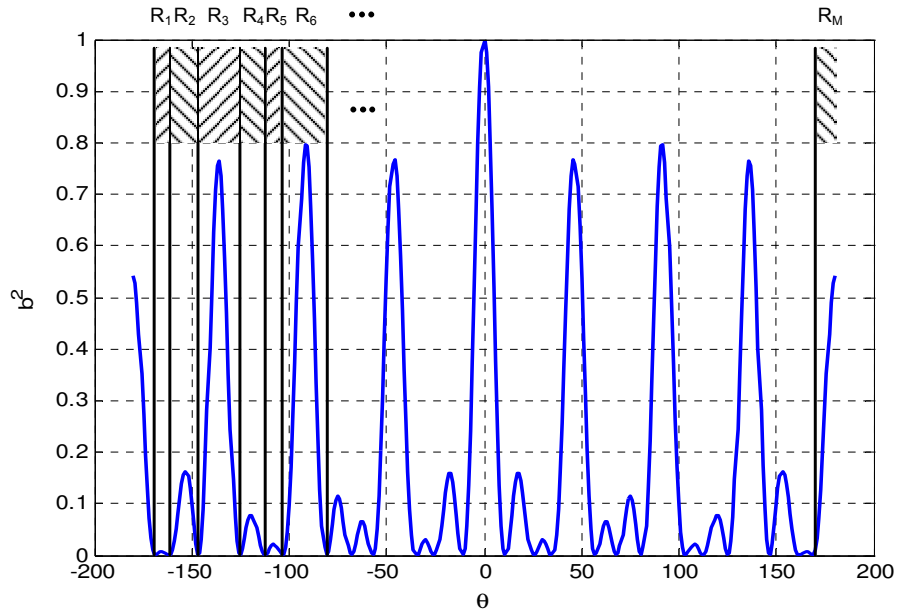
Figure 3-6 Partitioning of b^2

As it was stated before, as SNR gets low, the probability of gross error in each region increases but the peak point in each region does not change, which means the most probable candidate of erroneous angle estimate does not change with SNR. Since the probability of gross errors is continuous with respect to θ, it is true to state that

$$P_{ge}\left(\theta_{peak}, \theta_{peak} \in R_i\right) \geq P_{ge}\left(\forall \theta, \theta \in R_i\right) \quad i = 1, 2, \cdots, M . \tag{3-28}$$

23

Therefore, the total probability of gross error can be calculated by only considering the peak values in each region. This is due to the assumption that if the spectrum value of an angle, which is in a certain region, exceeds the spectrum value of the correct incidence angle, then most probably the spectrum value of the peak angle in that region also exceeds the spectrum value of the correct incidence angle. Hence, the total probability of gross error will be

$$P_{ge} = P\{\psi_1 > \psi_c \ or \ \psi_2 > \psi_c \ or \cdots or \ \psi_M > \psi_c\}$$
$$= P\{|r_1|^2 > |r_c|^2 \ or \ |r_2|^2 > |r_c|^2 \ or \cdots or \ |r_M|^2 > |r_c|^2\},$$

(3-29)

where each r_i $i=1,2,..,M$ corresponds to the peak values in each region. Similarly,

$$P_{ge} = 1 - P\{|r_1|^2 < |r_c|^2 \ and \ |r_2|^2 < |r_c|^2 \ and \cdots and \ |r_M|^2 < |r_c|^2\}$$
$$= 1 - \int_0^\infty \int_0^{r_c} \cdots \int_0^{r_c} p(\psi_1, \cdots, \psi_M, \psi_c) d\psi_1 \cdots d\psi_M d\psi_c$$

(3-30)

The joint probability density function in (3-30) can be written by using the same analysis in development of (3-25). But the resulting integral will be difficult to solve even numerically.

In order to find a numerical result the following analysis is useful.

The probability density functions of individual ψ_c and ψ_i $i=1,2,...,M$ are in quadratic forms and have the non-central chi-squared forms with two degrees of freedom [28];

$$p(\psi_c) = \frac{1}{N\sigma^2} \exp\left[-\frac{\psi_c - N^2\alpha^2}{N\sigma^2}\right] I_0\left(\frac{2\sqrt{\psi_c}\alpha}{\sigma^2}\right).$$

(3-31)

$$p(\psi_i) = \frac{1}{N\sigma^2} \exp\left[-\frac{\psi_i - N^2 b^2 \alpha^2}{N\sigma^2}\right] I_0\left(\frac{2\sqrt{\psi_i}b\alpha}{\sigma^2}\right) \qquad i = 1,2,\cdots,M.$$

(3-32)

Since the contributions of the greater values of b^2 to the mean values of the random variables are greater; each $p(\psi_i)$ can be assumed to be a Gaussian random variable. The mean and the variance of each random variable can be found as

$$m_{\psi_c} = \int_0^\infty \psi_c \, p(\psi_c) d\psi_c = N\sigma^2 + N^2\alpha^2$$

$$\sigma_{\psi_c}^2 = \int_0^\infty \psi_c^2 \, p(\psi_c) d\psi_c - m_{\psi_{ci}}^{\;2} = N^2\sigma^4 + 2N^3\sigma^2\alpha^2$$

$$m_{\psi_m} = \int_0^\infty \psi_c \, p(\psi_c) d\psi_c = N\sigma^2 + \left|\mathbf{A}_m^H \mathbf{A}_c\right|^2 \alpha^2 \qquad (3\text{-}33)$$

$$\sigma_{\psi_m}^2 = \int_0^\infty \psi_m^2 \, p(\psi_m) d\psi_m - m_{\psi_m}^{\;2} = N^2\sigma^4 + 2N\left|\mathbf{A}_m^H \mathbf{A}_c\right|^2 \sigma^2\alpha^2$$

The random variables are correlated and the covariance can be found by

$$\rho_{ij} = \int_0^\infty \int_0^\infty \psi_i \psi_j \, p(\psi_i,\psi_j) d\psi_i d\psi_j - m_{\psi_i} m_{\psi_j} \qquad i,j = 1,2,\cdots,M \; . \qquad (3\text{-}34)$$

$p(\psi_i, \psi_j)$ can be found by the same way as (3-25).

After finding the means, the variances and the covariance, joint pdf can be written as

$$p(\psi_1,\cdots,\psi_M,\psi_c) = \frac{1}{(2\pi)^{M+1/2}|C|^{1/2}} \exp\left[-\frac{1}{2}(\psi - \mu)^T C^{-1}(\psi - \mu)\right] \qquad (3\text{-}35)$$

and probability of gross errors can be found numerically by using (3-30). Linear combinations of non-central chi-squared random variables were considered in [29] and the exact distribution was given. In order to have a simpler form, some approximations were also given that the linear combination of the non-central chi-squared distributions is also a non-central chi-square distribution [30] and in that sense joint pdf of the random variables in (3-30) can be considered as Gaussian.

Numerical computation of multivariate normal probabilities in the form of (3-30) can be carried out by using the procedure given in [31].

3.3 Probability of Gross Errors for Multiple Snapshots

For multiple snapshots (3-10) can be written as

$$
\begin{aligned}
P_{gem} = P\{\psi_m > \psi_c\} &= P\left\{\sum_{k=1}^{K}|r_m(k)|^2 > \sum_{k=1}^{K}|r_c(k)|^2\right\} \\
&= \int_0^\infty \int_{\psi_c}^\infty p(\psi_c,\psi_m)d\psi_m d\psi_c
\end{aligned}
\tag{3-36}
$$

For this case ψ_m and ψ_c can be considered as the summation of $2K$ random variables:

$$
\begin{aligned}
\psi_c &= \sum_{k=1}^{K}\left[r_{cR}^2(k)+r_{cI}^2(k)\right] \\
\psi_m &= \sum_{k=1}^{K}\left[r_{mR}^2(k)+r_{mI}^2(k)\right]
\end{aligned}
\tag{3-37}
$$

where r_{cR}, r_{cI}, r_{mR} and r_{mI} are real Gaussian random variables. Thus, both ψ_m and ψ_c will have non-central chi-square forms with $2K$ degrees of freedom, with the following density functions:

$$
p(\psi_c) = \frac{1}{N\sigma^2}\left(\frac{\psi_c}{s_c^2}\right)^{\frac{(K-1)}{2}}\exp\left[-\frac{\psi_c+s_c^2}{N\sigma^2}\right]I_{K-1}\left[\frac{2\sqrt{\psi_c}s_c}{N\sigma^2}\right],
\tag{3-38}
$$

$$
p(\psi_m) = \frac{1}{N\sigma^2}\left(\frac{\psi_m}{s_m^2}\right)^{\frac{(K-1)}{2}}\exp\left[-\frac{\psi_m+s_m^2}{N\sigma^2}\right]I_{K-1}\left[\frac{2\sqrt{\psi_m}s_m}{N\sigma^2}\right],
\tag{3-39}
$$

where

$$s_c^2 = \sum_{k=1}^{K} N^2 |g(k)|^2 , \tag{3-40}$$

$$s_m^2 = \sum_{k=1}^{K} \left| A_m^H A_c \right|^2 |g(k)|^2 . \tag{3-41}$$

Note that ψ_m and ψ_c always have positive valued means. As the number of snapshots gets higher, these positive means get larger values. It is known that for this case it can be assumed that ψ_m and ψ_c have approximately Gaussian distributions and their joint distribution will also be Gaussian. These two random variables are not independent. Their covariance can be estimated by using the following:

$$E\{\psi_c \psi_m\} = E\left\{ \left[\sum_{k=1}^{K} |r_c (k)|^2 \right] \left[\sum_{l=1}^{K} |r_m (l)|^2 \right] \right\}. \tag{3-42}$$

Since different snapshots are independent from each other,

$$E\left\{ |r_c (k)|^2 |r_m (l)|^2 \right\} = E\left\{ |r_c (k)|^2 \right\} E\left\{ |r_m (l)|^2 \right\} \quad k \neq l . \tag{3-43}$$

(3-42) can be written as

$$E\{\psi_c \psi_m\} = \sum_{k=1}^{K} E\left\{ |r_c (k)|^2 |r_m (k)|^2 \right\} + \sum_{k=1}^{K} E\left\{ |r_c (k)|^2 \right\} \sum_{\substack{l=1 \\ l \neq k}}^{K} E\left\{ |r_m (k)|^2 \right\}. \tag{3-44}$$

For each snapshot, all the expected values inside (3-44) can be calculated by using the probability density functions derived in Section 3.2:

$$Cov\{\psi_c \psi_m\} = E\{\psi_c \psi_m\} - E\{\psi_c\} E\{\psi_m\}. \tag{3-45}$$

The joint probability density function can be written as

$$p(\psi_c, \psi_m) = \frac{1}{(2\pi)|C|^{1/2}} \exp\left[-\frac{1}{2} (\psi - \mu)^T C^{-1} (\psi - \mu) \right], \tag{3-46}$$

27

where C is the covariance matrix and μ is the mean vector. The probability of gross error for each angle can be calculated by using (3-36).

In Figure 3-7, the probability of gross error for each angle is plotted. A UCA with eight elements and an aperture of 2λ are chosen as in the previous section. SNR is chosen as *-20 dB* and the number of snapshots is equal to *101*.
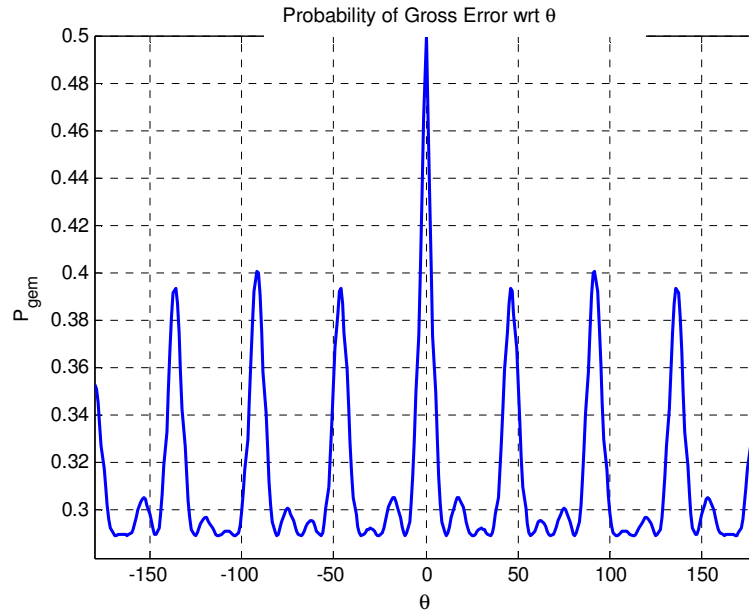
Figure 3-7 Calculated probability of gross error for the UCA when SNR = *-20 dB*

The same response is obtained as in the single snapshot case. Hence, it is true to state that as in the single snapshot case, probability of gross errors gets higher if the value of b^2 gets higher. b^2 is given in (3-27) and rewritten here for convenience:

$$b^2 = \frac{\left|\mathbf{A}^H(\theta_m)\mathbf{A}(\theta_c)\right|^2}{N^2} \, . \tag{3-47}$$

By using the same technique described in the previous section, the total probability of gross error for a given incidence angle can be obtained by evaluating the integral

$$P_{ge} = 1 - P\left\{ \begin{array}{c} \sum_{k=1}^{K} |r_1(k)|^2 < \sum_{k=1}^{K} |r_c(k)|^2 \ and \ \sum_{k=1}^{K} |r_2(k)|^2 < \sum_{k=1}^{K} |r_c(k)|^2 \ and \\ \cdots and \ \sum_{k=1}^{K} |r_M(k)|^2 < \sum_{k=1}^{K} |r_c(k)|^2 \end{array} \right\} . (3\text{-}48)$$

$$= 1 - \int_0^\infty \int_0^{r_c} \cdots \int_0^{r_c} p(\psi_1, \cdots, \psi_M, \psi_c) d\psi_1 \cdots d\psi_M d\psi_c$$

When the number of integrands increases in (3-48), evaluation of the integral as well as the calculation of required parameters to evaluate the integral such as the first and the second order statistics and the covariance matrix of the random variables, gets complicated and requires large amount of time to produce results. On the other hand, calculation of the total probability of gross error for a given incidence angle is still possible by using the method described here. As far as known it is the first approximate calculation of the probability of gross errors in the literature.

3.4 Alternative Interpretation of Individual Pairwise Probability of Gross Errors of Different Angles

In this section, an alternative way of interpretation will be given. This interpretation was published in [26] and is based on the derivation of "Error Probability for Multichannel Binary Signals" given in App. B of [28]. According to this interpretation, the probability of deciding a different angle θ_m instead of the correct DOA θ_c is given as

$$P_{gem} = Q\left[\sqrt{\frac{NS}{2}\left(1-\sqrt{1-b^2}\right)}, \sqrt{\frac{NS}{2}\left(1+\sqrt{1-b^2}\right)}\right]$$

$$-e^{\frac{NS}{2}}\left[I_0\left(\frac{b\ NS}{2}\right)-\frac{1}{2^{2K-1}}I_0\left(\frac{b\ NS}{2}\right)\sum_{m=0}^{K-1}\binom{2K-1}{m}\right.$$

$$-\frac{1}{2^{2K-1}}\sum_{m=0}^{K-1}I_m\left(\frac{b\ NS}{2}\right)\left[\left(\frac{1+\sqrt{1-b^2}}{b}\right)^m - \left(\frac{1-\sqrt{1-b^2}}{b}\right)^m\right] \tag{3-49}$$

$$\left.\sum_{k=0}^{K-1-m}\binom{2K-1}{m}\right].$$

where I_m is the mth order modified Bessel function of the first kind and Q is the Marcum's Q function which is given by

$$Q(\alpha,\beta) = \int_{\beta}^{\infty} te^{-\frac{t^2+\alpha^2}{2}} I_0(\alpha t)dt . \tag{3-50}$$

In (3-49), b is given in (3-27) and S is the signal energy to noise power spectral density $S=E/N_0$ where E is the energy of the received bandpass signal on any of the sensors;

$$E = \frac{1}{2B}\sum_{k=1}^{K} g^*(k)g(k). \tag{3-51}$$

In [26], the union bound that serves as a loose upper bound on total probability of gross errors is given after obtaining the pairwise error probabilities by (3-49). The derivation of pairwise error probabilities which was given in Section 3.2 and Section 3.3 yields the same results with this interpretation. The reason to suggest the method in Section 3.2 and Section 3.3 is that, it makes the approximation to the total gross error probability possible.

This interpretation has a comparable computational complexity with the one that we suggested. Therefore, the only advantage of this interpretation is to have an expression for the pairwise probability of gross errors in closed form as in (3-49).

3.5 Cramer-Rao Bound for Direction of Arrival Estimation

The log likelihood function is given in (3-3) for the signal model in Section 2.2 and it is repeated here:

$$L(\theta) = -KN \ln(\pi\sigma^2) - \frac{1}{\sigma^2} \sum_{k=1}^{K} |\mathbf{x}(k) - \mathbf{A}(\theta)\mathbf{g}(k)|^2 . \tag{3-52}$$

The CRB provides a bound on the covariance matrix of any unbiased estimate of Θ. The covariance matrix of the estimation errors is given by

$$\mathbf{C}(\Theta) \overset{\Delta}{=} E\left\{ (\hat{\Theta} - \Theta)(\hat{\Theta} - \Theta)^T \right\}. \tag{3-53}$$

The multiple-parameter CRB states that

$$\mathbf{C}(\Theta) \geq \mathbf{C}_{CR}(\Theta) \overset{\Delta}{=} \mathbf{J}^{-1} . \tag{3-54}$$

The matrix $\mathbf{J}$ is referred to as Fisher's information matrix [27].

The nonrandom (conditional) signal model is given by

$$\mathbf{x}(k) = \mathbf{A}(\theta)\mathbf{g}(k) + \mathbf{n}(k) \qquad k = 1,2,\ldots,K . \tag{3-55}$$

In (3-55), $\mathbf{g}(k)$ and θ are given as vectors so that the derived CRB will be valid for multiple simultaneous M distinct signals.

The unknown parameters that will be estimated are

$$\Theta = \begin{bmatrix} \theta, \mathbf{g}, \sigma^2 \end{bmatrix}, \tag{3-56}$$

where $\mathbf{g}$ is a real vector that contains the signal values at each snapshot time.

$$\mathbf{g} = \begin{bmatrix} \text{Re}\{\mathbf{g}(1)\}^T, \text{Im}\{\mathbf{g}(1)\}^T, \text{Re}\{\mathbf{g}(2)\}^T, \text{Im}\{\mathbf{g}(2)\}^T, \cdots, \text{Re}\{\mathbf{g}(K)\}^T, \text{Im}\{\mathbf{g}(K)\}^T \end{bmatrix}^T, \tag{3-57}$$

where each $\mathbf{g}(k)$ is an M dimensional vector.

The unknown parameters are given in (3-56) and we let the FIM be in the structure

$$\mathbf{J} = \left[\begin{array}{c|c|c} \mathbf{J}_{\theta\theta} & \mathbf{J}_{\theta\mathbf{g}} & \mathbf{J}_{\theta\sigma^2} \\ \hline \mathbf{J}_{\mathbf{g}\theta} & \mathbf{J}_{\mathbf{g}\mathbf{g}} & \mathbf{J}_{\mathbf{g}\sigma^2} \\ \hline \mathbf{J}_{\sigma^2\theta} & \mathbf{J}_{\sigma^2\mathbf{g}} & \mathbf{J}_{\sigma^2\sigma^2} \end{array} \right], \tag{3-58}$$

where each J_{xy} is given by

$$J_{ij} = E\left\{ \frac{\partial L}{\partial \Theta_i} \frac{\partial L}{\partial \Theta_j} \right\}, \tag{3-59}$$

and for the general case it will be

$$J_{ij} = K \mathrm{tr}\left[\mathbf{K}_x^{-1} \frac{\partial \mathbf{K}_x}{\partial \Theta_i} \mathbf{K}_x^{-1} \frac{\partial \mathbf{K}_x}{\partial \Theta_j} \right] + 2K\,\mathrm{Re}\left\{ \frac{\partial \mathbf{m}^H}{\partial \Theta_i} \mathbf{K}_x^{-1} \frac{\partial \mathbf{m}}{\partial \Theta_j} \right\} \tag{3-60}$$

where $\mathbf{K}_x$ is the covariance matrix of the received signal and $\mathbf{m}$ is the mean vector of the received signal. The derivation of (3-60) can be found in Appendix A.

For the conditional signal model case

$$\begin{aligned} \mathbf{K}_x &= \sigma^2 \mathbf{I} \\ \mathbf{m}(k) &= \mathbf{A}(\boldsymbol{\theta})\mathbf{g}(k) \end{aligned}. \tag{3-61}$$

To find $\mathbf{J}_{\theta\theta}$ we use

$$\frac{\partial L}{\partial \theta_i} = \frac{1}{\sigma^2} \sum_{k=1}^{K} \mathbf{g}^H(k)\mathbf{D}^H(\theta_i)\mathbf{n}(k) + \mathbf{n}^H(k)\mathbf{D}(\theta_i)\mathbf{g}(k)$$

$$J_{\theta_i\theta_j} = \frac{2}{\sigma^2}\,\mathrm{Re}\left\{ \sum_{k=1}^{K} \mathbf{g}^H(k)\mathbf{D}^H(\theta_i)\mathbf{D}(\theta_j)\mathbf{g}(k) \right\} \tag{3-62}$$

$$\mathbf{J}_{\theta\theta} = \frac{2}{\sigma^2}\,\mathrm{Re}\left\{ \sum_{k=1}^{K} \mathbf{g}^H(k)\mathbf{D}^H(\boldsymbol{\theta})\mathbf{D}(\boldsymbol{\theta})\mathbf{g}(k) \right\}$$

32

where

$$\mathbf{D}(\boldsymbol{\theta}) = \frac{\partial \mathbf{A}(\boldsymbol{\theta})}{\partial \boldsymbol{\theta}}.$$
(3-63)

In order to get the second principal submatrix $\mathbf{J_{gg}}$, we need to differentiate L with respect to each element of matrix $\mathbf{g}$:

$$\frac{\partial L}{\partial g_R(k)} = \frac{2}{\sigma^2} \text{Re}\{\mathbf{A}^H(\boldsymbol{\theta})\mathbf{n}(k)\}$$

$$\frac{\partial L}{\partial g_I(k)} = \frac{2}{\sigma^2} \text{Im}\{\mathbf{A}^H(\boldsymbol{\theta})\mathbf{n}(k)\}$$
(3-64)

Elements of $\mathbf{J_{gg}}$ are,

$$E\left\{ \frac{\partial L}{\partial g_R(k)} \left(\frac{\partial L}{\partial g_R(k)} \right)^T \right\} = E\left\{ \frac{\partial L}{\partial g_I(k)} \left(\frac{\partial L}{\partial g_I(k)} \right)^T \right\} = \frac{2}{\sigma^2} \text{Re}\{\mathbf{A}^H(\boldsymbol{\theta})\mathbf{A}(\boldsymbol{\theta})\}$$

$$E\left\{ \frac{\partial L}{\partial g_R(k)} \left(\frac{\partial L}{\partial g_I(k)} \right)^T \right\} = E\left\{ -\frac{\partial L}{\partial g_I(k)} \left(\frac{\partial L}{\partial g_R(k)} \right)^T \right\} = -\frac{2}{\sigma^2} \text{Im}\{\mathbf{A}^H(\boldsymbol{\theta})\mathbf{A}(\boldsymbol{\theta})\}$$
.(3-65)

The noise samples are uncorrelated for different snapshots, hence, the elements of $\mathbf{J_{gg}}$ that correspond to different snapshots will be zero. $\mathbf{J_{gg}}$ will be in the form of

$$J_{gg} = \frac{2}{\sigma^2} \begin{bmatrix} \mathbf{V}_R & -\mathbf{V}_I & & \vdots & & \\ \mathbf{V}_I & \mathbf{V}_R & & \cdots & & \mathbf{0} \\ \hline & \vdots & & \ddots & & \vdots \\ \hline & \mathbf{0} & & \cdots & \mathbf{V}_R & -\mathbf{V}_I \\ & & & & \mathbf{V}_I & \mathbf{V}_R \end{bmatrix}$$
(3-66)

where

$$\mathbf{V}_R = \text{Re}\{\mathbf{A}^H(\boldsymbol{\theta})\mathbf{A}(\boldsymbol{\theta})\}$$

$$\mathbf{V}_I = \text{Im}\{\mathbf{A}^H(\boldsymbol{\theta})\mathbf{A}(\boldsymbol{\theta})\}$$
(3-67)

The third principle sub-matrix is a scalar. By using (3-60) with (3-61)

$$J_{\sigma^2\sigma^2} = K\mathrm{tr}\left[\frac{1}{\sigma^2}\mathbf{I}\frac{1}{\sigma^2}\mathbf{I}\right].$$
$$= \frac{KN}{\sigma^4}$$

(3-68)

Similarly, by using (3-60) with (3-61), it is seen that σ^2 is not coupled with other parameters and

$$\mathbf{J}_{\theta\sigma^2} = \mathbf{J}_{\sigma^2\theta} = 0$$
$$\mathbf{J}_{\mathbf{g}\sigma^2} = \mathbf{J}_{\sigma^2\mathbf{g}} = 0.$$

(3-69)

The other off-diagonal term will be evaluated by first writing

$$\frac{\partial L}{\partial g_R(k)}\left(\frac{\partial L}{\partial \theta}\right)^T = \frac{2}{\sigma^2}\mathrm{Re}\left\{\mathbf{A}^H(\mathbf{\theta})\mathbf{D}(\mathbf{\theta})\mathbf{g}(k)\right\}$$
$$\frac{\partial L}{\partial g_I(k)}\left(\frac{\partial L}{\partial \theta}\right)^T = \frac{2}{\sigma^2}\mathrm{Im}\left\{\mathbf{A}^H(\mathbf{\theta})\mathbf{D}(\mathbf{\theta})\mathbf{g}(k)\right\}.$$

(3-70)

We define

$$\mathbf{\Delta}_R(k) = \frac{2}{\sigma^2}\mathrm{Re}\left\{\mathbf{A}^H(\mathbf{\theta})\mathbf{D}(\mathbf{\theta})\mathbf{g}(k)\right\}$$
$$\mathbf{\Delta}_I(k) = \frac{2}{\sigma^2}\mathrm{Im}\left\{\mathbf{A}^H(\mathbf{\theta})\mathbf{D}(\mathbf{\theta})\mathbf{g}(k)\right\}.$$

(3-71)

By combining the above results, the Fisher's information matrix becomes,

$$\mathbf{J} = \left[\begin{array}{ccc:c:ccc:c} \mathbf{J}_{\theta\theta} & \mathbf{\Delta}^T{}_R(1) & \mathbf{\Delta}^T{}_I(1) & \cdots & \mathbf{\Delta}^T{}_R(K) & \mathbf{\Delta}^T{}_I(K) & \mathbf{0} \\ \mathbf{\Delta}_R(1) & \mathbf{V}^R & -\mathbf{V}^I & & \mathbf{0} & \mathbf{0} & \mathbf{0} \\ \mathbf{\Delta}_I(1) & \mathbf{V}^I & \mathbf{V}^R & & \mathbf{0} & \mathbf{0} & \mathbf{0} \\ \hdashline \vdots & & & \ddots & & & \vdots \\ \hdashline \mathbf{\Delta}_R(K) & \mathbf{0} & \mathbf{0} & & \mathbf{V}^R & -\mathbf{V}^I & \mathbf{0} \\ \mathbf{\Delta}_I(K) & \mathbf{0} & \mathbf{0} & & \mathbf{V}^I & \mathbf{V}^R & \mathbf{0} \\ \hdashline \mathbf{0} & \mathbf{0} & \mathbf{0} & \cdots & \mathbf{0} & \mathbf{0} & \dfrac{KN}{\sigma^4} \end{array}\right].$$

(3-72)

CRB on θ can be found by taking inverse of the upper left portion of the Fisher information matrix and taking the upper left section of the inverse. That is, CRB on θ is the upper left subsection of the matrix

$$\begin{bmatrix} \mathbf{J}_{\theta\theta} & \mathbf{\Delta}^T \\ \mathbf{\Delta} & \mathbf{J}_{gg} \end{bmatrix}^{-1}. \tag{3-73}$$

Hence,

$$CRB(\mathbf{\theta}) = \left[\mathbf{J}_{\theta\theta} - \mathbf{\Delta}^T \mathbf{J}_{gg}^{-1} \mathbf{\Delta}\right]^{-1}. \tag{3-74}$$

Next, by observing that

$$\begin{bmatrix} \mathbf{V}^R & -\mathbf{V}^I \\ \mathbf{V}^I & \mathbf{V}^R \end{bmatrix}^{-1} = \begin{bmatrix} \mathbf{W}^R & -\mathbf{W}^I \\ \mathbf{W}^I & \mathbf{W}^R \end{bmatrix} \tag{3-75}$$

where

$$\mathbf{W} = \mathbf{V}^{-1} \tag{3-76}$$

and

$$\begin{bmatrix} \mathbf{W}^R & -\mathbf{W}^I \\ \mathbf{W}^I & \mathbf{W}^R \end{bmatrix} \begin{bmatrix} \mathbf{\Delta}_R(k) \\ \mathbf{\Delta}_I(k) \end{bmatrix} = \begin{bmatrix} \mathbf{W}^R \mathbf{\Delta}_R(k) - \mathbf{W}^I \mathbf{\Delta}_I(k) \\ \mathbf{W}^I \mathbf{\Delta}_R(k) + \mathbf{W}^R \mathbf{\Delta}_I(k) \end{bmatrix},$$
$$= \begin{bmatrix} \mathrm{Re}\{\mathbf{W}\mathbf{\Delta}(k)\} \\ \mathrm{Im}\{\mathbf{W}\mathbf{\Delta}(k)\} \end{bmatrix} \tag{3-77}$$

we obtain

$$\begin{bmatrix} \mathbf{\Delta}_R^T(k) & \mathbf{\Delta}_I^T(k) \end{bmatrix} \begin{bmatrix} \mathrm{Re}\{\mathbf{W}\mathbf{\Delta}(k)\} \\ \mathrm{Im}\{\mathbf{W}\mathbf{\Delta}(k)\} \end{bmatrix} = \mathrm{Re}\{\mathbf{\Delta}^H(k)\mathbf{W}\mathbf{\Delta}(k)\}. \tag{3-78}$$

CRB on θ can be obtained and by using (3-62), (3-67) and (3-71) it is simplified to

35

$$CRB(\theta) = \left[\mathbf{J}_{\theta\theta} - \sum_{k=1}^{K} \mathrm{Re}\left\{ \mathbf{\Delta}^{H}(k)\mathbf{W}\mathbf{\Delta}(k) \right\} \right]^{-1}$$

$$= \left[\frac{2}{\sigma^2} \mathrm{Re}\left\{ \sum_{k=1}^{K} \mathbf{g}^{H}(k)\mathbf{D}^{H}(\theta)\mathbf{D}(\theta)\mathbf{g}(k) \right\} \right. \qquad ,(3\text{-}79)$$

$$\left. - \frac{2}{\sigma^2} \sum_{k=1}^{K} \mathrm{Re}\left\{ \mathbf{g}^{H}(k)\mathbf{D}^{H}(\theta)\mathbf{A}(\theta)\left[\mathbf{A}^{H}(\theta)\mathbf{A}(\theta)\right]^{-1}\mathbf{A}^{H}(\theta)\mathbf{D}(\theta)\mathbf{g}(k) \right\} \right]^{-1}$$

$$CRB(\theta) = \left[\frac{2}{\sigma^2} \sum_{k=1}^{K} \mathrm{Re}\left\{ \mathbf{g}^{H}(k)\mathbf{D}^{H}(\theta)\left[\mathbf{I} - \mathbf{A}(\theta)\left[\mathbf{A}^{H}(\theta)\mathbf{A}(\theta)\right]^{-1}\mathbf{A}^{H}(\theta)\right]\mathbf{D}(\theta)\mathbf{g}(k) \right\} \right]^{-1} .(3\text{-}80)$$

This result will be used in Chapter 4, when we will attempt to propose a metric function that serves as an optimization constraint on array geometry.

CHAPTER 4

PROPOSED METRIC AND THE ARRAY

OPTIMIZATION

Probability of gross errors and the Cramer-Rao bound for estimation errors, i.e., the bound on fine errors have been derived in the previous chapter. For a good array design, one should minimize both errors. In this chapter, we will state a metric function that can be used to minimize both parameters in an array design problem.

In this chapter, we state the relation between the locations of the array elements and both the probability of gross errors and the CRB. The main emphasis of this chapter is that a single function which is given in (4-1) directly reflects the behavior of the functions derived for both CRB and the probability of gross errors and hence can be used to minimize both.

Considering the effects of the gross errors in array optimization process has received limited attention in the literature [21][22]. Available work on this subject proposes similar functions to optimize the array performance. These functions are offered intuitively which applied to linear array models and yielded satisfactory results. As far as known to this author, the metric function presented in this chapter is a novel function and the idea behind to use this function is theoretically justified.

The last part of this chapter contains the outline of a generic genetic optimization algorithm used to obtain the results presented in the next chapter.

4.1 Minimization of Probability of Gross Errors and CRB

In the previous chapter it is shown that the probability of gross error for a given incidence angle follows the value of b^2 which is given as

$$b^2 = \frac{\left|\mathbf{A}^H(\theta_m)\mathbf{A}(\theta_c)\right|^2}{N^2},$$

(4-1)

where θ_c is the correct incidence angle and θ_m is any other angle different from the correct incidence angle. N is the number of sensors in the array. We have stated that the function in (4-1) is a measure of similarity between the array steering vectors and if this similarity increases, then the probability of making the wrong decision gets higher as well. Obviously, when these two angles are taken to be the same, the similarity will be equal to the highest value that it can take.

$$b^2 = \frac{\left|\mathbf{A}^H(\theta_c)\mathbf{A}(\theta_c)\right|^2}{N^2} = \frac{N^2}{N^2} = 1$$

(4-2)

In this section, we will attempt to show that the similarity between a steering vector that corresponds to a specific angle and the other vectors that lie in its small angular neighborhood, can be used as a measure on the CRB of that array. To achieve this, we will define a new function which shows the similarity between two steering vectors separated by an offset, that is;

$$B(\theta,\phi) = \frac{\left|\mathbf{A}^H(\theta)\mathbf{A}(\theta+\phi)\right|^2}{N^2}.$$

(4-3)

In order to obtain the similarity measure between two steering vectors that lie in a small angular neighborhood, we will analyze the new function given in (4-3) around $\phi=0$.

$A(\theta)$ is the antenna steering vector given in (2-9). Without loss of the validity of derivation given in Section 2.1, the center of the array can be taken as the reference point for the array. Hence (2-9) can be rewritten as

$$A(\theta)=\begin{bmatrix} e^{j\frac{\omega}{c}((x_1-x_c)\cos\theta+(y_1-y_c)\sin\theta)} \\ e^{j\frac{\omega}{c}((x_2-x_c)\cos\theta+(y_2-y_c)\sin\theta)} \\ \vdots \\ e^{j\frac{\omega}{c}((x_N-x_c)\cos\theta+(y_N-y_c)\sin\theta)} \end{bmatrix}, \tag{4-4}$$

where x_c and y_c are the coordinates of the center of the array and given by,

$$\begin{aligned} x_c &= \frac{1}{N}\sum_{i=1}^{N}x_i \\ y_c &= \frac{1}{N}\sum_{i=1}^{N}y_i \end{aligned} \tag{4-5}$$

The value of b^2 around θ_m equals θ_c can be found by following the analysis:

In order to find the behavior of the function B around $\phi=0$,

$$\begin{aligned} A^H&(\theta)A(\theta+\phi) \\ &= \sum_{i=1}^{N} e^{j\frac{\omega}{c}[(x_i-x_c)(\cos(\theta+\phi)-\cos(\theta))+(y_i-y_c)(\sin(\theta+\phi)-\sin(\theta))]} \\ &= \sum_{i=1}^{N}\cos\left[\frac{\omega}{c}[(x_i-x_c)(\cos(\theta+\phi)-\cos(\theta))+(y_i-y_c)(\sin(\theta+\phi)-\sin(\theta))]\right] \\ &\quad + j\sum_{i=1}^{N}\sin\left[\frac{\omega}{c}[(x_i-x_c)(\cos(\theta+\phi)-\cos(\theta))+(y_i-y_c)(\sin(\theta+\phi)-\sin(\theta))]\right] \end{aligned} \tag{4-6}$$

$$\begin{aligned} \left|A^H(\theta)A(\theta+\phi)\right|^2 &= \left[\sum_{i=1}^{N}\cos\left[\frac{\omega}{c}[(x_i-x_c)(\cos(\theta+\phi)-\cos(\theta))+(y_i-y_c)(\sin(\theta+\phi)-\sin(\theta))]\right]\right]^2 \\ &\quad + \left[\sum_{i=1}^{N}\sin\left[\frac{\omega}{c}[(x_i-x_c)(\cos(\theta+\phi)-\cos(\theta))+(y_i-y_c)(\sin(\theta+\phi)-\sin(\theta))]\right]\right]^2 \end{aligned} \tag{4-7}$$

If we expand (4-7) around $\phi=0$,

$$\left|A^H(\theta)A(\theta+\phi)\right|^2$$

$$\cong\left[\sum_{i=1}^{N}\left(1-\frac{\omega^2\phi^2}{2c^2}\left[(y_i-y_c)\cos\theta-(x_i-x_c)\sin\theta\right]^2\right)\right]^2$$

$$+\left[\sum_{i=1}^{N}\left(\frac{\omega\phi}{c}\left[(y_i-y_c)\cos\theta-(x_i-x_c)\sin\theta\right]\right.\right.$$

$$\left.\left.-\frac{\omega\phi^2}{2c}\left[(x_i-x_c)\cos\theta+(y_i-y_c)\sin\theta\right]\right)\right]^2 \qquad (4-8)$$

The second part of (4-8) evaluates to zero, since we have (4-5).

This is reasonable since around $\phi=0$, B is purely real. Hence,

$$\left|A^H(\theta)A(\theta+\phi)\right|^2\cong N-\frac{\omega^2\phi^2}{2c^2}\sum_{i=1}^{N}\left[(y_i-y_c)\cos\theta-(x_i-x_c)\sin\theta\right]^2. \qquad (4-9)$$

If we consider the CRB on estimation of θ for a single source, and evaluate it in terms of the array element locations we have

$$CRB(\theta)=\left[\frac{2}{\sigma^2}\sum_{k=1}^{K}\mathrm{Re}\left\{g^*(k)\mathbf{D}^H(\theta)\left[\mathbf{I}-\mathbf{A}(\theta)\left[\mathbf{A}^H(\theta)\mathbf{A}(\theta)\right]^{-1}\mathbf{A}^H(\theta)\right]\mathbf{D}(\theta)g(k)\right\}\right]^{-1}. \qquad (4-10)$$

The next step is to observe that $\mathbf{D}^H(\theta)\mathbf{A}(\theta)$ evaluates to zero when the array center is chosen as a reference point.

$\mathbf{D}(\theta)$ is given as

$$D(\theta) = \frac{\partial A(\theta)}{\partial(\theta)}$$

$$= \begin{bmatrix} -j\frac{\omega}{c}((x_1 - x_c)\sin\theta - (y_1 - y_c)\cos\theta)e^{j\frac{\omega}{c}((x_1 - x_c)\cos\theta + (y_1 - y_c)\sin\theta)} \\ -j\frac{\omega}{c}((x_2 - x_c)\sin\theta - (y_2 - y_c)\cos\theta)e^{j\frac{\omega}{c}((x_2 - x_c)\cos\theta + (y_2 - y_c)\sin\theta)} \\ \vdots \\ -j\frac{\omega}{c}((x_N - x_c)\sin\theta - (y_N - y_c)\cos\theta)e^{j\frac{\omega}{c}((x_N - x_c)\cos\theta + (y_N - y_c)\sin\theta)} \end{bmatrix}, \quad (4\text{-}11)$$

$$\mathbf{D}^H(\theta)\mathbf{A}(\theta) = \frac{\partial \mathbf{A}^H(\theta)}{\partial\theta}\mathbf{A}(\theta)$$

$$= j\frac{\omega}{c}\sum_{i=1}^{N}[(x_i - x_c)\sin\theta - (y_i - y_c)\cos\theta]$$

$$= j\frac{\omega}{c}\sin\theta\left[\sum_{i=1}^{N}x_i - Nx_c\right] - \frac{\omega}{c}\cos\theta\left[\sum_{i=1}^{N}y_i - Ny_c\right] \quad (4\text{-}12)$$

$$= 0$$

Hence CRB can be written as

$$CRB(\theta) = \left[\frac{2\sum_{k=1}^{K}g^*(k)g(k)}{\sigma^2}\mathbf{D}^H(\theta)\mathbf{D}(\theta)\right]^{-1}$$

$$= \left[\frac{2E}{N_0}\mathbf{D}^H(\theta)\mathbf{D}(\theta)\right]^{-1} \quad (4\text{-}13)$$

By using (4-11) in (4-13)

$$CRB(\theta) = \left[\frac{2E}{N_0}\frac{\omega^2}{c^2}\sum_{i=1}^{N}[(x_i - x_c)\sin\theta - (y_i - y_c)\cos\theta]^2\right]^{-1}. \quad (4\text{-}14)$$

If we compare (4-14) with the function $\left|\mathbf{A}^H(\theta)\mathbf{A}(\theta + \phi)\right|^2$ given in (4-9), we can conclude that minimization of $\left|\mathbf{A}^H(\theta)\mathbf{A}(\theta + \phi)\right|^2$ around $\phi=0$ results in smaller CRB so that less error on estimation of direction of arrival error. Since B is given by

41

$$B(\theta,\phi) = \frac{\left|\mathbf{A}^H(\theta)\mathbf{A}(\theta+\phi)\right|^2}{N^2}, \qquad (4\text{-}15)$$

minimization of B is the same as minimization of $\left|\mathbf{A}^H(\theta)\mathbf{A}(\theta+\phi)\right|^2$. Thus one can conclude that the minimization of the function B around $\phi=0$ yields less fine errors.

When ϕ is taken to be a larger value, we have already shown that in Section 3.3, (4-3) can be used as a measure of the similarity between two array steering vectors that are separated by the amount of ϕ. Since this value is directly proportional to the pairwise error probabilities, this gives us the probability of deciding the angle, that falls apart ϕ degrees from the correct angle, instead of the correct angle and hence, the gross error probability. This can be better visualized by using a generic example.

Let us choose an arbitrary two dimensional array which is given in Figure 4-1. Figure 4-2 shows the graph of $B(\theta,\phi)$ when the correct incidence angle, i.e., θ is chosen to be $100°$. B is a measure of the similarity between the array steering vectors that corresponds to different angle of arrivals. Therefore, Figure 4-2 demonstrates us that array steering vector at $100°$ is fairly similar to the array steering vector that lies $50°$ away from it which is $150°$. Therefore, all the peaks present in the graph are the potential erroneous estimate candidates at $100°$. The fine error performance of the array when the correct incidence angle is $100°$ can be extracted by the curvature around the main lobe as the analysis has shown. Steeper main lobe indicates the better fine error performance.

The three dimensional graph of $B(\theta,\phi)$ for all values of θ is given in Figure 4-3. It shows the overall performance of the array at all possible incidence angles. The graph in Figure 4-2, is obtained by cutting the three dimensional graph in Figure 4-3 by a plane at $\theta=100°$.
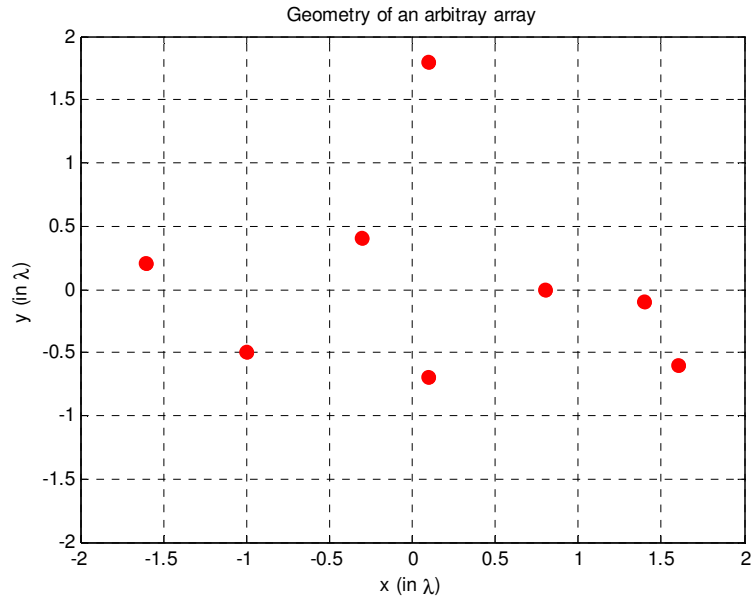
Figure 4-1 Geometry of an arbitrary array

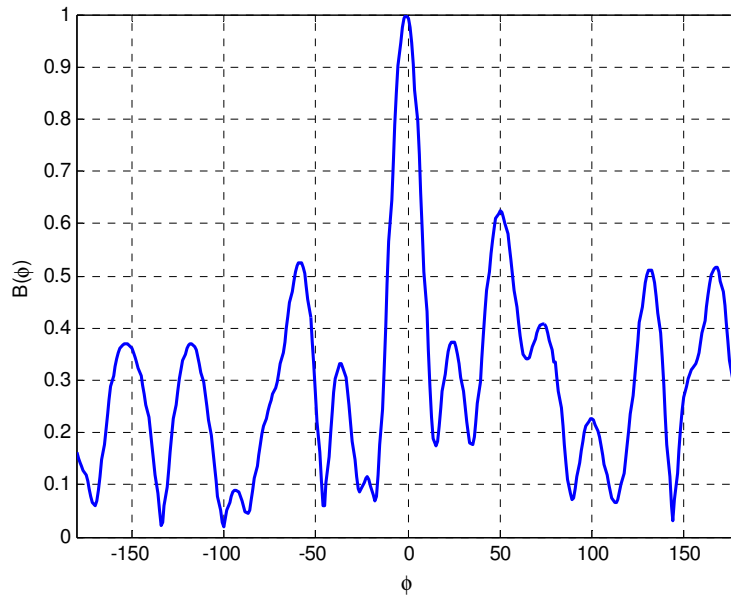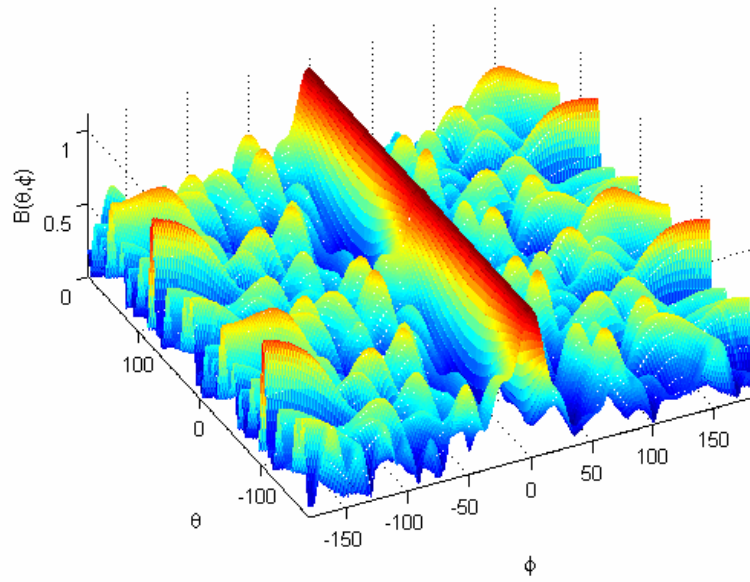Figure 4-2 *B(φ)* when *θ=100°*

Figure 4-3 Sketch of $B(\theta,\phi)$

The symmetry properties of the function $B(\theta,\phi)$ can be used to perform the calculations faster. There are two types of symmetry that the function $B(\theta,\phi)$ has. The first one is the symmetry that is caused by the magnitude square. Since,

$$\left| \mathbf{A}^{H}(\theta)\mathbf{A}(\theta+\phi) \right|^{2} = \left| \mathbf{A}^{H}(\theta+\phi)\mathbf{A}(\theta) \right|^{2} \tag{4-16}$$

then,

$$B(\theta,\phi) = B(\theta+\phi,-\phi). \tag{4-17}$$

An other type of symmetry, originates from the definition of the array steering vector: From (4-4), it can be deduced that

$$B(\theta,\phi) = B(\theta+\pi,\phi). \tag{4-18}$$

44

4.2 Proposed Metric

For a good array design we want less fine estimation error as well as less probability of gross errors. For a given angle of incidence we showed that probability of gross errors follows the pattern of the function *B* which is given as

$$B(\theta,\phi) = \frac{\left|\mathbf{A}^H(\theta)\mathbf{A}(\theta+\phi)\right|^2}{N^2} \ . \tag{4-19}$$

The same function can be a measure for CRB. We showed that in the previous section as well. The steepness of the curvature of *B* around $\phi=0$, which is the second derivative of the function, is directly linked to the CRB of the array for a given θ.

In order to design an array that has the least probability of gross error at any angle, the maximum value of $B(\phi)$ outside the main peak should be minimized for all angles θ.

If we consider the main peak around $\phi=0$, the steepness of the curvature of the main peak of $B(\phi)$ is proportional to the CRB of that angle θ. Again in order to design an array that has the least variance of fine errors, the maximum value of $B(\phi)$ at the main peak should be minimized for all angles θ.

The idea can be visualized by the help of Figure 4-4. Finding maximum along θ outside the main peak gives the worst case of probability of gross errors and finding the maximum along θ at the main peak gives the worst case of the CRB.
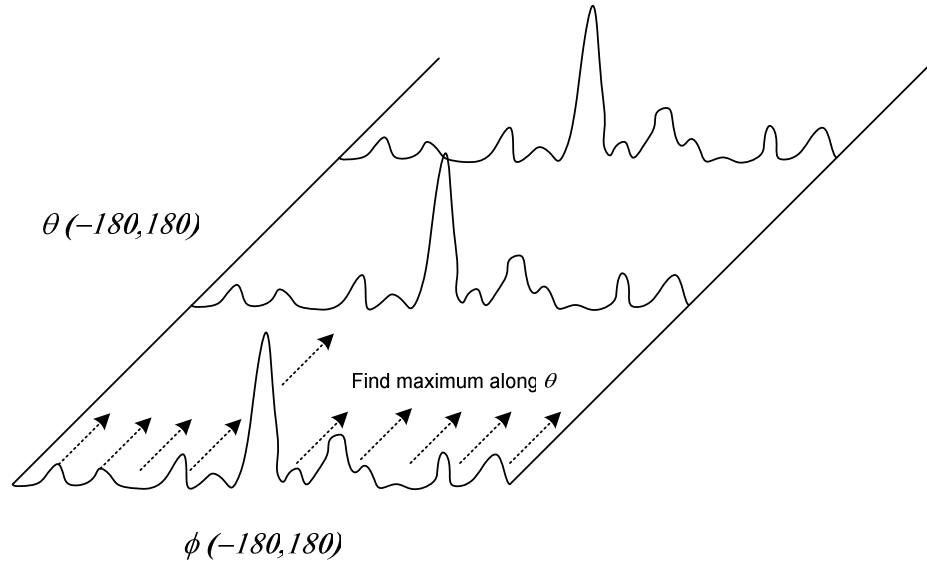
θ (−180,180)

Find maximum along θ

ϕ (−180,180)

Figure 4-4 Procedure of forming $M(\phi)$

Therefore, the following function can effectively be used to design the array:

$$M(\phi) \overset{\Delta}{=} \max_{\theta} B(\theta, \phi)$$

$$= \max_{\theta} \frac{\left| \mathbf{A}^H(\theta + \phi)\mathbf{A}(\theta) \right|^2}{N^2} \qquad (4\text{-}20)$$

It is equivalent to maximize the square root of $M(\phi)$ and since N is the number of sensors which is a constant and can be omitted, an equivalent metric function is

$$M_{eq}(\phi) = \max_{\theta} \left| \mathbf{A}^H(\theta + \phi)\mathbf{A}(\theta) \right|. \qquad (4\text{-}21)$$

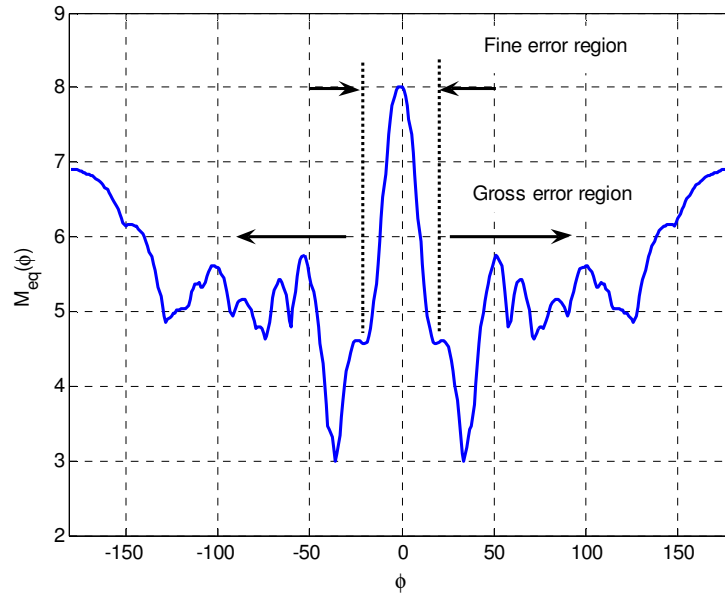For the array given in Figure 4-1, $M_{eq}(\phi)$ is sketched in Figure 4-5.

Figure 4-5 $M_{eq}(\phi)$ of the array

In Figure 4-5 both fine error and gross error regions are shown. It is seen that the risk of ambiguity is very high for this particular array. Following analysis is provided for the UCA of 8 elements given in Figure 4-6. Figure 4-7 shows the $M_{eq}(\phi)$ of the UCA.
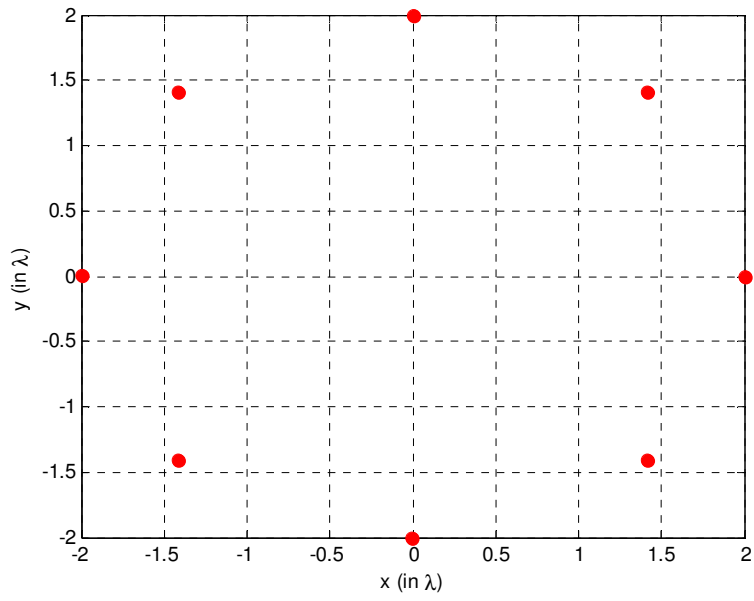
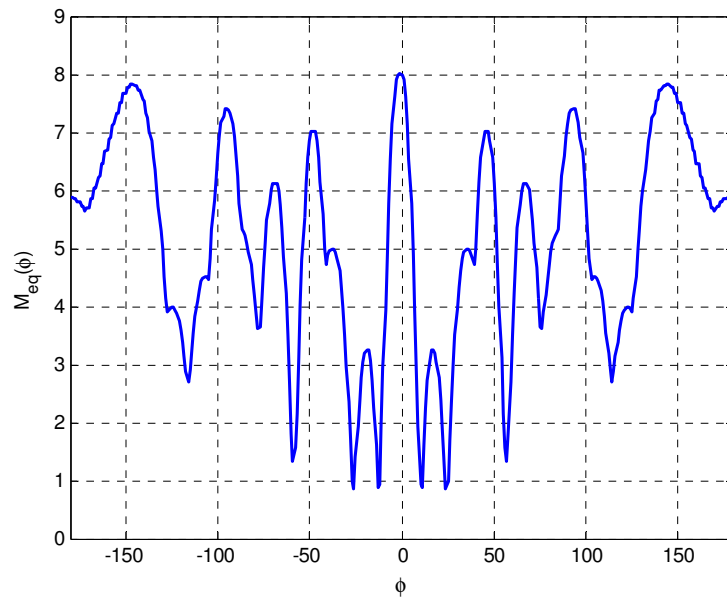Figure 4-6 UCA of 8 elements and aperture of 2λ

Figure 4-7 $M_{eq}(\phi)$ of the UCA

Figure 4-8 shows that the arbitrary array given in Figure 4-1, has a relatively good gross error performance compared to UCA. However, UCA has much better performance around the main peak and therefore has a better fine error variance as expected. The calculated CRB of both arrays are sketched in Figure 4-9 for SNR=*0 dB*. In this figure, CRB of both arrays are normalized with respect to the CRB of the UCA. Figure 4-9, validates the conclusion we drew from Figure 4-8. The CRB of the UCA is approximately 3 times better than that of the other array.

4.3 Optimization

The metric function which was given in (4-21) is a function that helps us to assess the performance figure of a certain array in terms of both gross and fine errors. Here is the optimization steps that we are going to use:

1. A bounded region that the sensors can be located is defined. Any arbitrary region can be specified.

2. The number of array elements is determined.

3. By using (3-36), the maximum allowed probability of gross error is set for a certain SNR.

4. Corresponding $M_{eq}(\phi)$ value is determined for the maximum allowed probability of gross error. As an example, Figure 4-10 and Figure 4-11 show the relation between the $M_{eq}(\phi)$ and P_{gem} based on the discussion in Section 3.3. These figures are generated for 101 and 11 snapshots.

5. The value found in step 4 is set as a threshold for $M_{eq}(\phi)$ for the gross error region.

6. An optimization is carried out to find the maximum curvature of the main beam that satisfies the threshold in step 4.
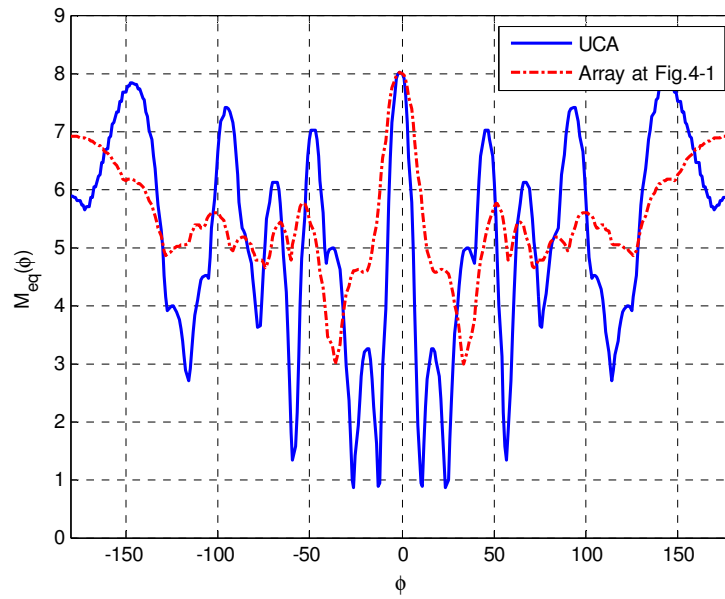
49

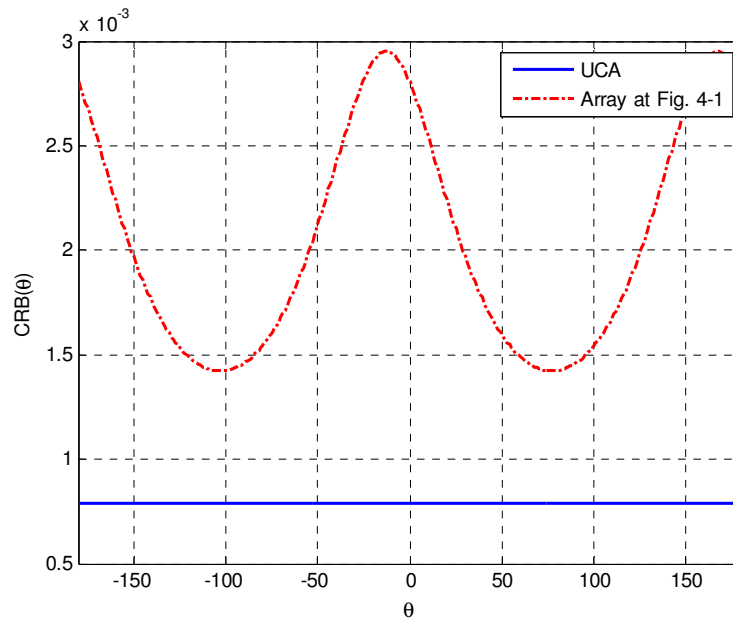Figure 4-8 $M_{eq}(\phi)$ of the UCA and the array given in Figure 4-1

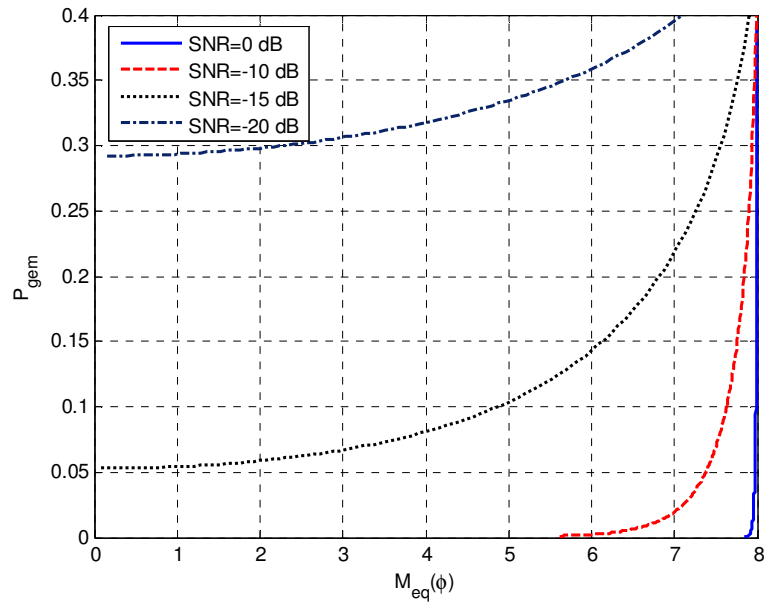Figure 4-9 Comparison of the CRB of both arrays

50

Figure 4-10 P_{gem} versus $M_{eq}(\phi)$ for *101* snapshots
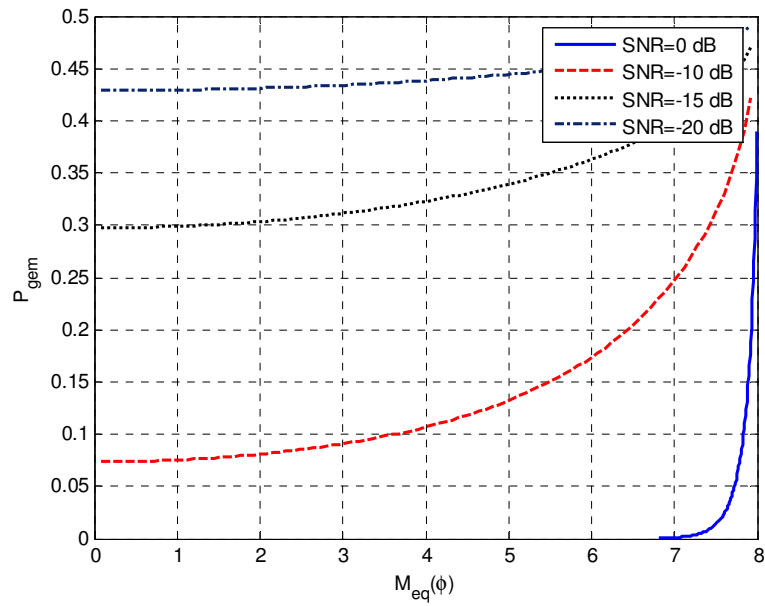

Figure 4-11 P_{gem} versus $M_{eq}(\phi)$ for *11* snapshots

At this point, a significant observation should be stated about the relation between the $M_{eq}(\phi)$ and P_{gem}. For the conditional maximum likelihood estimators, a sufficient statistic is given as in (3-8).

$$L_3(\theta) = \frac{1}{N} \sum_{k=1}^{K} \left| \mathbf{A}^H(\theta)\mathbf{x}(k) \right|^2 \tag{4-22}$$

where $x(k)$ was given in (2-11).

$$\mathbf{x}(k) = \mathbf{A}(\theta_c)g(k) + \mathbf{n}(k) \qquad k = 1, 2, \ldots, K \tag{4-23}$$

where θ_c represents the incidence angle of the incoming signal. If we use (4-23) in (4-22) we get

$$
\begin{aligned}
L_3(\theta) = \frac{1}{N} \sum_{k=1}^{K} \big[& \mathbf{A}^H(\theta)\mathbf{A}(\theta_c)g(k)g^*(k)\mathbf{A}^H(\theta_c)\mathbf{A}(\theta) \\
& + \mathbf{A}^H(\theta)\mathbf{A}(\theta_c)g(k)\mathbf{n}^H(k)\mathbf{A}(\theta) \\
& + \mathbf{A}^H(\theta)\mathbf{n}(k)g^*(k)\mathbf{A}^H(\theta_c)\mathbf{A}(\theta) \\
& + \mathbf{A}^H(\theta)\mathbf{n}(k)\mathbf{n}^H(k)\mathbf{A}(\theta) \big]
\end{aligned}
\tag{4-24}
$$

In (4-24), there are two noise cross signal terms and a noise cross noise term. When the SNR is sufficiently high, the noise cross signal terms dominate and it will be sufficient to calculate the relation between the $M_{eq}(\phi)$ and the P_{gem} for only one snapshot value. The relation between the $M_{eq}(\phi)$ and the P_{gem} for other snapshot values can be obtained by using the linear relation with the calculated one. On the other hand, if the SNR is not high enough, then the noise cross noise term cannot be ignored and the relation between the $M_{eq}(\phi)$ and the P_{gem} should be calculated for all desired snapshot values.

4.3.1 Optimization Algorithm

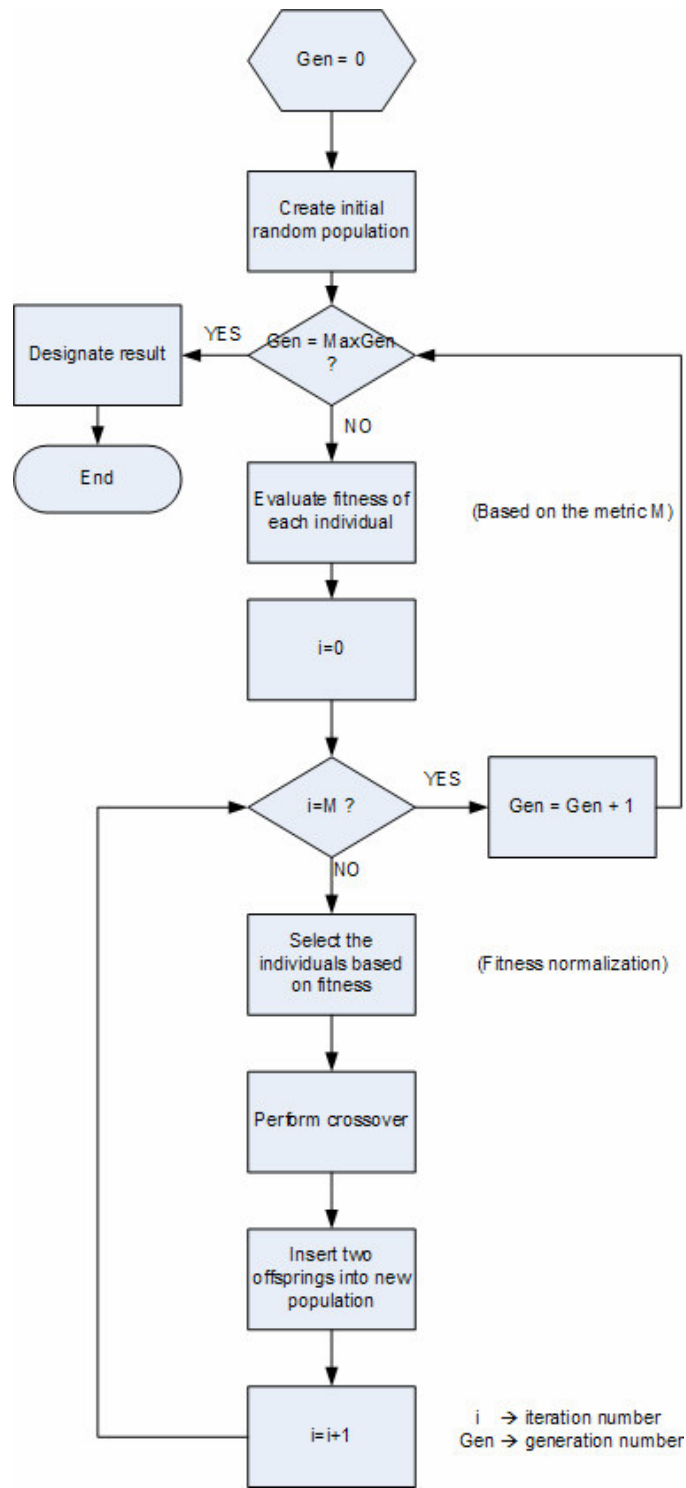A generic genetic algorithm is used to perform the optimization [32]. The algorithm is shown in Figure 4-12.

Figure 4-12 The applied genetic algorithm

The purpose of the genetic algorithm is to adapt the array geometry to certain conditions. Array geometry has the form of the coordinates of the sensor array elements. Assuming N array elements it has the structure $\{(x_1,y_1), (x_2,y_2), ...,(x_N,y_N)\}$.

Initially, a sample population is created. The sample population consists of different individuals that correspond to a single array structure. The size of the sample population is decided by considering the array size and the number of elements. Sample population is created randomly but is subject to a certain criterion. The array elements are forced to lie in the given bounded region. In an array structure, any two array elements can not be closer to each other than a certain distance. This is provided by controlling the creation of the sample population and as well as the mutual coupling and mutation operations. Structure of the sample population is given in Table 4-1.

Table 4-1 Structure of the population of individuals

Individual Number	Individuals	
	Sensor Locations	Fitness
1	$S_1=\{(x_1,y_1), (x_2,y_2), ..., (x_N,y_N)\}$	F_1
2	$S_2=\{(x_1,y_1), (x_2,y_2), ..., (x_N,y_N)\}$	F_2
3	$S_3=\{(x_1,y_1), (x_2,y_2), ..., (x_N,y_N)\}$	F_3
:	:	:
:	:	:
MaxPop	$S_{MaxPop}=\{(x_1,y_1), (x_2,y_2), ..., (x_N,y_N)\}$	F_{MaxPop}

Each individual that passes the threshold set for the gross errors is assigned a fitness value. The fitness is set to zero for the individuals that cannot pass the threshold For the others, the fitness value is determined by using the curvature of the main lobe.

After the sample population is created and fitness values are determined, the crossover operation is performed. Crossover is carried out by choosing two parents, namely, *parent1* and *parent2* and producing two new offsprings, namely, *child1* and *child2*. In order to choose the two parents, a selection procedure is performed by giving more chance to higher fitness valued individuals. This selection procedure is usually called weighted roulette wheel operation in the literature. The crossover procedure is visualized in Figure 4-13.

A cross point is randomly determined and two parent's chromosomes, namely, their sensor location positions, are exchanged. Hence, the offsprings are produced.

In order to achieve a more extensive search, mutation may be produced at the crossover phase. Mutation is a procedure that occurs with a certain probability and replaces the mutant child's chromosomes with new ones. This is carried out again within certain rules. Newly generated array elements must lie in the bounded region and cannot be closer to the other array elements than a certain distance. The process of generation of the new population is depicted in Figure 4-14.

After the crossover, a new generation is constructed and fitness values of all are determined. Until a certain number of generations is produced or the improvement of the fitness values slows down, the algorithm halts.
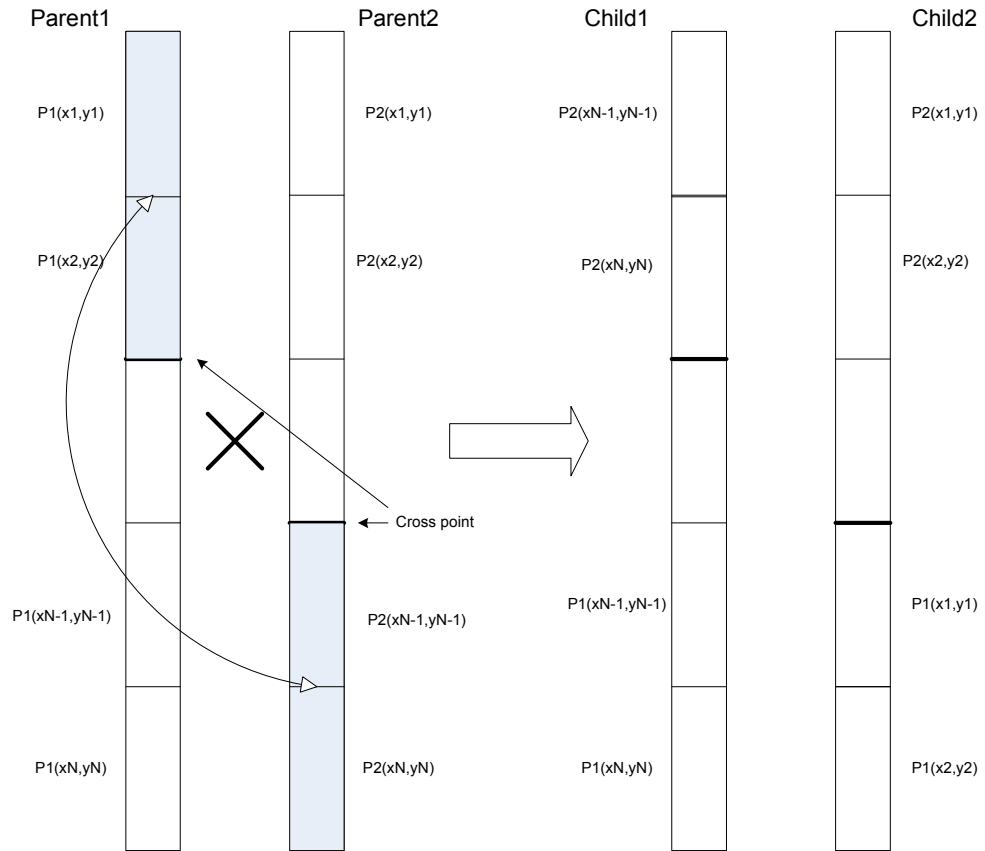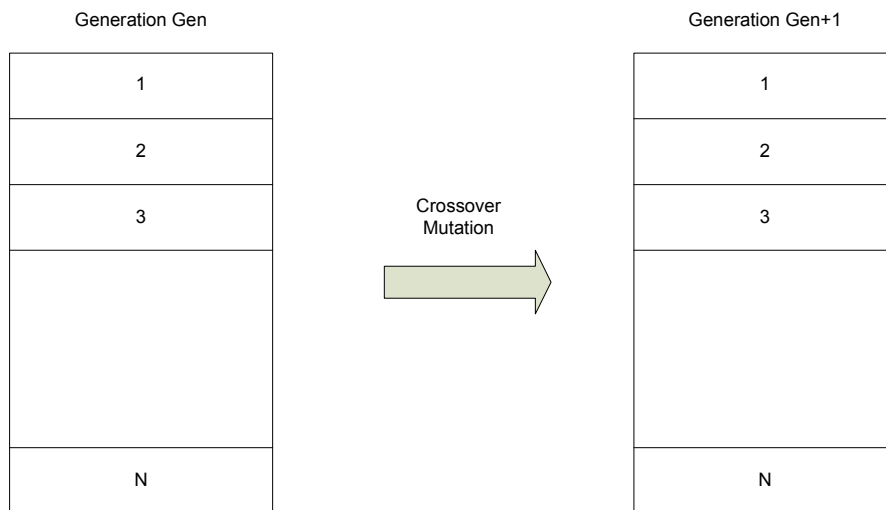
Figure 4-13 Crossover

Figure 4-14 Production of a new generation

CHAPTER 5

RESULTS

In this chapter, the optimization procedure outlined in the previous chapter is applied to certain regions and the results are discussed.

Firstly, optimization is performed on a circular aperture and two different apertures are used to demonstrate the effect of the aperture length on the procedure. Both examples use the same number of sensors and the thresholds are set to a value to assure that the gross error specifications of the array restrict the fine error performance from reaching to its maximum possible figure. Results are compared to the UCA.

The next example is arranged to show the outcome of the method in more realistic circumstances. The procedure is applied to place the array elements on an aircraft.

Finally, different threshold values are set for the previous examples, in order to see the effect on optimized array geometries.

Throughout the simulations, some default values are chosen for the number of snapshots that the MUSIC algorithm uses. The method proposed in this work is independent of the number of snapshots as long as the required calculations such as the ones presented in Figure 4-10 and Figure 4-11 are carried out. Thus, the number of snapshots can be chosen according to the requirements of the specific application of interest.

5.1 Circular Aperture of 2λ with 8 Elements

For the first example, bounded region is set to a circle of 2λ which is a relatively short aperture that will possibly have some application areas on mobile platforms. For this particular example, the maximum allowed P_{gem} is set to 0.15 at SNR=-15 dB when the number of snapshots is 101. By using Figure 4-10, $M_{eq}(\phi)$ can be found as 6. This value is set as a threshold and the optimization is performed. The array shown in Figure 5-1 was obtained. The array element locations are depicted in Table 5-1.

Table 5-1 Array element locations of the optimized array of the circular aperture of 2λ case

Array Element Number	1	2	3	4	5	6	7	8
x (in λ)	-0.4	0	0	0.8	-1.6	-0.6	1.9	1.9
y (in λ)	0.9	-1.6	1.7	1.4	0.2	-0.8	0.1	-0.4

The dashed curve in Figure 5-1 shows the bounded region. The corresponding metric function of the array is shown in Figure 5-2.
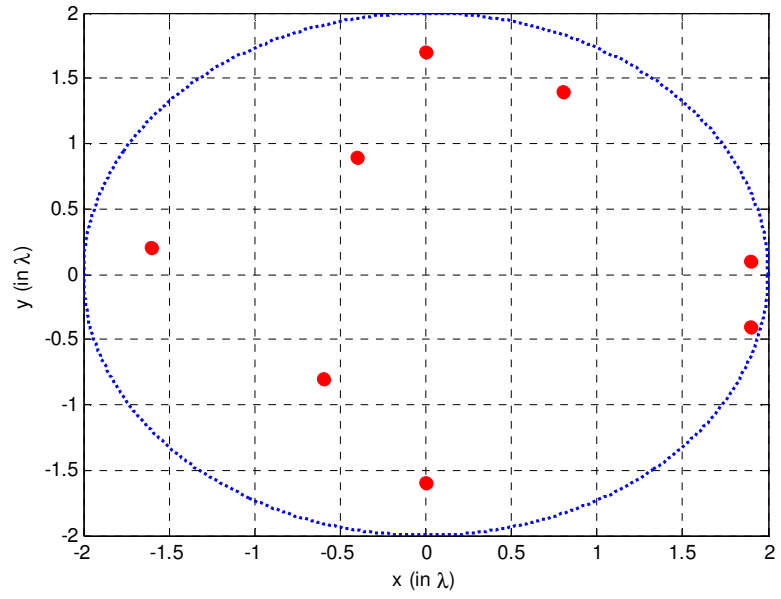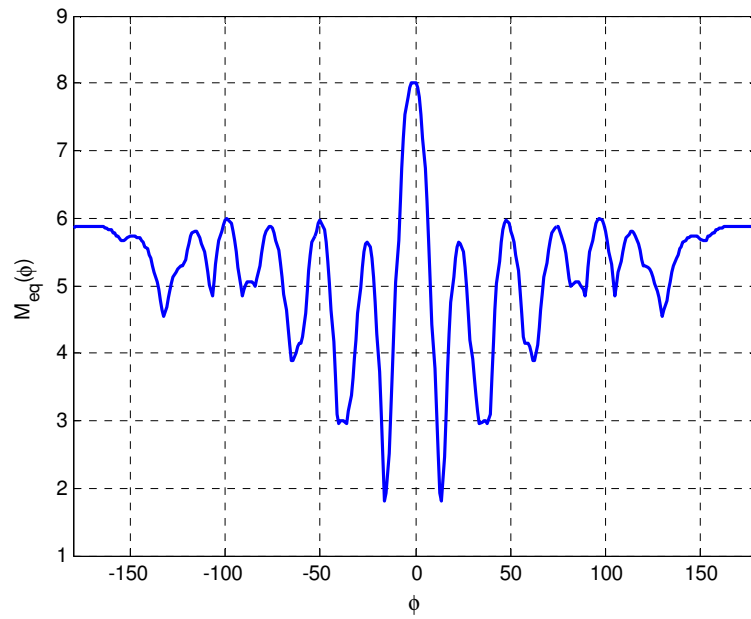
Figure 5-1 The optimized array

Figure 5-2 The metric function of the optimized array

Note that the sidelobe levels are under the threshold. The optimized array is compared with the UCA that uses the same aperture and is given in Figure 5-3. Array element locations of UCA are listed in Table 5-2 and the metric function of the UCA which was previously given in Figure 4-7 is sketched again in Figure 5-4 for convenience.

Table 5-2 Array element locations of the UCA that has the aperture of 2λ

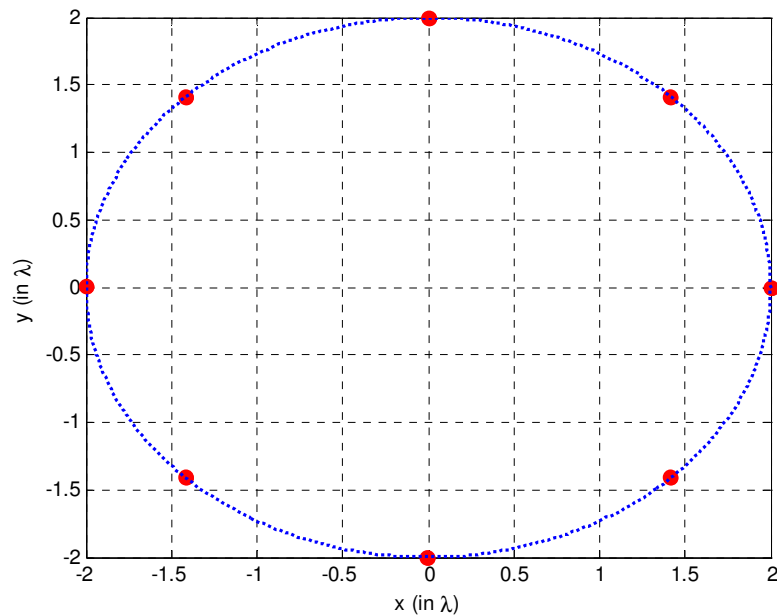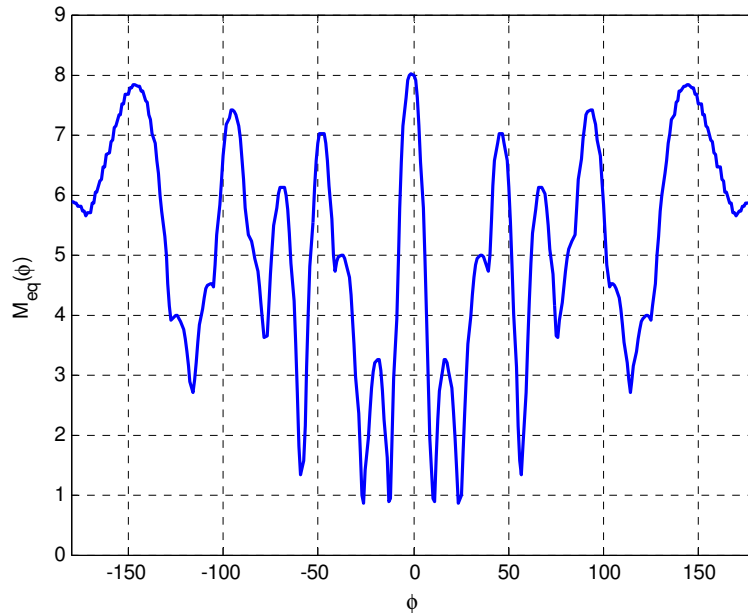| Array Element Number	1	2	3	4	5	6	7	8
x (in λ)	1.41	0	-1.41	-2	-1.41	0	1.41	2
y (in λ)	1.41	2	1.41	0	-1.41	-2	-1.41	0

Figure 5-3 Geometry of the UCA

Figure 5-4 Metric function of the UCA

If the two metric functions are compared, it can be seen that probability of gross error is significantly reduced. It can be observed from Figure 5-4 that the highest peak value of the UCA's metric function is around 7.8. Thus, we can deduce from Figure 4-10 that under the same conditions, i.e. for *101* snapshots and *-15 dB* SNR, probability of gross errors can reach *0.35* for the UCA, while this value is *0.15* for the optimized array. On the other hand, if we zoom in on the metric function graphs of both arrays, around $\phi=0$, as in Figure 5-5, it can be seen that CRB of the UCA is slightly better than that of the optimized array. This result is expected since the UCA uses the full aperture, by paying the price of increased probability of gross errors. Calculated CRB of both arrays are also compared in Figure 5-6. In this figure, CRB is normalized to the CRB of UCA in order to compare the estimation errors of both arrays. Effect of the expansion of the main lobe is seen in this figure clearly. A small relaxation in CRB pulls the probability of gross errors to much lower values. In other words, a smart trade off is performed for a much less

61

ambiguity risk to a bit worse performance for high SNR values. This will be much more obvious when we look at the MUSIC spectra and the total error variances.

MUSIC spectra of a single run of the MUSIC estimator for UCA and optimized array are given for different bearing angles and for different SNR values: Figure 5-7 shows the function b and the MUSIC spectra of UCA for different SNR values at incidence angle $0°$. As SNR gets lower, the peaks of the MUSIC spectrum get higher at the peaks of b. Hence, the gross error risk would be significantly high at those incidence angles. If it is compared to the optimized array given in Figure 5-8, it is clearly seen that, since the peaks of the function b are much lower than the peaks of UCA, the MUSIC spectrum is considerably flat at those values. Similar observations can be made at different incidence angles. Figure 5-9 and Figure 5-10 show the function of b and the MUSIC spectra at $15°$ and Figure 5-11 and Figure 5-12 show the same information at $\theta=45°$. It is evident from the figures that gross errors are highly probable under $-6\ dB$ SNR values when the UCA is used. In contrast, the gross errors are much less probable when the optimized array is used even in $-9\ dB$ SNR values.
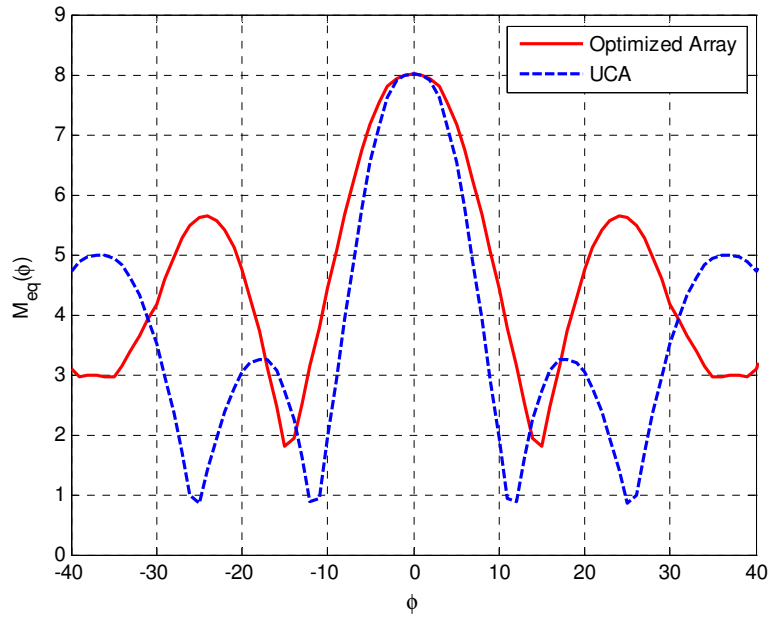
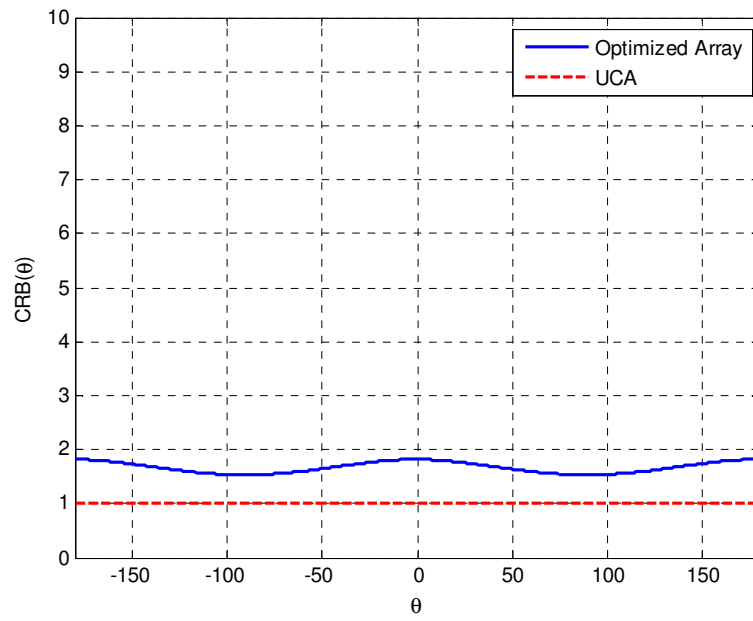Figure 5-5 Comparison of the UCA and the optimized array

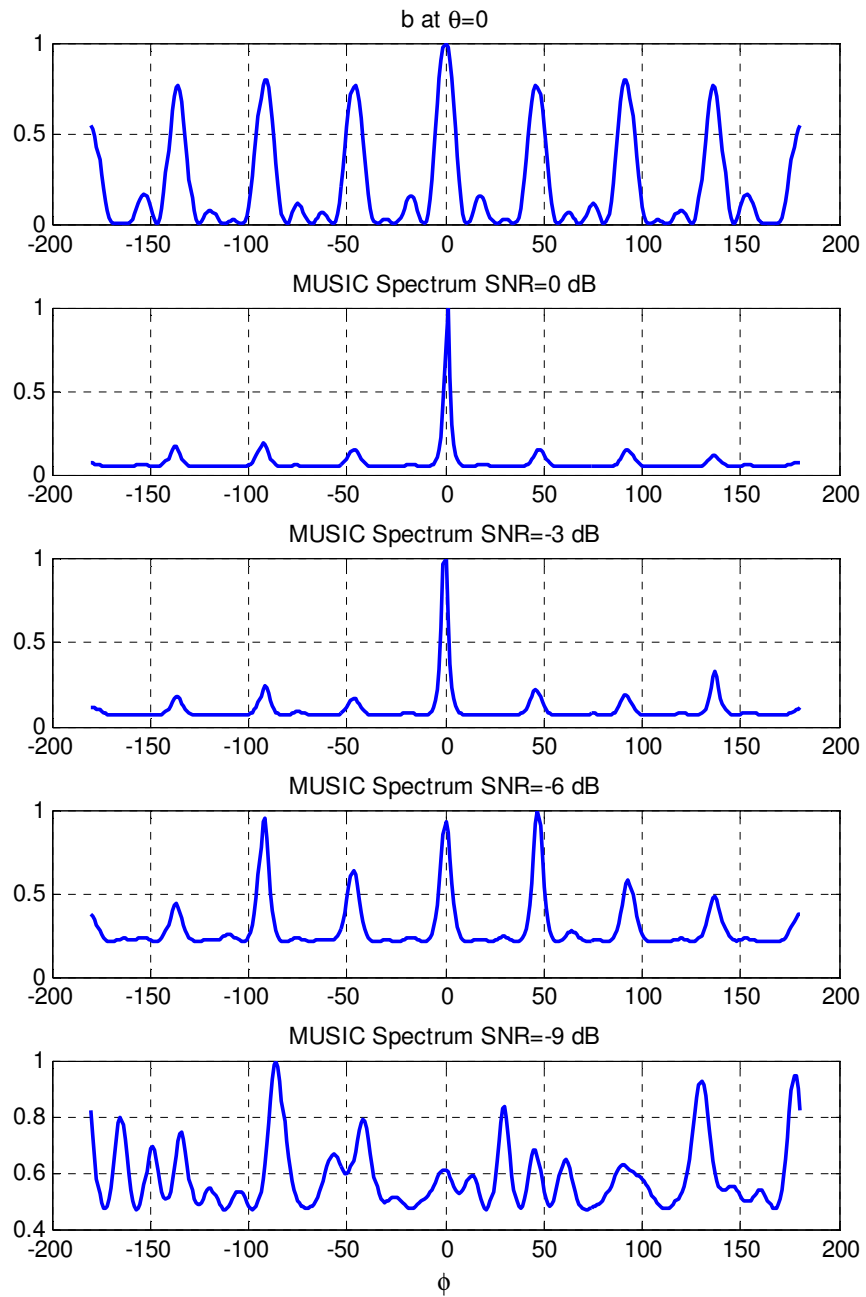Figure 5-6 Comparison of the CRB of both arrays

Figure 5-7 MUSIC spectrum of the UCA when the incidence Angle is 0° and SNR=0,-3,-6,-9 dB
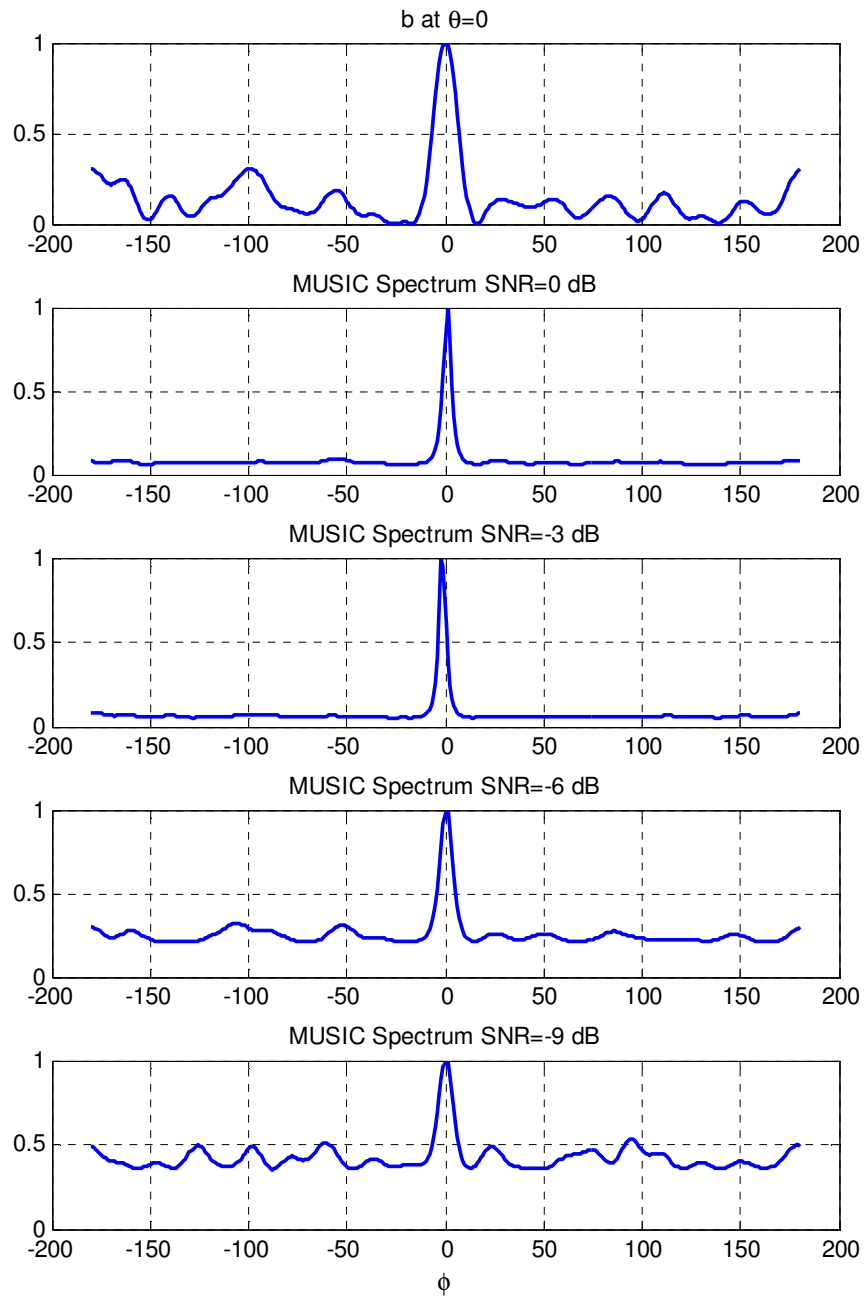
Figure 5-8 MUSIC spectrum of the optimized array when the incidence angle is 0°
and SNR = 0,-3,-6,-9 dB

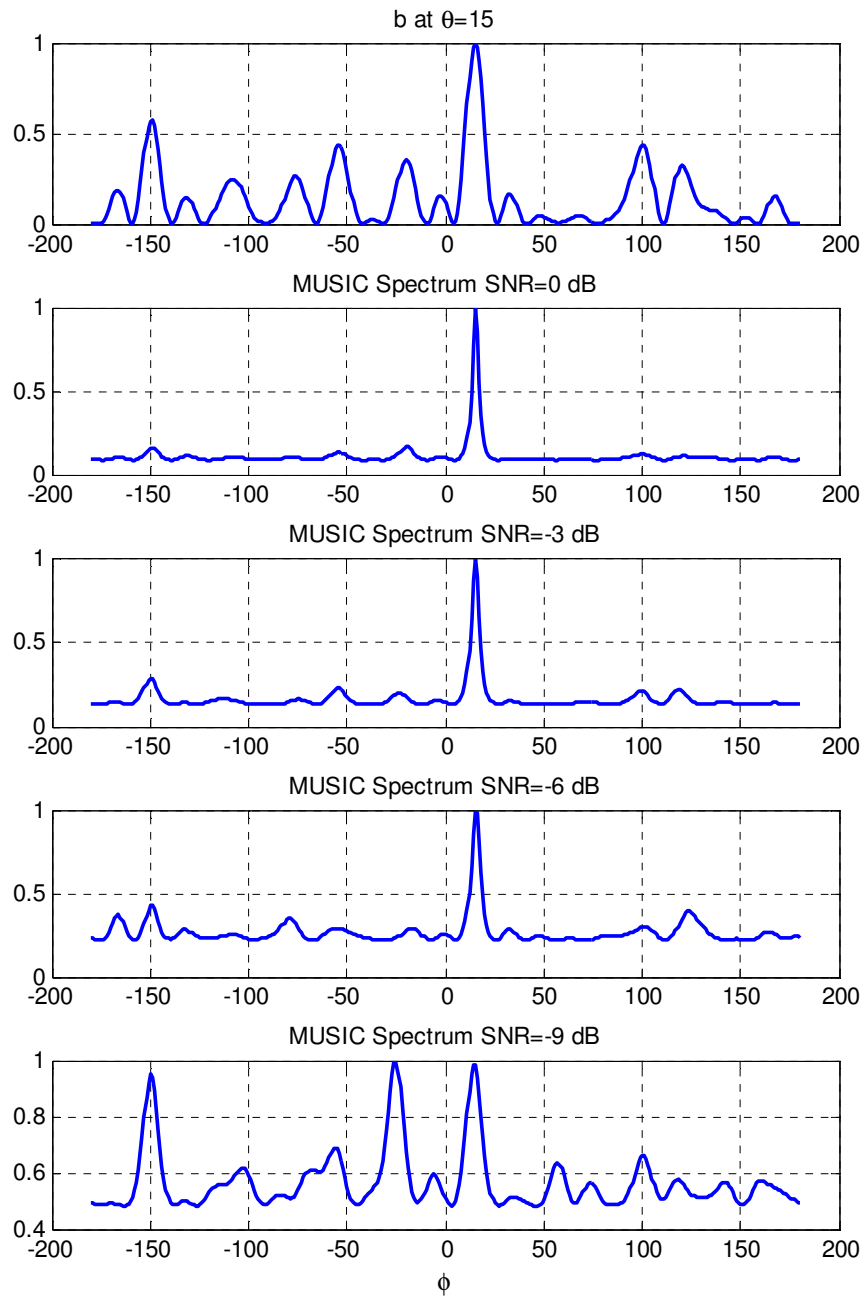Figure 5-9 MUSIC spectrum of the UCA when the incidence angle is 15° and SNR=0,-3,-6,-9 dB
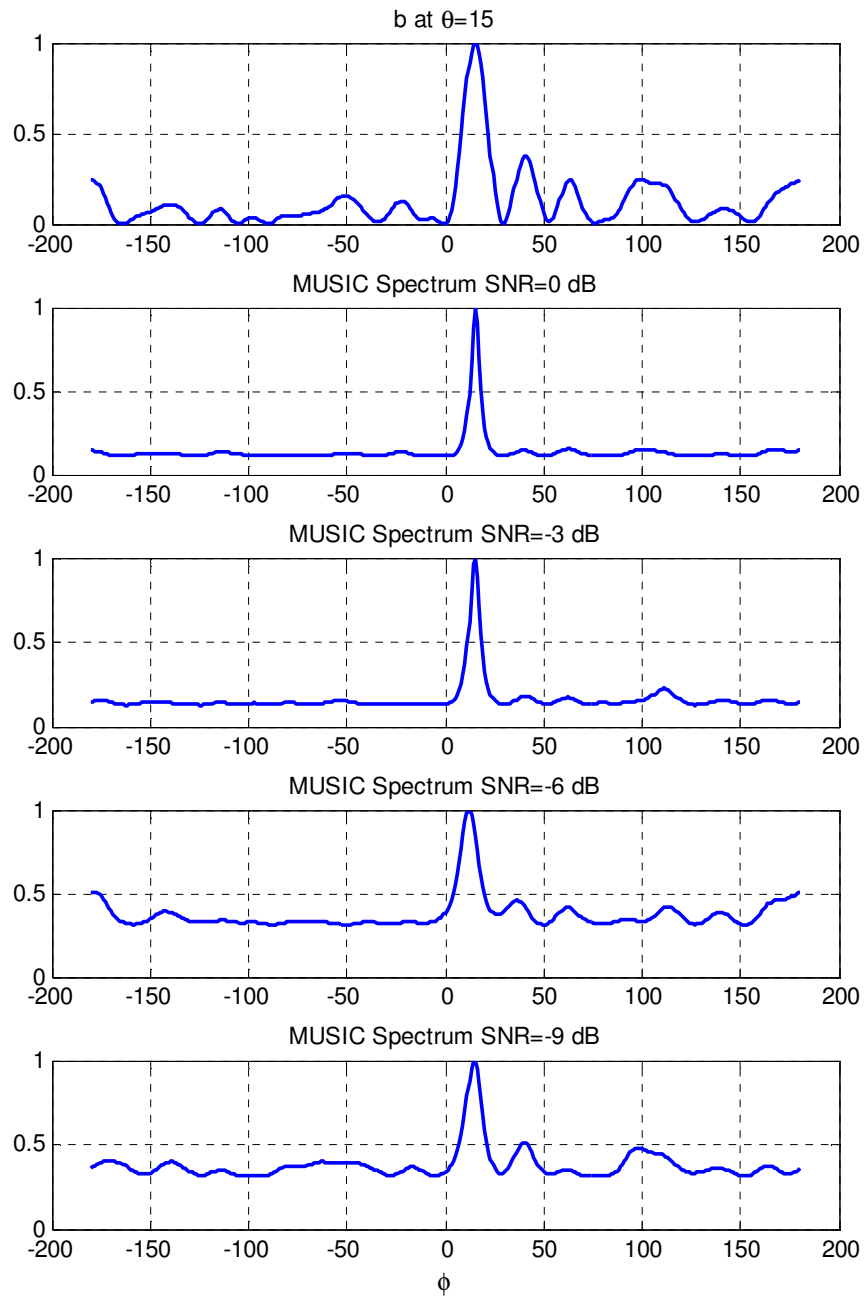
Figure 5-10 MUSIC spectrum of the optimized array when the incidence angle is 15° and SNR = 0,-3,-6,-9 dB
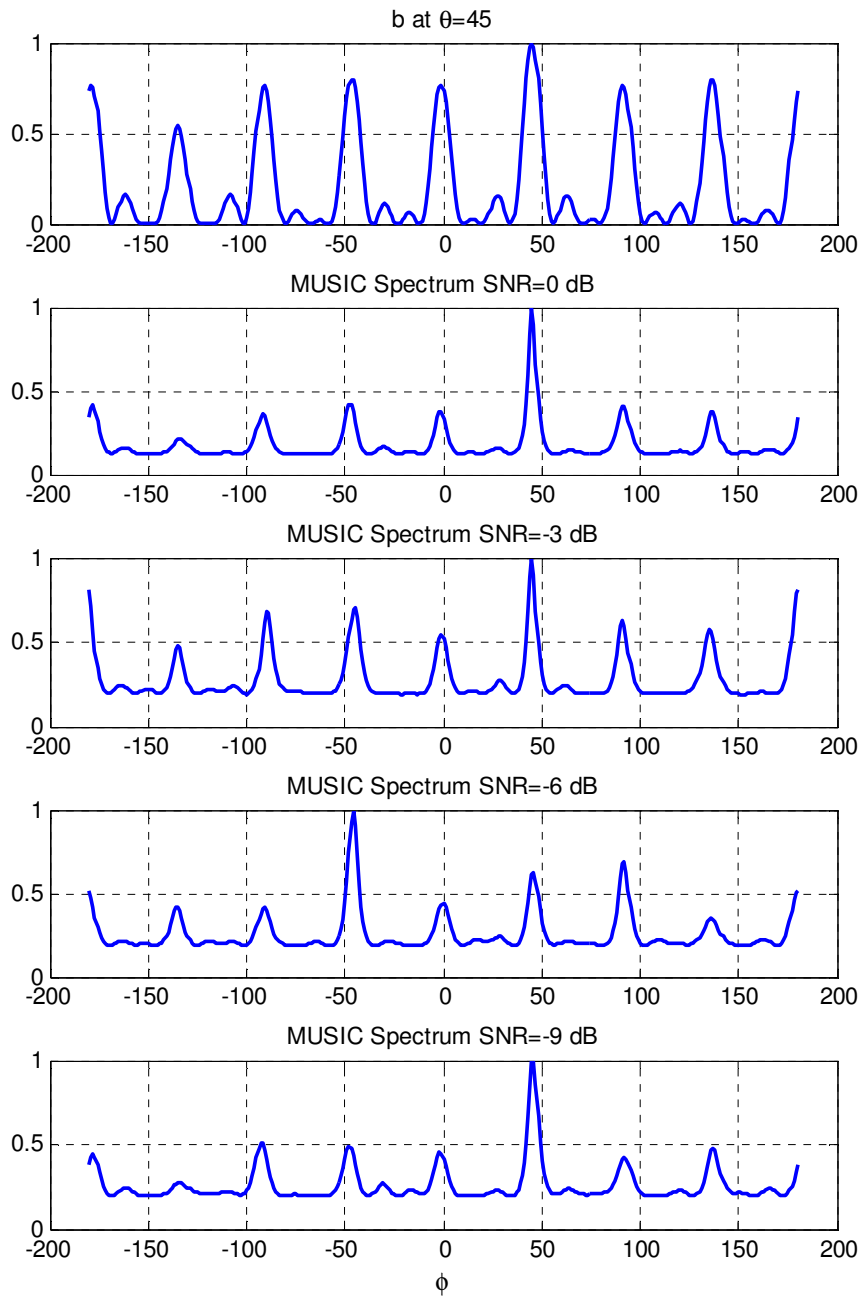
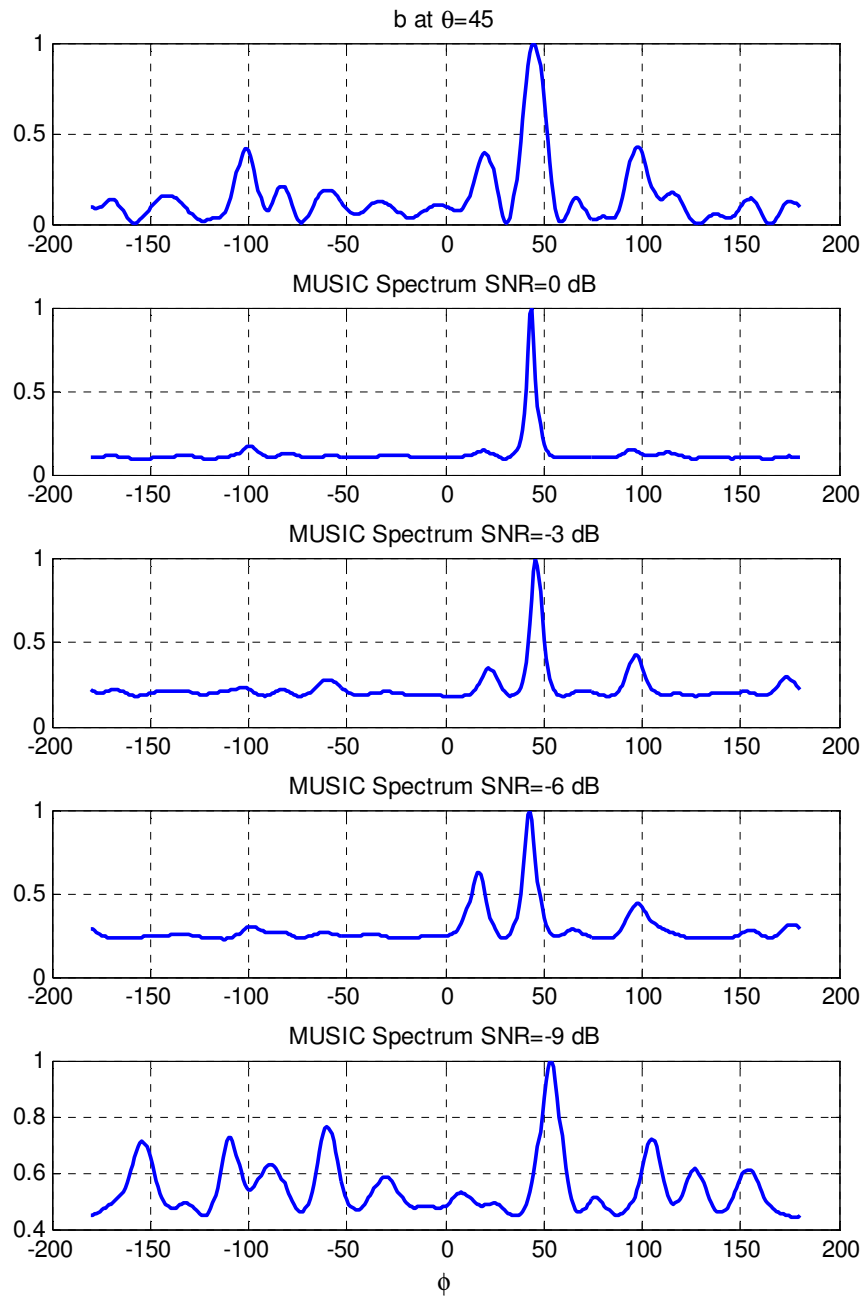Figure 5-11 MUSIC spectrum of the UCA when the incidence angle is 45° and SNR=0,-3,-6,-9 dB

Figure 5-12 MUSIC spectrum of the optimized array when the incidence angle is 45° and SNR = 0,-3,-6,-9 dB

One more remark on these figures is that, as SNR gets lower, the main peaks of the MUSIC spectra that correspond to the optimized array gets rounder compared with the MUSIC spectra of the UCA which indicates larger fine errors. This is apparent from Figure 5-12 that the estimated angle is slightly larger than $50°$ when the incidence angle is $45°$ at *-9 dB* SNR. If it is compared with Figure 5-11, although the MUSIC estimator made a gross error at *-6 dB* SNR, it made a correct estimate at *-9 dB* for that particular run and the peak is observed to be sharper than the MUSIC spectrum of the optimized array. The fine error performances of both arrays will be analyzed further in the text by the simulation results on estimation error variances.

By observing the MUSIC spectra, the probability of gross errors for the optimized array are expected to decrease in comparison to the case of the UCA. This makes the estimation error variances to reduce significantly at low SNR values. However, since the CRB of UCA is lower than that of the optimized array, estimation error variance is expected to be larger than that of the UCA at high SNR values. This expectation is justified as can be seen in the following figure: Figure 5-13 shows the total probability of gross errors of both arrays when the incidence angle is $45°$. Gross error is defined as the estimated bearing which is out of the main beam of the function *b*. If the estimated angle is in the main beam of *b*, it is considered as a fine error. The figure shows that at $45°$, the probability of gross error is significantly reduced by the optimization.
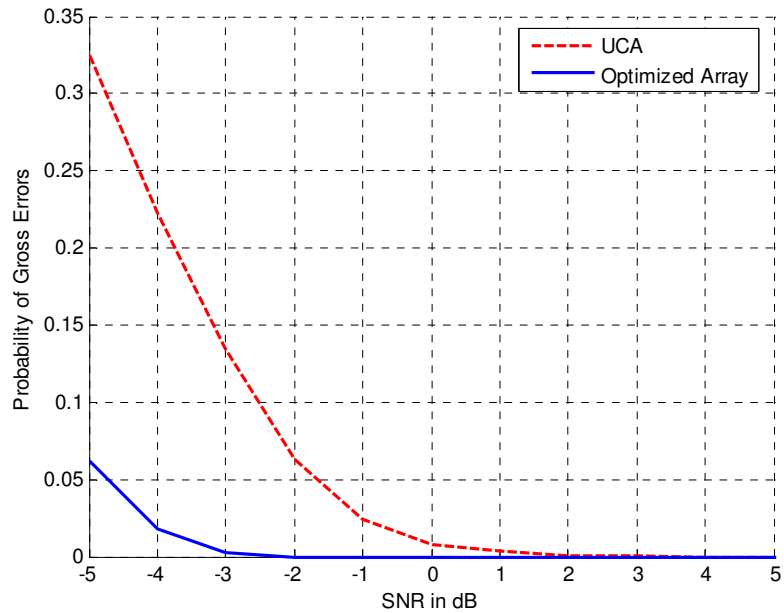
Figure 5-13 Comparison of the probability of gross errors when the incidence angle is 45°

Another observation can be made by comparing the total estimation variances for different SNR values. Figure 5-14 shows the result for incidence angle *45°*. Both the gross and the fine errors are considered together in this figure. Simulations were carried out by taking 5000 different runs in each SNR value and statistics are calculated by using the MUSIC estimation results. The graph in the figure fits well to the expected results. Since the UCA has more gross errors than the optimized array, at low SNR region optimized array has a lower estimation error variance. As the SNR gets higher, UCA is expected to have a lower estimation error variance. This can be seen if the high SNR region of Figure 5-14 is zoomed, as shown in Figure 5-15. Above the *4 dB* SNR point, estimation error variance of the UCA gets lower than that of the optimized array which supports our expectation.
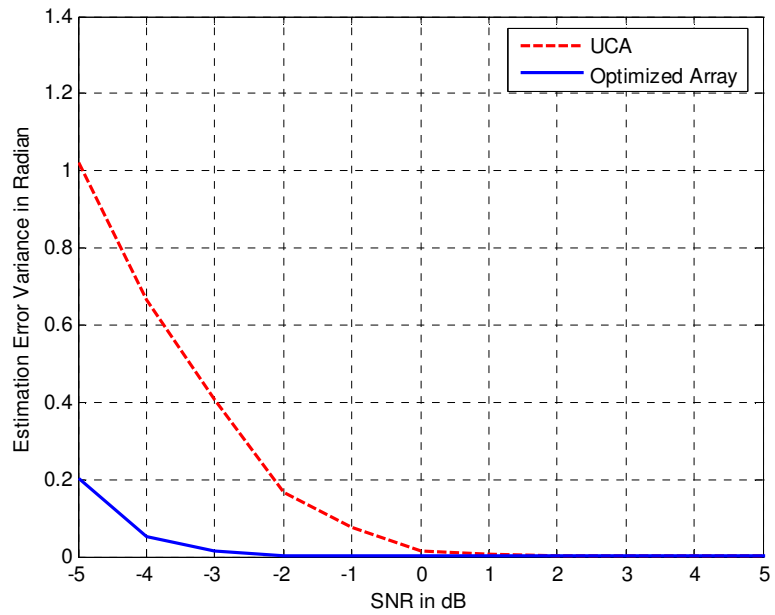
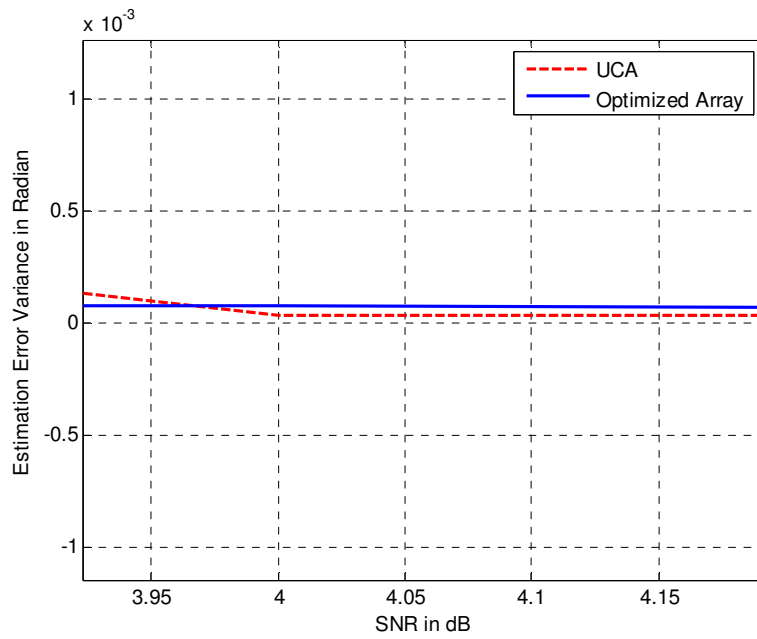Figure 5-14 Comparison of the estimation error variances when the incidence angle
is 45°

Figure 5-15 Effect of the main lobe expansion to the error variances

Since we have made the observations only for the incidence angle at *45°* these results do not reflect the overall array performance. Figure 5-16, Figure 5-17 and Figure 5-18 show the results when the incidence angle is randomly changed in each run, hence they are representative for the overall array performance. The results are the generalization of the previous analyses which were carried out at *45°* and it can be deduced that the estimation error variance is significantly reduced by the optimization process when compared to the UCA. By comparing the equal estimation error variance points of both arrays in Figure 5-17, we can say that in low SNR region, significant amount of performance can be gained by using a non-uniform array that is optimized by the method outlined in this work.

In Figure 5-18, Figure 5-17 is zoomed at high SNR region to show the fine error performance is dominant at high SNR and the UCA has better performance at those values, as expected.
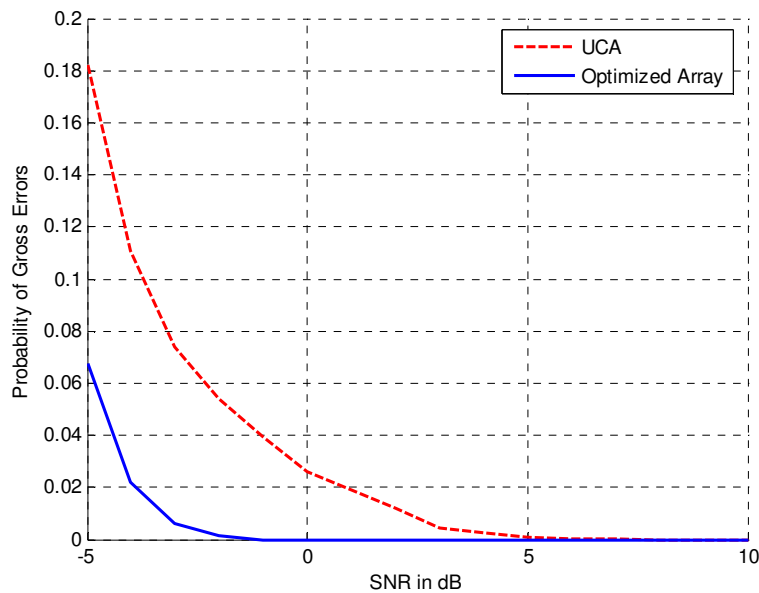

Figure 5-16 Comparison of the probability of gross errors for random incidence angle
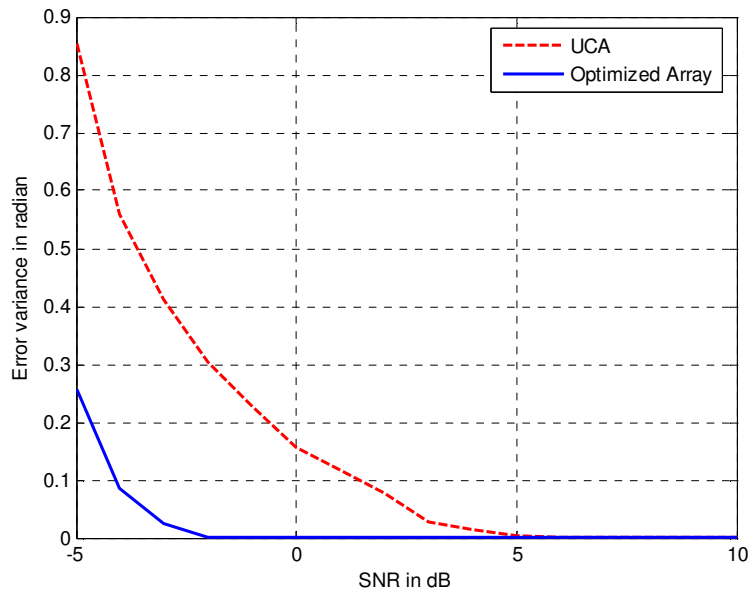
Figure 5-17 Comparison of the estimation error variances for random incidence angle
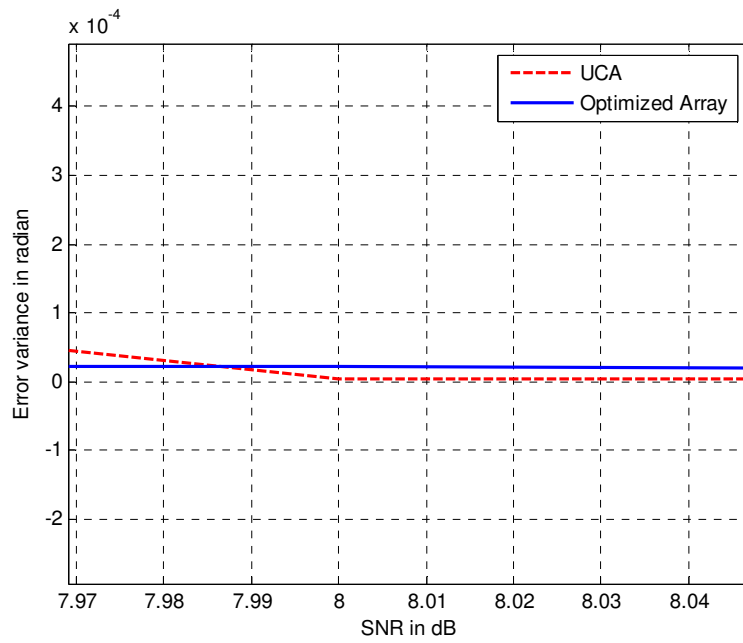

Figure 5-18 Effect of the main lobe expansion to the error variances

Up to this point, we have given extensive comparisons between the optimized array and the UCA which uses the entire specified region of 2λ, as the aperture size. However, the optimized array does not use the total aperture in order to compromise between the gross errors and fine errors. This raises the question, what will be the performance of the UCA, compared to the optimized array, which does not use the full aperture but a narrower aperture instead, to minimize the gross errors?

We have already shown by the theoretical analyses and verified by the simulations that the metric function given in (4-21) represents the gross and fine errors for any antenna array. Therefore, the comparison of the UCA with the optimized array will be carried out by changing the aperture size of the UCA and comparing the metric functions.

In order to perform this two cases will be generated: First case is the one for the UCA and the optimized array have the same fine error performance. The aperture radius of the UCA has been shrunk until the main lobes of the metric functions of both arrays will be equal in width. This condition is satisfied when the aperture radius of the UCA is 1.4λ. The metric functions of both arrays are shown in Figure 5-19. Note that, the main lobe of the metric functions of both arrays have the same lobe width, so that they will have the same fine error estimation performance. In Figure 5-20, calculated CRB of the optimized array and the UCA are shown with respect to the incidence angle. This sketch validates that the worst CRB value of the optimized array is almost the same as the UCA. This is due to the fact that the main lobe width of our metric function reflects the worst possible fine error performance. Since the condition of equal fine error performances is satisfied, we can analyze the gross error performances of the optimized array and the UCA that has an aperture of 1.4λ.
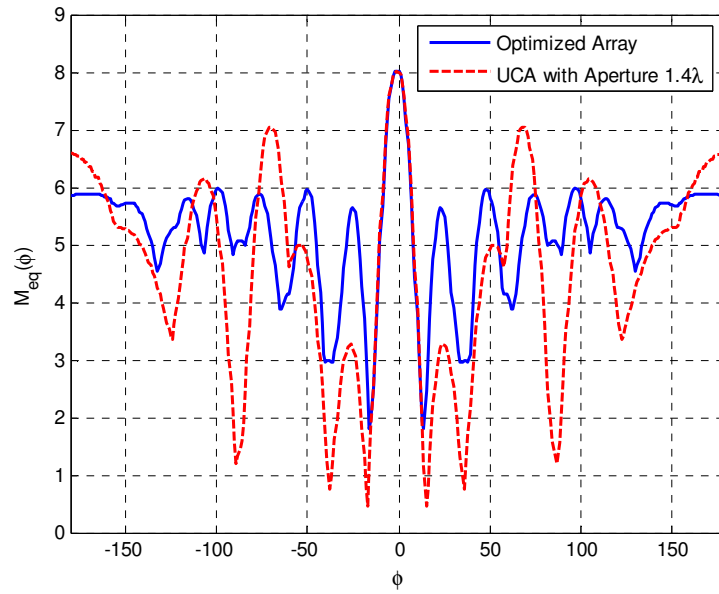
Figure 5-19 Metric functions of the optimized array and the UCA with aperture
length *1.4 λ*
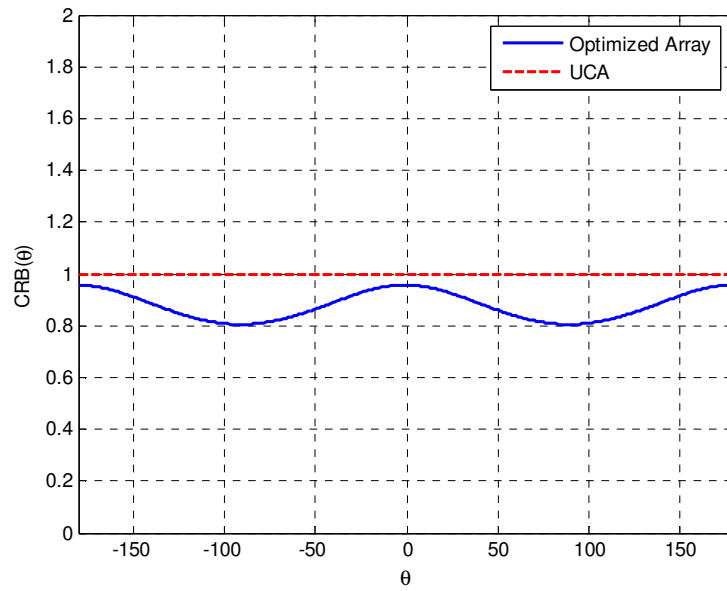
Figure 5-20 CRB of the optimized array and the UCA with aperture length *1.4 λ*

Figure 5-19 indicates that while the fine error performances of both arrays are almost equal, expected gross error performance of UCA is worse than that of the optimized array. This is because the metric function of the UCA has higher peaks than the optimized array. The simulation results support this observation and Figure 5-21 shows the estimation error variance of the optimized array is lower in low SNR region.
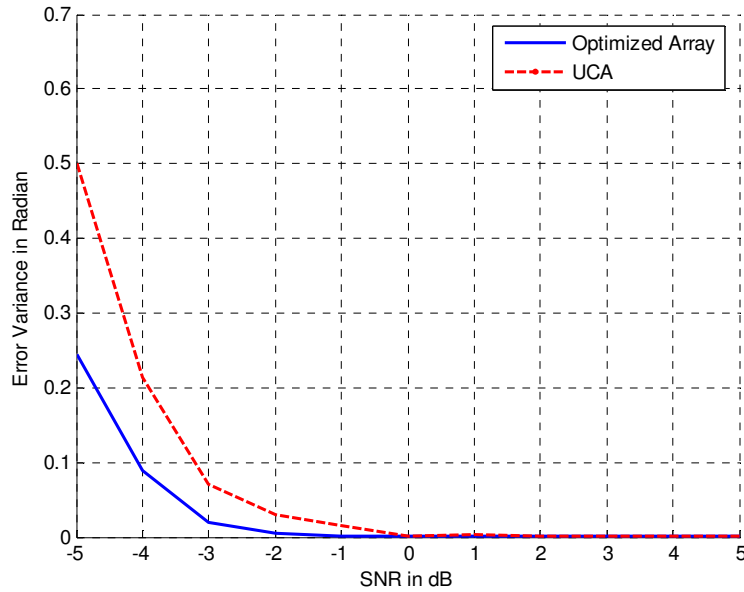
Figure 5-21 Estimation error variances of the optimized array and the UCA with aperture length *1.4 λ*

We mentioned that these two arrays would have almost the same fine error performances and validated this by analyzing the CRB of both arrays as shown in Figure 5-20. Figure 5-22 shows the SNR region where the fine errors dominate the error variance: The error variances are almost the same.
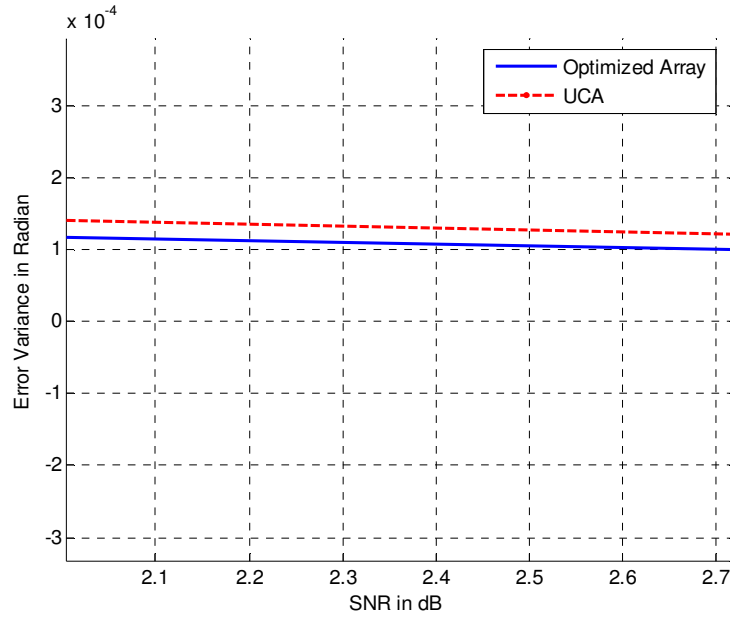
Figure 5-22 Fine error performances of the optimized array and the UCA with aperture length *1.4 λ*

The next step is to shorten the aperture length of the UCA further and generate the second case which is the one that the UCA and the optimized array have the same gross error performance. In order to satisfy this condition the aperture radius of UCA has been shrunk until the peaks of the metric function of the UCA reduce to the threshold level which was the initial design criterion of the optimized array. This condition occurs when the aperture length of the UCA is *0.73 λ.*

The metric functions, which are shown in Figure 5-23, show that the main lobe of the UCA is much wider than that of the optimized array when the required gross error specification is satisfied. Therefore, the CRB of the UCA is expected to be higher and no significant difference of the gross error performance is expected between the two arrays. This expectation is validated by the simulations. Figure 5-24 shows the estimation error variances of the two arrays. In low SNR region, the performances of the arrays are quite similar. However, in the high SNR region

78

which is zoomed in Figure 5-25, it is seen that the optimized array has a better performance than that of the UCA which has the narrower aperture. Figure 5-26 shows that the calculated CRB of the optimized array is much less than that of the UCA at all incidence angles.
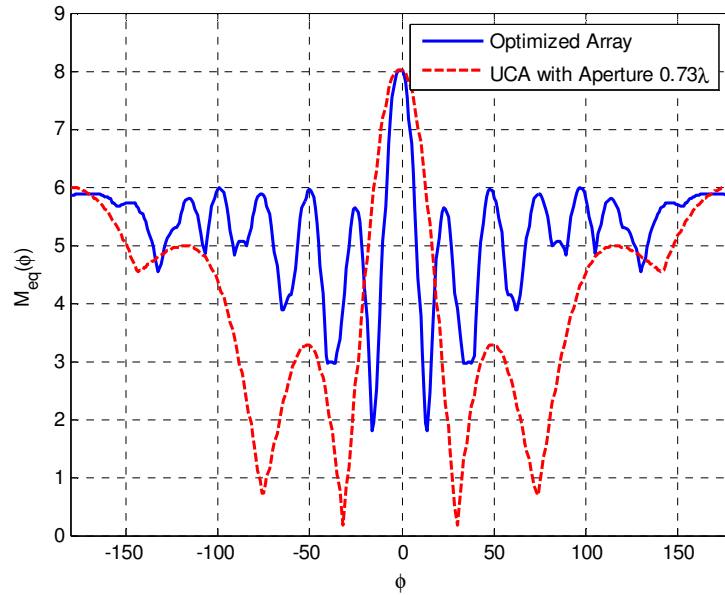
Figure 5-23 Metric functions of the optimized array and the UCA with aperture length *0.73 λ*

As a result, we can conclude that using the non-uniform array structure for which the element locations are optimized by using the metric function proposed, yields a better estimation performance than the UCA does.
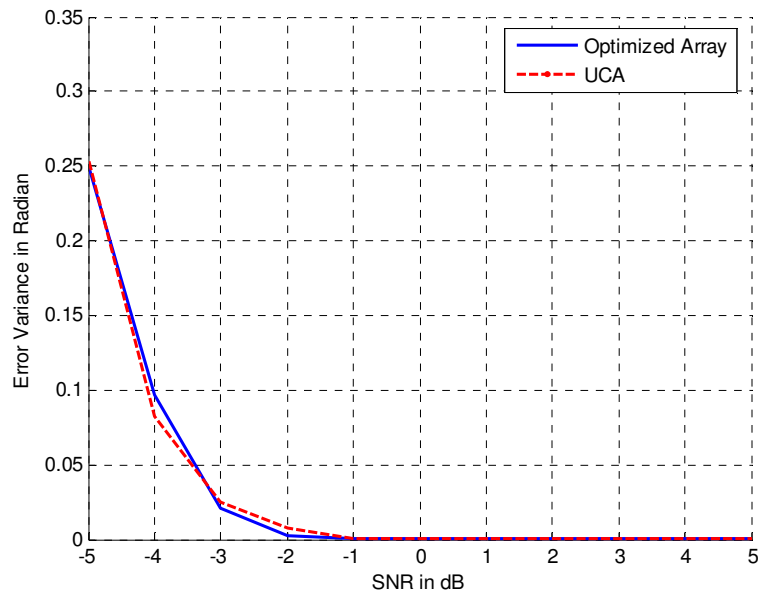
Figure 5-24 Estimation error variances of the optimized array and the UCA with aperture length *0.73 λ*
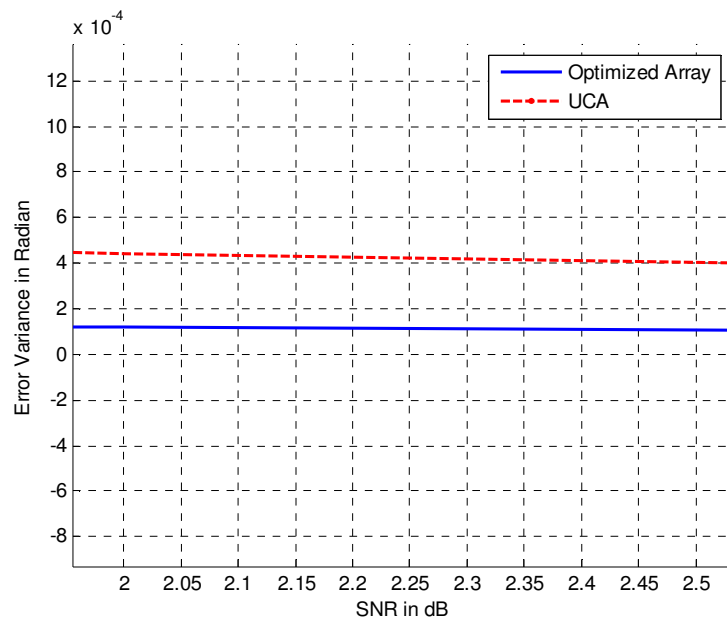
Figure 5-25 Fine error performances of the optimized array and the UCA with aperture length *0.73 λ*
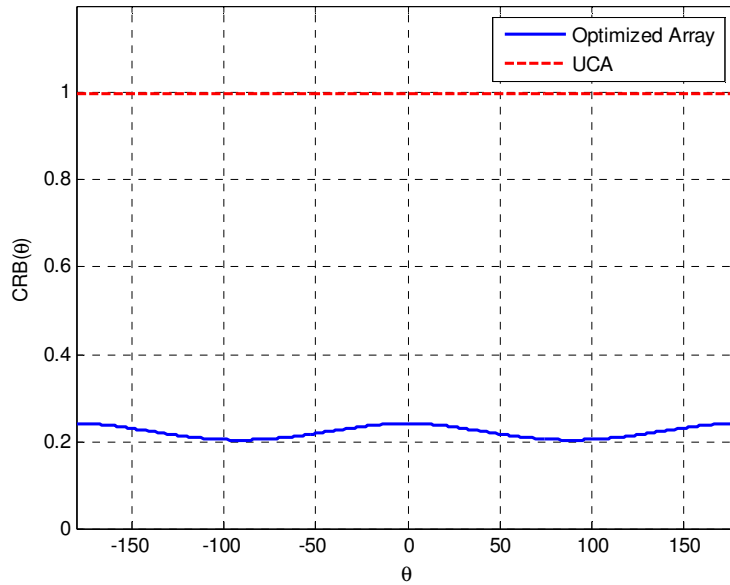
Figure 5-26 CRB of the optimized array and the UCA with aperture length *0.73 λ*

Before proceeding, a few comments should be stated here on how the sensors are placed by the optimization procedure. The array elements are spread out to use the full aperture to get a higher resolution while they are kept together, sometimes in couples or triplets, in order to satisfy the gross error probability requirements. This behaviour is intuitively logical and similar observations have been made in array geometry optimization literature and an intuitive approach of using the array elements in clusters for large aperture arrays has been proposed [17][20].

All of these observations such as the symmetry, closely spaced elements and using the aperture as a whole are intuitively used in such applications. The optimization procedure we have offered makes this implementation more controllable by putting the gross error and the fine error probabilities into the process and, moreover, makes it more flexible by allowing to change the requirements depending on the application. This flexibility can be attained by using different probability of gross error thresholds, initially.

5.1.1 Effect of Setting Different Probability of Gross Error Thresholds for the Optimization Algorithm

Some applications require operation in low SNR environments. In such applications, the array element locations should be decided accordingly. The optimization procedure we proposed has the ability to adjust the probability of gross errors for a certain SNR value and makes the design more flexible for different conditions. In this section, we will examine the effect of setting different thresholds for the gross error probability in optimization of the sensor locations.

Different thresholds are set for the uniform circular region which has a radius of 2λ. The same geometry is used in Section 5.1. In Section 5.1, the threshold was set to 6 and the array shown in Figure 5-1 was obtained. Here, $M_{eq}(\phi)$ threshold is set to 7 and the array shown in Figure 5-27 is obtained. The array element locations are listed in Table 5-3. In Figure 5-27, dashed line shows the bounded region. The metric function of the array is shown in Figure 5-28.

Table 5-3 Array element locations of the optimized array when the threshold is 7

Array Element Number	1	2	3	4	5	6	7	8
x (in λ)	0.2	0.6	-1.3	0.1	-1.5	1.5	1.9	-1.2
y (in λ)	-1.7	1.6	1.0	2.0	0.2	0.6	-0.1	-0.2

In this example we raise the probability of gross error threshold to a higher value. This may be a suitable condition if the fine error performance of the array is more important or high resolution is needed for the application and the array is supposed to operate in high SNR region which is above *0 dB*. It is seen from Figure 5-27 that the array sensors have moved apart from each other, closer to the bound of the

allocated region, since we relaxed the threshold a little bit. Therefore, better fine error can be achieved with this array compared to the array given in Figure 5-1. Although we move the threshold to a higher state, it still imposes some bound on the probability of gross errors and hence the array elements are clustered in pairs to achieve the requirement.
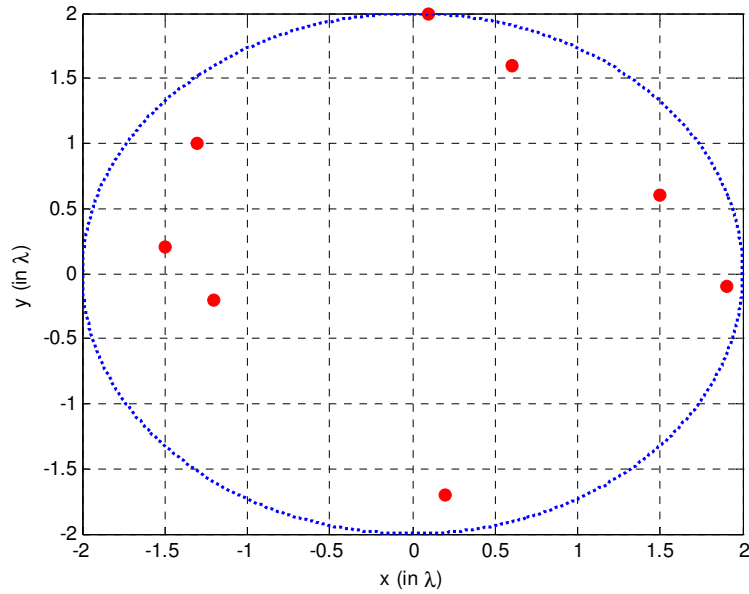
Figure 5-27 The optimized array
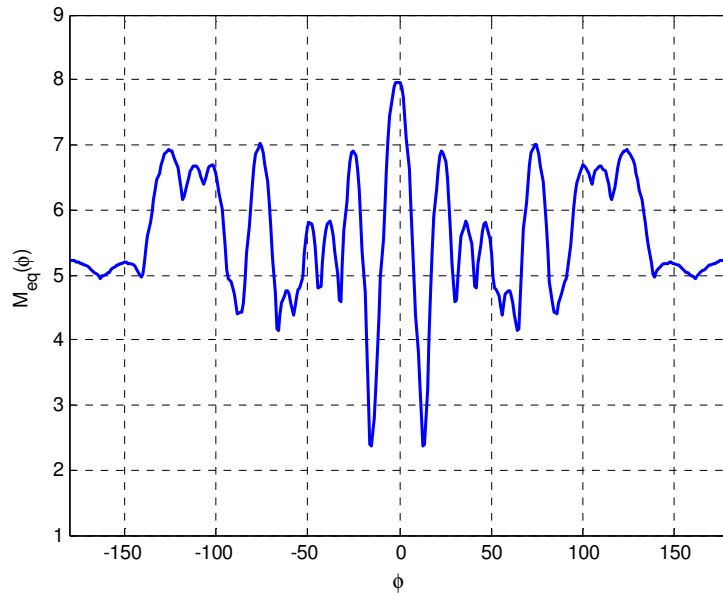
Figure 5-28 The metric function of the optimized array

The next step is to set the threshold to a lower value and see the optimization results. For this example we set the threshold on $M_{eq}(\phi)$ to 5 and performed the optimization to obtain the array shown in Figure 5-29. The array element locations are listed in Table 5-4. The metric function of the array is shown in Figure 5-30.

Table 5-4 Array element locations of the optimized array when the threshold is 5

Array Element Number	1	2	3	4	5	6	7	8
x (in λ)	0.3	-0.2	0.2	-1.4	-0.7	-1.0	0.2	0.3
y (in λ)	-0.9	-0.7	0.2	-0.1	0.6	0.3	1.0	0.6
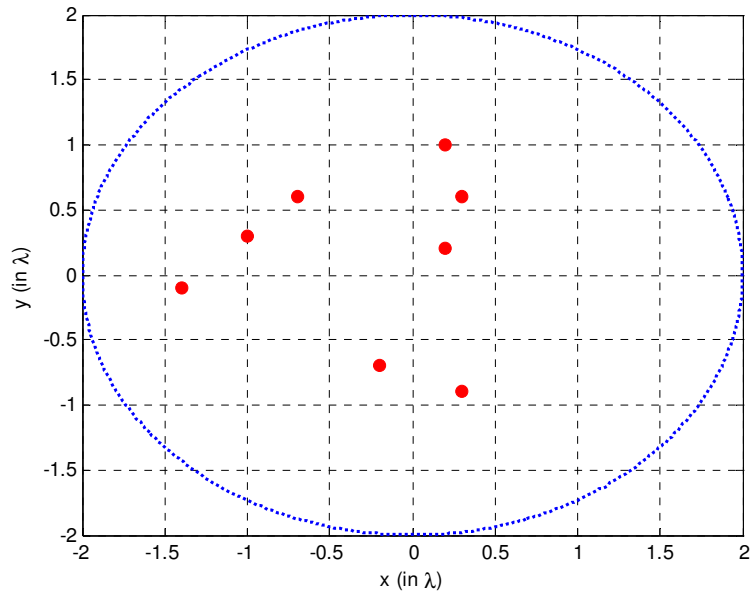
Figure 5-29 The optimized array
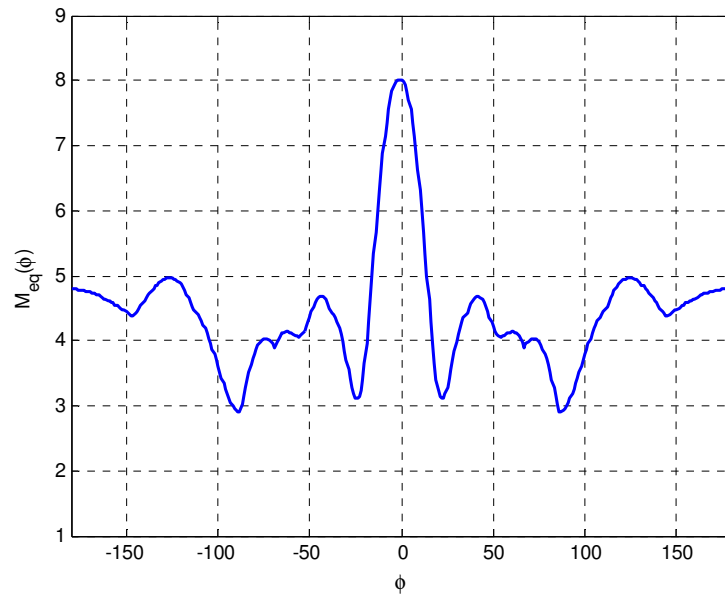
Figure 5-30 The metric function of the optimized array

When a tight bound is applied on the gross error probability, the fine error performance clearly gets worse. The metric function in Figure 5-30 has a wider main lobe than the metric functions in Figure 5-28 and Figure 5-2. As expected, the distance between the sensor array elements are set to lower values in order to satisfy the relatively low probability of gross error specification. As a result, the total aperture size shrinks and hence the fine error performance gets worse.

Figure 5-31 shows the estimation error variances of the arrays shown in Figure 5-27 and Figure 5-29. If we compare this figure with Figure 5-17 we can observe that the estimation error variance curve of the optimized array with a threshold at *6* falls in between the two curves shown in Figure 5-31. Figure 5-32 shows the error variances at high SNR region. From these figures, we verify that as the total array aperture gets smaller the probability of gross errors gets lower and fine errors get higher.
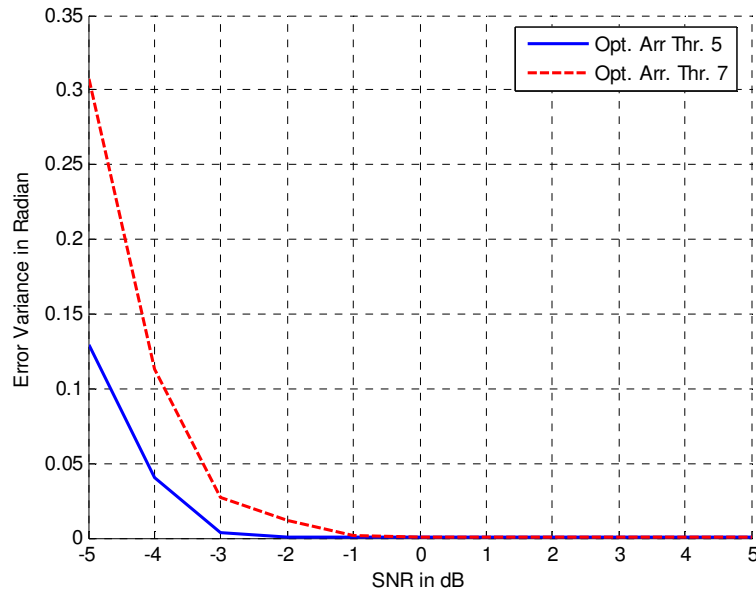
Figure 5-31 Error variances for the arrays optimized for different thresholds
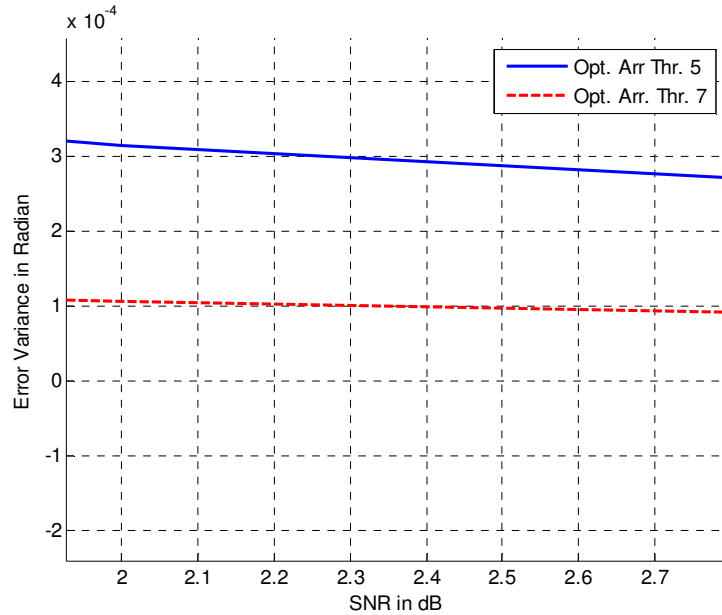
Figure 5-32 Comparison of error variances at high SNR values

5.2 Circular Aperture of 10λ with 8 Elements

As the allowed region gets larger, the arrays that utilize the whole region can be used to gain better DOA estimation resolution. However, as the array elements get further away from each other, the risk of ambiguities drastically increases and the gross errors may be intolerable. This particular example is given in order to show the advantage of using non-uniform arrays when the allowed region is large and the number of array elements is limited. For this purpose, we extent the allowed region to a circle of radius *10λ* and number of array elements is kept limited to 8. The analysis will be quite the same as in the previous section, yet the gain of using an optimized array in this situation is expected to increase considerably.

For this particular problem we set the threshold value at 7.2 which keeps the pairwise probability of gross errors under *%3* for *-10 dB* SNR and *101* snapshots.

The optimized array and the bounded region are given in Figure 5-33. The coordinates of the sensors of the optimized array are given in Table 5-5.

Table 5-5 Array element locations of the optimized array of the circular aperture of 10λ case

Array Element Number	1	2	3	4	5	6	7	8
x (in λ)	3.5	0.1	-6.7	7.1	-1.4	4.1	4.4	-2.1
y (in λ)	-8.1	7.2	0.6	-0.9	-8	2.6	2.3	-3.5
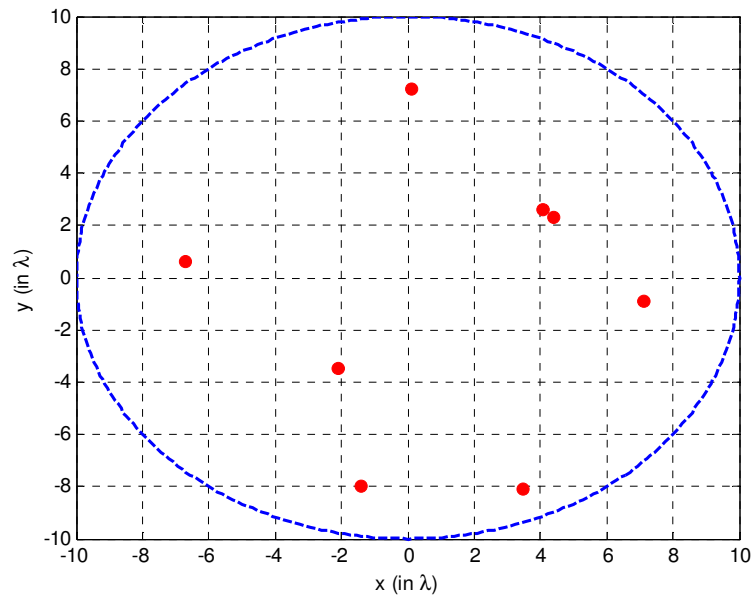
Figure 5-33 The optimized array

At this point it is seen that some of the array elements are kept close to each other while the others are placed near the edge of the allowed region as we discussed before.

The metric function of the optimized array is given in Figure 5-34. Since the aperture length is high, the peak of the metric function around $\phi=0$ is very steep. The other peaks of the metric function are kept below the threshold to keep the probability of gross errors within the limit.
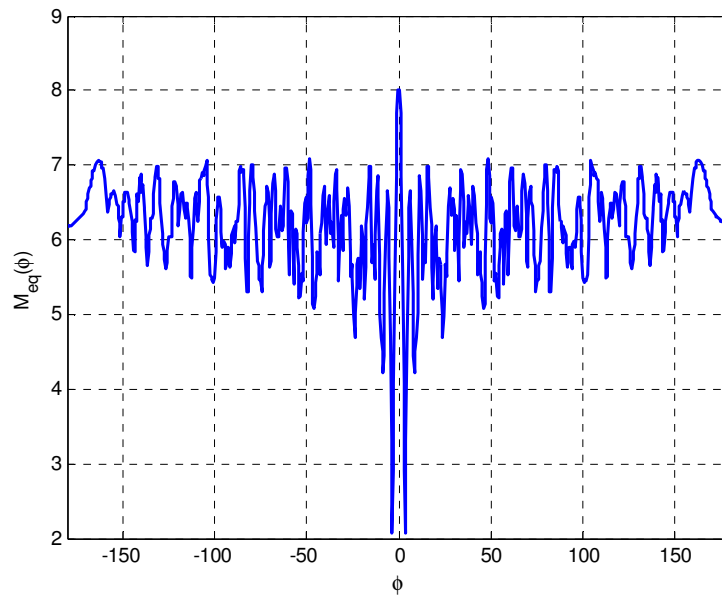
Figure 5-34 The metric function of the optimized array

The optimized array is compared to the UCA of the same aperture given in Figure 5-35 and the coordinates of array elements are given in Table 5-6. The metric function of the UCA is given in Figure 5-36. Note that since the aperture length is large, the probability of gross error is very high for the UCA. There are numerous "almost ambiguous" angles observed.

Table 5-6 Array element locations of the UCA that has the aperture of 10λ

Array Element Number	1	2	3	4	5	6	7	8
x (in λ)	7.07	0	-7.07	-10	-7.07	0	7.07	10
y (in λ)	7.07	10	7.07	0	-7.07	-10	-7.07	0
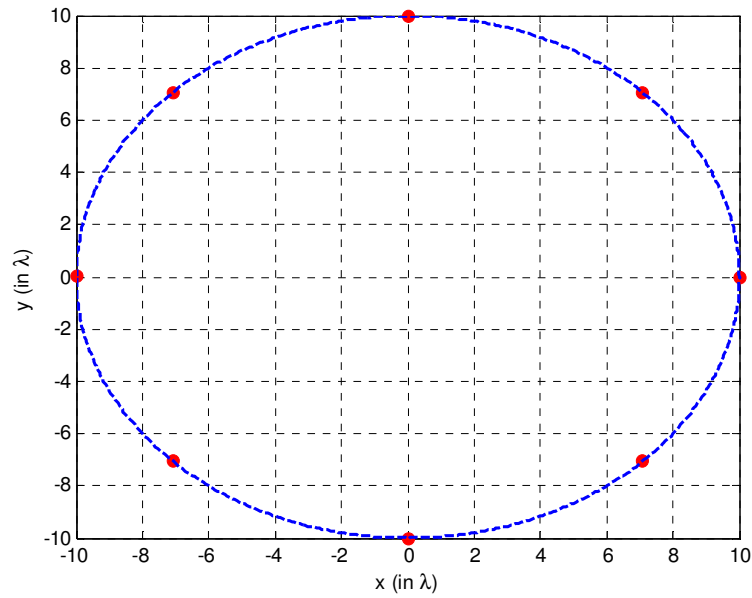
Figure 5-35 Geometry of the UCA
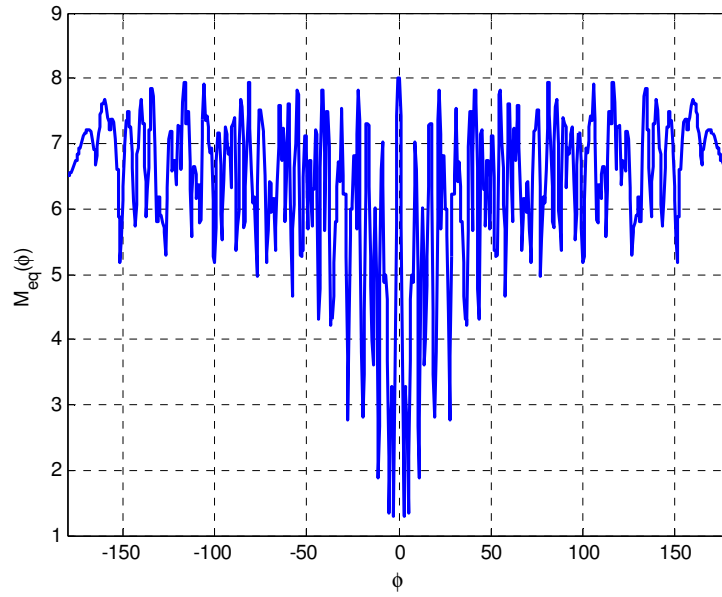
Figure 5-36 The metric function of the UCA

Increasing the aperture of the array means better resolution in the DOA estimation. Hence, the advantage of the UCA that spreads out to whole aperture is the reduced CRB. This can be observed from Figure 5-37 and Figure 5-38. Figure 5-37 shows the main lobe of the metric functions given in Figure 5-34 and Figure 5-36 that correspond to the optimized array and the UCA, respectively. Apparently, the UCA has a steeper main lobe and hence a better fine error performance. Figure 5-38 shows the calculated CRB's of both arrays. The effect of a steeper main lobe can also be observed in Figure 5-38. The CRB of the UCA is lower than that of the optimized array, which is the expected result.

In order to see the advantage of using the optimized array we will focus on the probability of the gross errors. The same probability of gross errors and the estimation error variance analyses have been carried out as we have performed in the previous case. Figure 5-39 shows the total probability of gross errors of both arrays when the incidence angle is randomly changed and Figure 5-40 shows the

estimation error variances for both arrays. For the low SNR region, the gain of using the optimized array is increased drastically, as expected.

By using the results of the last two sections, it can be stated that for the conditions of a large bounded region and a limited number of sensors, using non-uniform arrays is inevitable and the placing of array elements can be carried out successfully by using the optimization procedure outlined in this work.

The next example will be given in order to see how the optimization procedure places the sensors on a more realistic platform. The bounded region will be chosen in such a way that reflects the characteristics of an aircraft and optimization will be carried out.
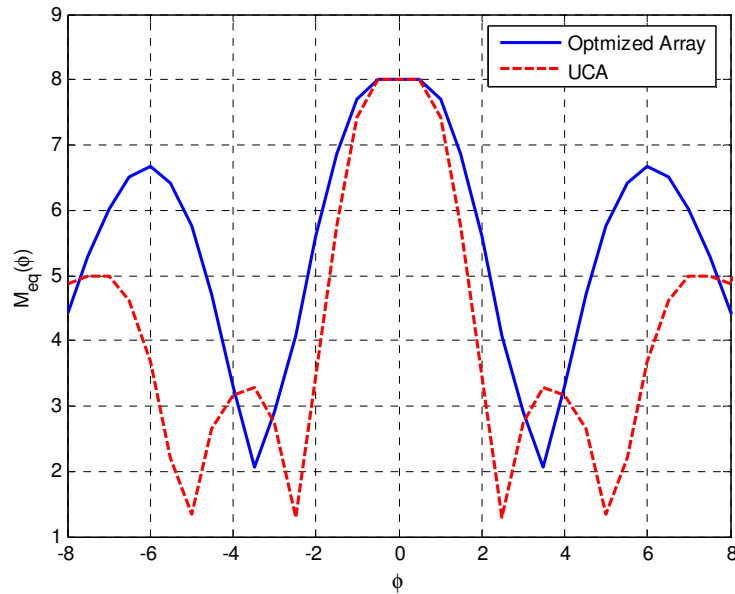
Figure 5-37 Comparison of the UCA and the optimized array
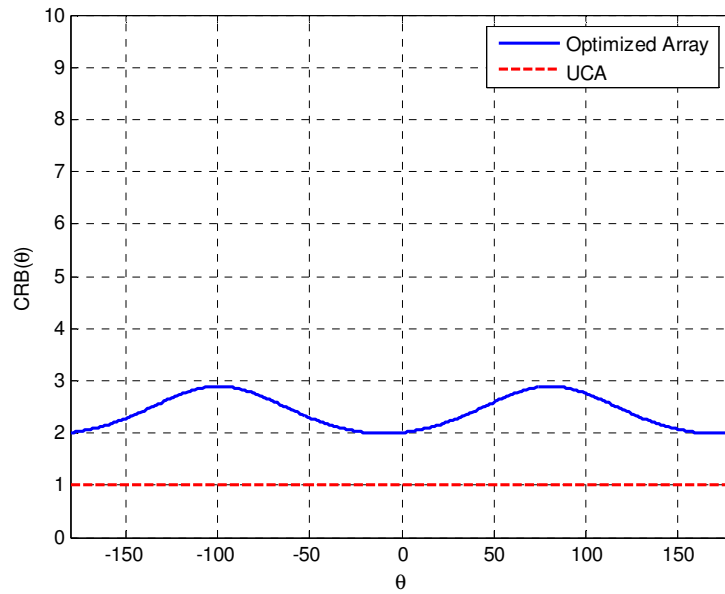
Figure 5-38 Comparison of the CRB of both arrays
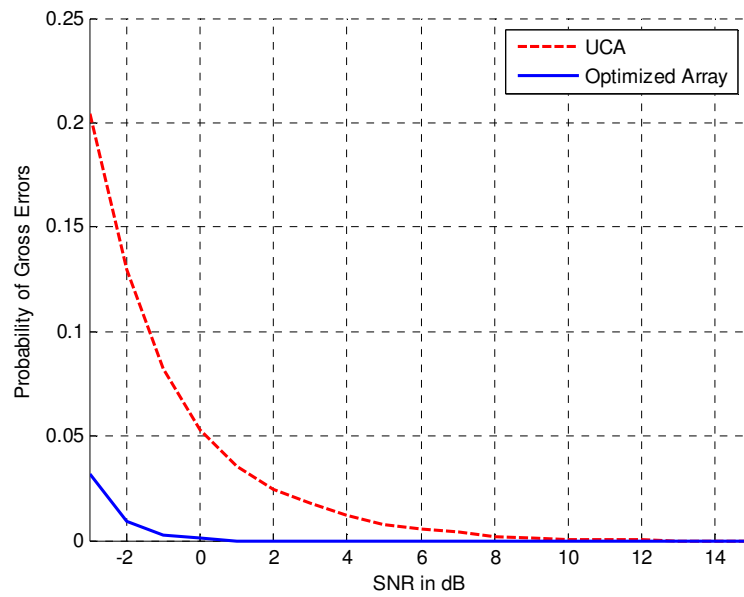
Figure 5-39 Comparison of the probability of gross errors for random incidence
angle
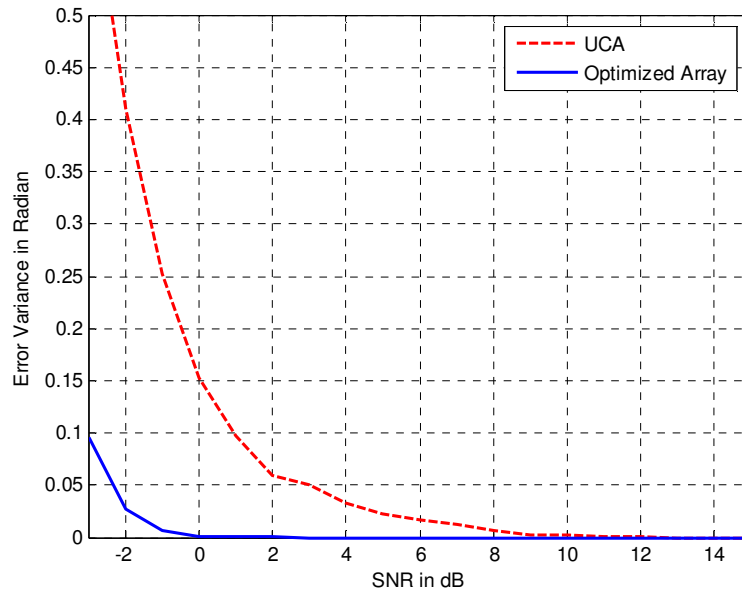
Figure 5-40 Comparison of the estimation error variances for random incidence angle

5.3 Placing Sensors on an Aircraft

One of the most critical problems in avionics that deserves significant attention is the placement of the antenna array elements on an aircraft with a good estimation performance. Although this complicated problem has many real life issues that are hard to solve, we will ignore some of the complications and assume a simple aircraft model, isotropic antenna elements and apply the optimization method introduced in this work, just to give an idea for the resulting geometry.

The first step of the algorithm is to set the bounded region where the sensors will be placed. In this case, the bounded region is set to the whole body of the aircraft and plotted in Figure 5-41.
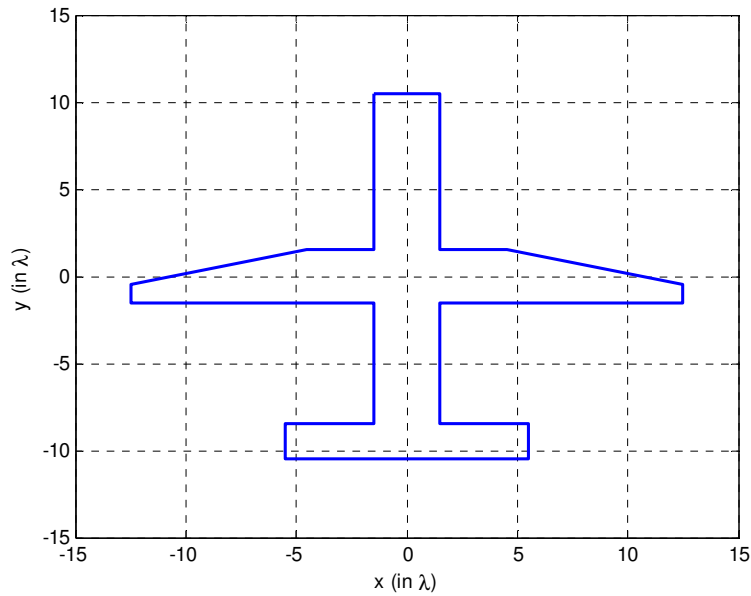
Figure 5-41 The aircraft model

The next step is to set the number of array elements and the threshold value. In this example, 8-element and 9-element arrays are optimized. The threshold is set to 7.7 for the 8-element case and 8.6 and for the 9-element case. These thresholds are relatively high and relax the requirements for the gross errors.

The optimization results are given in Figure 5-42 and Figure 5-44 for the 8 and 9-element cases, respectively. Figure 5-43 and Figure 5-45 show the metric function of both arrays. Note that the sensor elements in both cases are placed nearly symmetric at the edge of the bounded region so that the full aperture is used to increase the fine error performance. Additionally, in order to avoid the high gross error probabilities in such a wide aperture, the array elements are used in closely spaced pairs or triples.
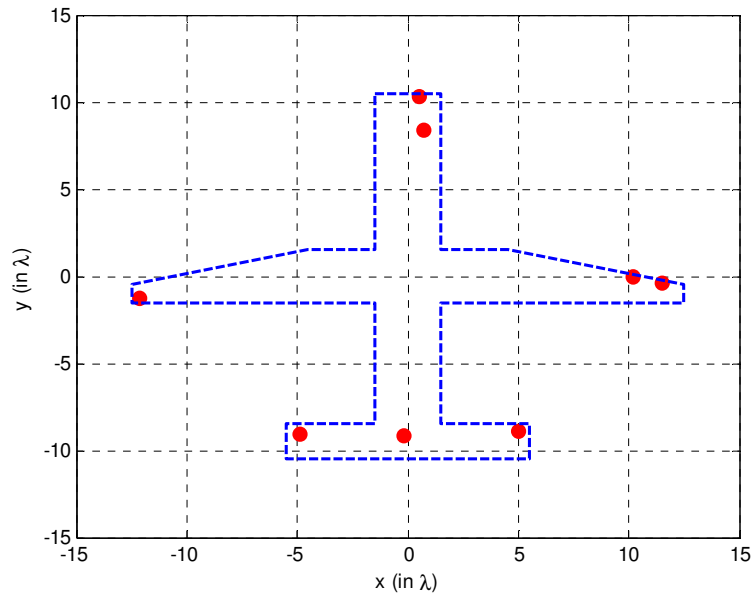
Figure 5-42 The optimized array of 8 elements when the threshold is 7.7
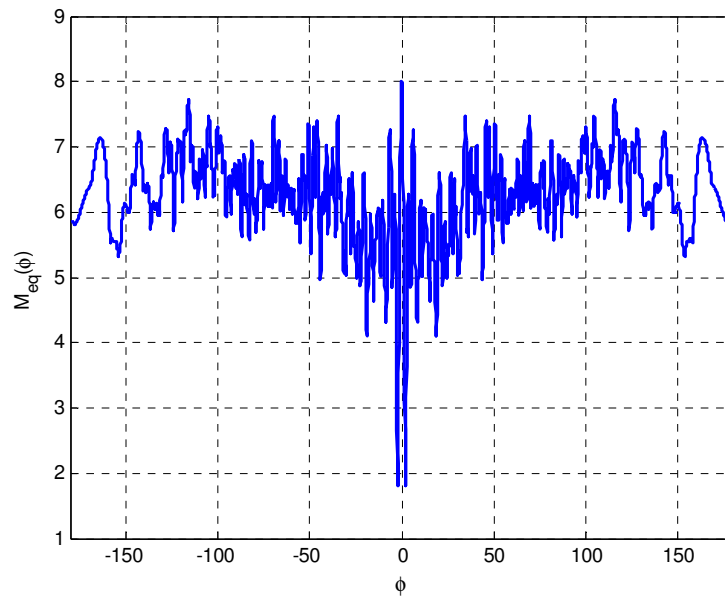
Figure 5-43 The metric function of the optimized array of 8 elements
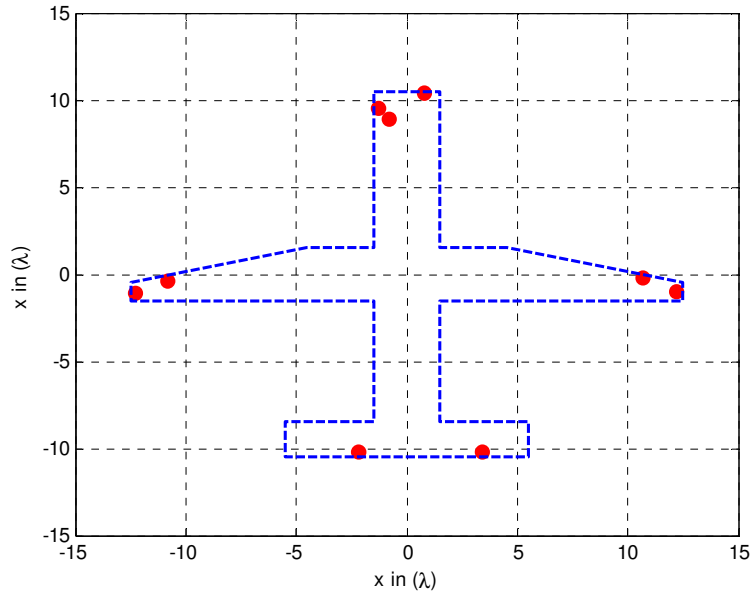
Figure 5-44 The optimized array of 9 elements when the threshold is 8.6
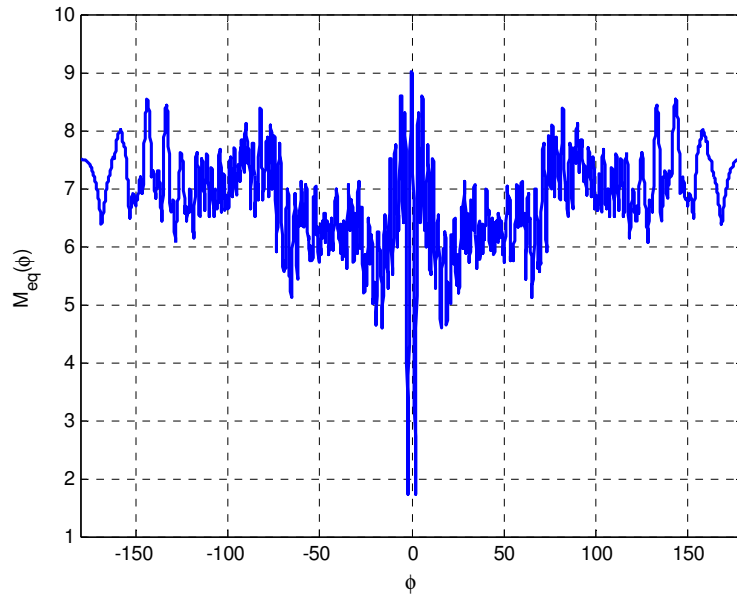
Figure 5-45 The metric function of the optimized array of 9 elements

The last example is on application of a different threshold value to the optimization of the array that is going to be placed on the aircraft given in Figure 5-41. For this example the number of array elements is 8 which is the same as before and the threshold on the metric function is set to 7 instead of 7.7. The optimized array and the metric function of this array are given in Figure 5-46 and Figure 5-47, respectively.

The same discussion also applies to this example: As we limit the probability of gross errors to a lower value, optimized array's elements are placed close to each other. The array elements are gathered together at the middle of the aircraft. Although the aperture of the array gets smaller compared to the previous example, it is still considerably large and to satisfy the lower probability of gross error specification the array elements are placed in closely spaced pairs and the symmetry is preserved.
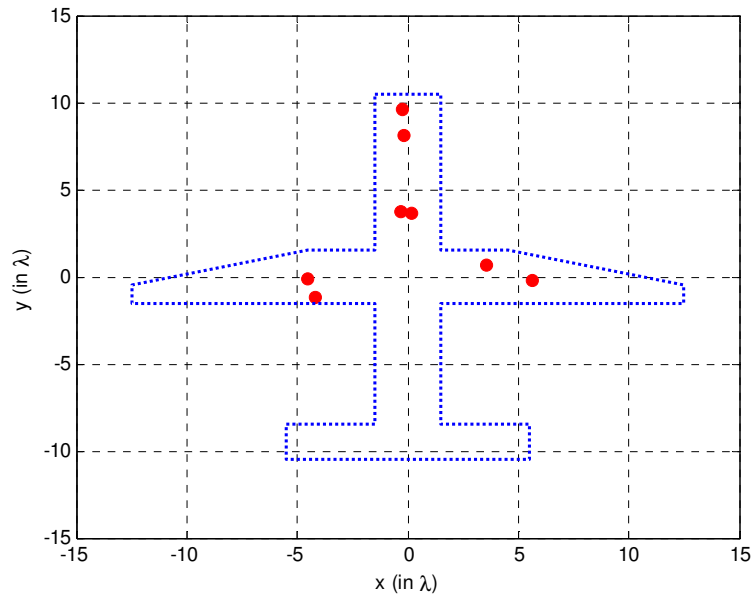
Figure 5-46 The optimized array of 8 elements when the threshold is 7
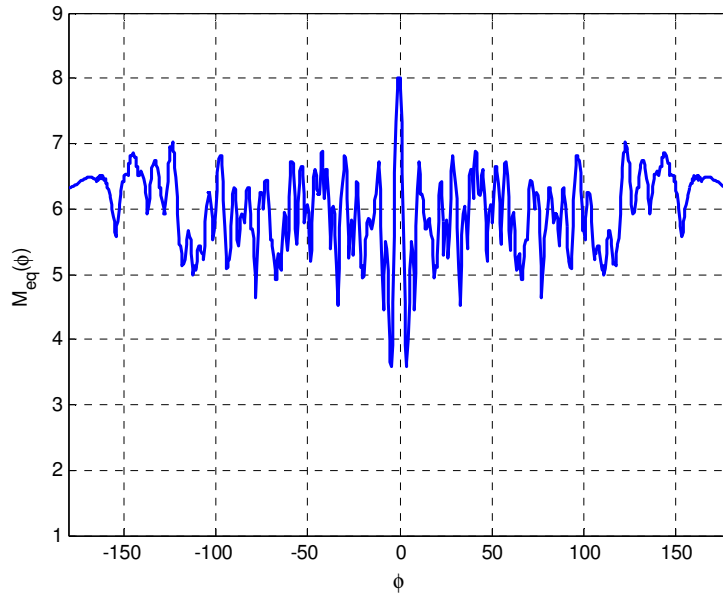
Figure 5-47 The metric function of the array

5.4 Array Performances When There Are Multiple Incident Signals

It is obvious that dealing with more than one incoming signal adds considerable complexity resulting from the angle separation of the signals, the correlation between the signals or the power differences between the signals. Although these issues are kept out of the scope of this work, a special case of the multiple signal condition is simulated here just to give an idea about how the estimation performances would be for the case of multiple incident signals.

We stated that (4-3) can be used to calculate the similarity between the array steering vectors that belong to different incidence angles and proposed a metric function to minimize the similarity of the array steering vectors. Although we assumed only one incoming signal throughout all our analyses and simulations, intuitively it will not be unexpected that minimizing the similarity results in better estimation performance when there is more than one incident signal at a time.

In this section we compare the estimation performances of the optimized array and the UCA when there are two incoming signals. The optimized array in Section 5.1 and the UCA that has the aperture length of 2λ are compared in terms of the probability of gross errors and the estimation of error variances for different SNR values. In these simulations, the incidence angles of the two arrays are randomly changed in each run of the simulation and 5000 runs are carried out for each SNR value to collect the statistics. The incident waves are restricted to have an angle separation of more than 10 degrees. The two incoming signals are assumed to be uncorrelated and equal in power. A priori knowledge of the number of incoming signals is assumed.

Figure 5-48 shows the estimation error variances of the UCA and the optimized array. The error variance is calculated separately for each incident wave. Figure 5-49 shows the comparison of the probability of gross errors of the two arrays. In this figure, the estimation error that is greater than a certain value in at least one of the two signals DOA estimation is considered as the gross error.
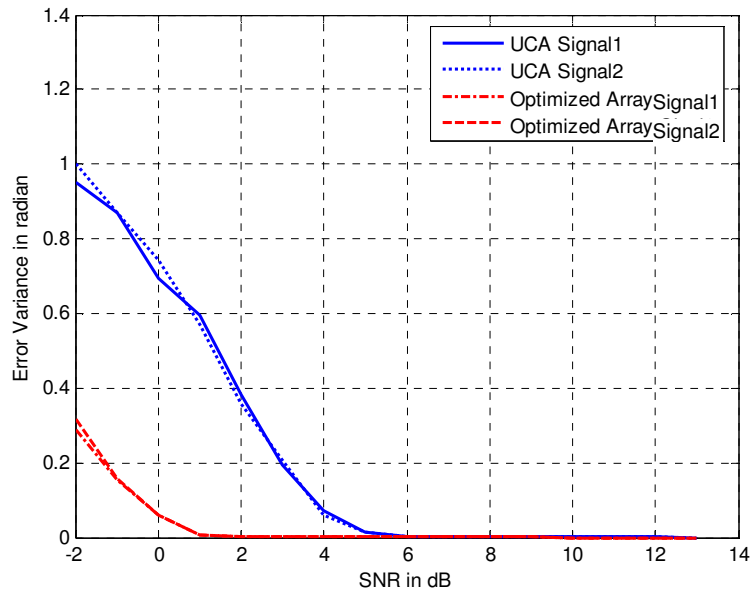
Figure 5-48 Estimation error variances of the UCA and the optimized array when there are two incident signals
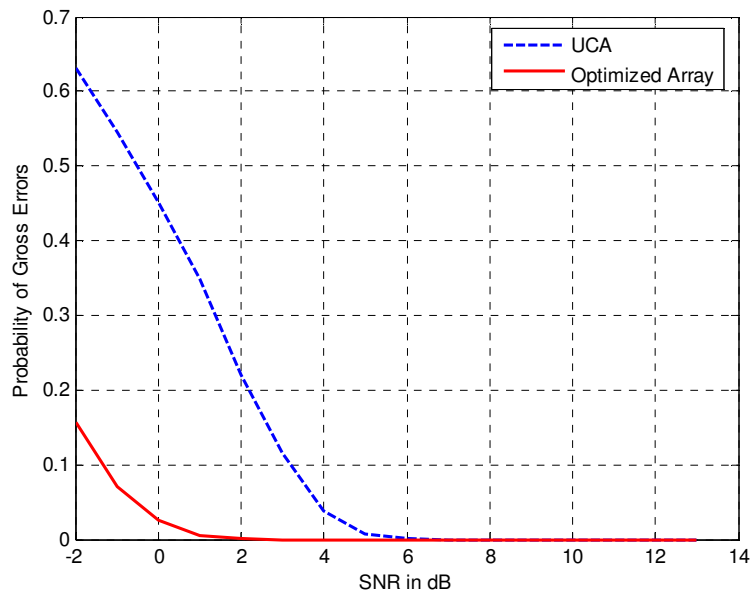
Figure 5-49 Probability of gross errors of the UCA and the optimized array when there are two incident signals

Although this simulation is a particular special case of the multiple signal condition, it indicates us that the estimation performance of the non-uniform optimized array that is optimized by using the procedure described in this thesis is better than the UCA. This is an intuitively expected result. However, this discussion should be extended by a detailed analysis of the multiple signal case which is not in the scope of this thesis and remains as a future work.

CHAPTER 6

CONCLUSIONS

In this work, we have searched an answer to the question: How can the array sensors be correctly positioned for a better direction of arrival estimation?

The conventional approach to the solution of the problem could have been the minimization of Cramer-Rao Bound of the array. This approach has been applied and analyzed in the literature. Unfortunately, this approach is valid only for high SNR conditions. In low and moderate SNR conditions, analyses show that the gross errors have much greater effect on direction of arrival estimation variance than fine errors have. Therefore, in order to improve the direction of arrival estimation performance of an array, gross errors were also considered.

For this purpose, we first propose a method to calculate the pairwise gross error probability which was previously handled in [26]. We established a mathematical link between the probability of gross errors and the function

$$b^2 = \frac{\left| \mathbf{A}^H(\theta_m) \mathbf{A}(\theta_c) \right|^2}{N^2}, \tag{6-1}$$

where $\mathbf{A}$ is the array manifold vector, θ_m is the angle of possible erroneous estimate, θ_c is the incidence angle and N is the number of array elements.

The method that we propose allows us to develop the calculation of the pairwise error probabilities further to calculate the total probability of gross errors of an array for a given incidence angle. An upper bound was proposed by using the union bound of the pairwise error probabilities is proposed before [26]. This bound is not tight and gives very coarse results in low SNR values. The method we proposed in this thesis is an approximation of the total probability of gross errors, which is a novel method. It requires the numerical calculations of means, variances and the covariance matrix of numerous correlated random variables. The number of random variables is equal to the number of the peaks in the function b^2. Hence, if the array aperture increases, the number of the peaks will drastically increase. As the number of random variables increases the numerical calculation becomes complicated and it takes too much time to produce results. Therefore, when the b^2 graph has several peaks, forming the covariance matrix and numerically calculating the result of (3-30) becomes a cumbersome task. On the other hand, the described method has an academic value, since it is the first attempt to obtain an approximate gross error probability, although it needs some further simplifications.

Nevertheless, pairwise error probabilities have provided us sufficient information to propose our metric function:

$$M_{eq}(\phi) = \max_{\theta} \left| \mathbf{A}^H (\theta + \phi) \mathbf{A}(\theta) \right|.$$ (6-2)

We also showed that the curvature of the metric function around $\phi=0$, which corresponds to the main lobe of the metric function, reflects the behavior of the CRB. This function allows us to optimize the array's fine error performance with the constraint on probability of gross errors, by setting a threshold on it.

This metric function can be considered as a similarity measure of two different array steering vectors. Similar measures have already been offered in the literature [21][22]. These measures were offered intuitively and limited theoretical analyses have been given. The main contribution of this work is to establish the link between the proposed metric function and the two important constraints that can be used in

array design by providing extensive theoretical analyses. These two constraints are the fine error and gross error specifications and the metric function allows us to control both parameters at the same time and therefore cuts down the optimization effort considerably.

The proposed optimization method is a procedure that uses the advantage of the metric function and tries to improve fine error variance under the constraint of a maximum allowed probability of gross errors. A generic genetic algorithm was implemented as an optimization tool. The results show that the overall direction of arrival estimation performance is significantly improved by using non-uniformly optimized arrays.

It should be kept in mind that the proposed metric function minimizes the maximum possible probability of gross error and the worst fine error performance for the array for any incidence angle. Therefore the resulting optimized arrays do not yield the same estimation performance for all possible incidence angles and they do not possess structural symmetry, necessarily.

Since the convergence of the genetic algorithm is not guaranteed, the optimized arrays given in this thesis should be considered as local optima. If we investigate the optimized arrays, some general conclusions can be drawn such as the symmetric pairwise placements of the array elements or the usage of the aperture according to the gross error probability specifications, which were discussed in the main body of the text. However, we can not guarantee that the outcome of the optimization procedure is the global optimum for the given conditions. In order to illustrate this, the outcomes of three consecutive optimization runs are shown in Figure 6-1, Figure 6-2 and Figure 6-3.

105
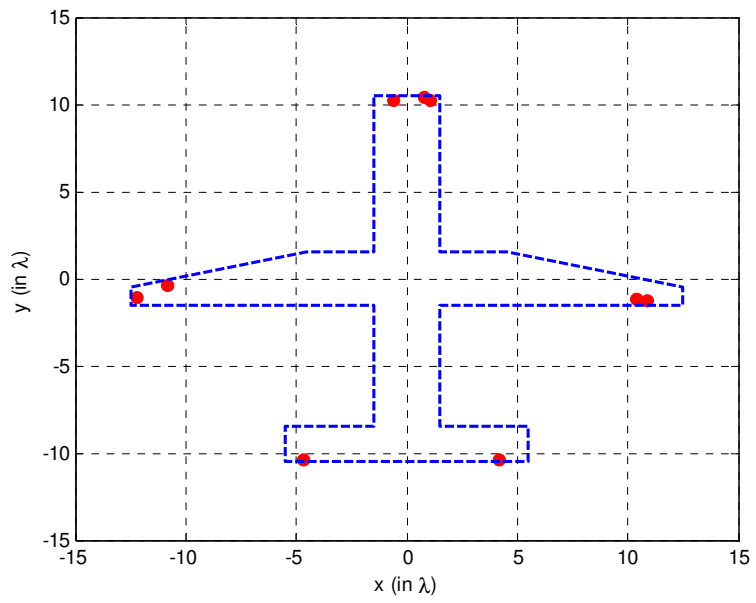
Figure 6-1 First run of the optimization algorithm
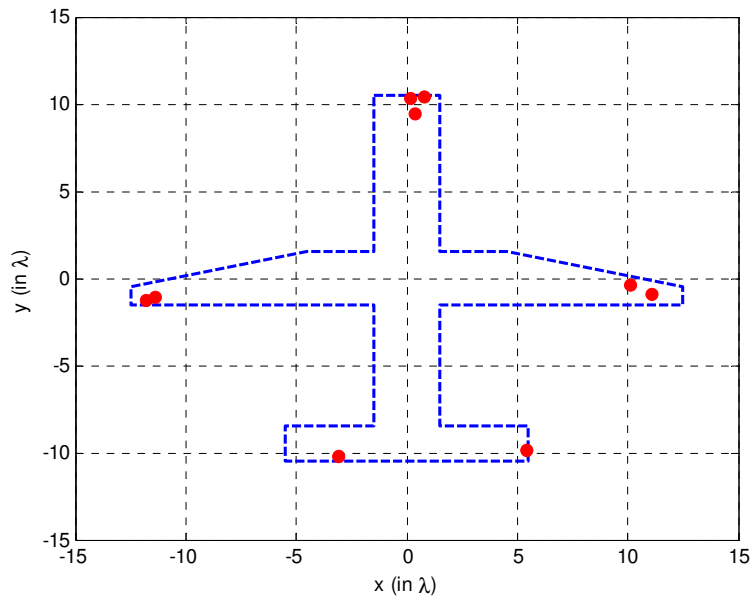
Figure 6-2 Second run of the optimization algorithm

106
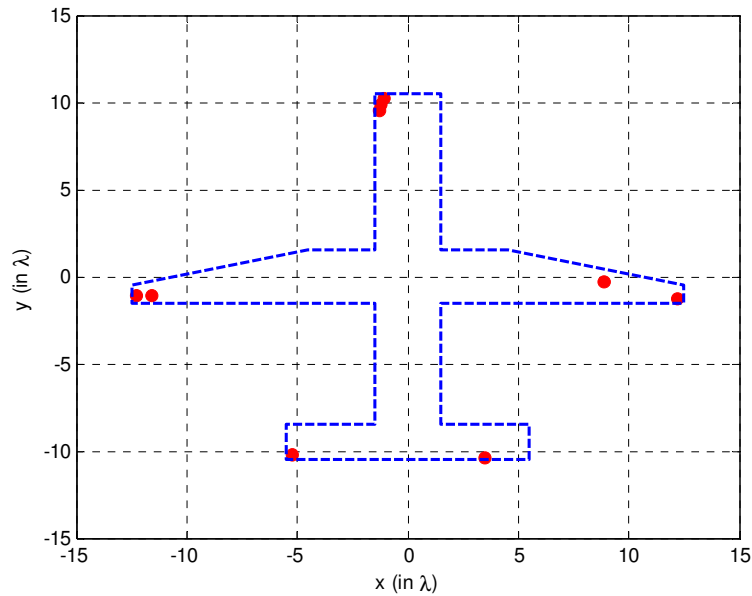
Figure 6-3 Third run of the optimization algorithm

These three arrays are almost equal in their performances together with the array given in Figure 5-44. All of these arrays have very similar topologies, there are only small displacement differences between the arrays. Although the placement of the array elements fits the observations we have made, it shows that some further optimization is possible by giving a small displacement to the array elements in order to reach the global optimum. Therefore, as a future work, a gradient based optimization algorithm can be applied after the genetic algorithm, to obtain better results. On the other hand, the similarity of the distribution of the array elements between the arrays which are almost equal in their performance, indicates the performance insensitivity of the array to small displacements of the sensors, which is desirable in the implementation.

In order to keep the analyses simple, we assumed that the sensors are isotropic and there is no mutual coupling between them. However, in real life problems, these assumptions are not valid. The analyses in this work can also be applied to the

107

directive antennas easily and mutual coupling can be included in the analyses after a suitable modeling. Similarly, the discussion may be extended to three dimensional case by adding a new search dimension. By this way, it can be possible to place the sensors in an allocated volume rather than a two dimensional region. We imposed narrowband assumptions on the received signal and assumed coherent demodulation which can be possible when the carrier frequency of the received signal is known. The case where the received signal is wideband and coherent demodulation is not possible may be addressed as a future work. Also the analysis of the multiple incident signals can be performed by considering the angle separation of the signals, the correlation between the signals or the power differences between the signals.

An interesting advantage of the proposed method is that it can handle different incidence angles separately. In other words, by setting different threshold values for different sectors, one can adjust the array performance according to the region of interest.

REFERENCES

[1] A. T. Koç, "Direction Finding with a Uniform Circular Array Via Single Snapshot Processing", Ph.D. Dissertation, Middle East Technical University, January 1996

[2] H. Krim and M. Viberg, "Two Decades of Array Signal Processing Research", IEEE Signal Processing Magazine, pp. 67-94, July 1996

[3] A. T. Moffet, "Minimum Redundancy Linear Arrays", IEEE Transactions on Antennas and Propagation, vol. AP16, pp. 172-175, July 1968

[4] J. Leech, "On the Representation of *1, 2, …, n* by Differences", Journal of London Mathematical Society, vol. 31, pp. 160-169, July 1956

[5] M. Ishiguro, "Minimum Redundancy Linear Arrays for a Large Number of Antennas", Radio Science, vol. 15, pp. 1163-1170, November/December 1980

[6] D. Pearson, S. U. Pillai and Y. Lee, "An Algorithm for Near-Optimal placement of Sensor Elements", IEEE Transactions on Information Theory, vol. 36, pp. 1280-1284, November 1990

[7] E. J. Vertatschitsch and S. Haykin, "Impact of Linear Array Geometry on Direction-of-Arrival Estimation for a Single Source", IEEE Transactions on Antennas and Propagation, vol. 39, pp. 576-584, May 1991

[8] X. Huang, J. P. Reilly and M. Wong, "Optimal Design of Linear Array of Sensors", in Proc. Int. Conf. Acoust., Speech, Signal Process., Toronto, Canada, 1991, vol. 2, pp. 1405.1408.

[9] Stoica and A. Nehorai, "Performance Study of Conditional and Unconditional Direction-of-Arrival Estimation", IEEE Transactions on Acoustics Speech and Signal Processing, vol. 38, pp. 1783-1795, October 1990

[10] A. N. Mirkin and L. H. Sibul, "Cramér-Rao Bounds on Angle Estimation with a Two-Dimensional Array", IEEE Transactions on Signal Processing, vol. 39, pp. 515-517, February 1991

[11] A. J. Weiss and B. Friedlander, "On the Cramér-Rao Bound for Direction Finding of Correlated Signals", IEEE Transactions on Signal Processing, vol. 41, pp. 495-499, January 1993

[12] R. O. Nielsen, "Azimuth and Elevation Angle Estimation with a Three-Dimensional Array", IEEE Journal of Oceanic Engineering, vol. 19, pp. 84-86, January 1994

[13] Ü. Baysal and R. L. Moses, "On the Geometry of Isotropic Arrays", IEEE Transactions on Signal Processing, vol. 51, pp. 1469-1478, June 2003

[14] W. J. Bangs, "Array Processing with Generalized Beamformers", Ph.D. Dissertation, Yale University, September 1971

[15] Y. Hua and T. K. Sarkar, "A Note on the Cramér-Rao Bound for 2-D Direction Finding Based on 2-D Array", IEEE Transactions on Signal Processing, vol. 39, pp. 1215-1218, May 1991

[16] P. Stoica and A. Nehorai, "MUSIC, Maximum Likelihood, and Cramér-Rao Bound", IEEE Transactions on Acoustics Speech and Signal Processing, vol. 37, pp. 720-741, May 1989

[17] A. B. Gershman and J. F. Böhme, "A Note on Most Favorable Array Geometries for DOA Estimation and Array Interpolation", IEEE Signal Processing Letters, vol. 4, pp. 232-235, August 1997

[18] Ü. Öktel and R. L. Moses, "A Bayesian Approach to Array Geometry Design", IEEE Transactions on Signal Processing, vol. 53, pp. 1919-1923, May 2005

[19] C. W. Ang, C. M. See and A. C. Kot, "Optimization of Array Geometry for Identifiable High Resolution Parameter Estimation in Sensor Array Processing", in ICICS'97, Singapore, September 1997

[20] F. Athley, "Optimization of Element Positions for Direction Finding with Sparse Arrays", in 11th IEEE Signal Processing Workshop Statistical Signal Processing, Singapore, 2001

[21] M. Gavish and A. J. Weiss, "Array Geometry for Ambiguity Resolution in Direction Finding", IEEE Transactions on Antennas and Propagation, vol. 44, pp. 889-895, June 1996

[22] S. Özaydın, "Optimization of Array Geometry for Direction Finding", Master Thesis, Middle East Technical University, December 2003

[23] R. O. Schmidt, "A Signal Subspace Approach to Multiple Emitter Location and Spectral Estimation", Ph.D. Dissertation, Stanford University, November 1981

[24] H. L. V. Trees, Optimum Array Processing, New York: John Wiley and Sons, 2002

[25] T. Birinci and Y. Tanık, "Optimization of Non-Uniform Planar Array Geometry for Direction of Arrival Estimation", in EUSIPCO 2005, Antalya, Turkey, 2005

[26] F. Athley, "Threshold Region of Maximum Likelihood Direction of Arrival Estimators", IEEE Transactions on Signal Processing, vol. 53, pp. 1359-1373, April 2005

[27] H. L. V. Trees, Detection, Estimation and Modulation Theory, John Wiley and Sons, 2001

[28] J. G. Proakis, Digital Communications, Mc. Graw Hill, Inc., 3rd edition, 1995

[29] S. J. Press, "Linear Combination of Non-central Chi-Square Random Variables", Annals of Mathematical Statistics, vol. 37, pp. 480-487, 1966

[30] F. E. Satterthwaite, "An Approximate Distribution of Estimates of Variance Components", Biometrics, vol. 2, pp. 110-114, 1946

[31] A. Genz, "Numerical Computation of Multivariate Normal Probabilities", Statistics and Computing, vol. 14, pp. 251-260, August 2004

[32] J. R. Koza, Genetic Programming, MIT Press, 1992

APPENDIX A

DERIVATION OF (3-60)

For an N element array, the probability density for a single snapshot is

$$p(\mathbf{x}) = \frac{1}{|\pi\mathbf{K}_\mathbf{x}(\mathbf{\Theta})|}\exp\left[-\left(\mathbf{x}^H - \mathbf{m}_\mathbf{x}^H(\mathbf{\Theta})\right)\mathbf{K}_\mathbf{x}^{-1}(\mathbf{\Theta})\left(\mathbf{x} - \mathbf{m}_\mathbf{x}(\mathbf{\Theta})\right)\right], \qquad \text{(A-1)}$$

where $\mathbf{x}$ is an $Nx1$ complex Gaussian random variable and $\mathbf{\Theta}$ is an $Mx1$ unknown vector that contains the parameters of interest that we want to estimate.

Successive snapshots are statistically independent, the joint probability density for K snapshots can be found as,

$$p(x) = \prod_{k=1}^{K}\frac{1}{|\pi\mathbf{K}_\mathbf{x}(\mathbf{\Theta})|}\exp\left[-\left(\mathbf{x}_k^H - \mathbf{m}_\mathbf{x}^H(\mathbf{\Theta})\right)\mathbf{K}_\mathbf{x}^{-1}(\mathbf{\Theta})\left(\mathbf{x}_k - \mathbf{m}_\mathbf{x}(\mathbf{\Theta})\right)\right]. \qquad \text{(A-2)}$$

The log-likelihood function is

$$\begin{aligned}L_\mathbf{x}(\mathbf{\Theta}) &= \ln p(\mathbf{x}) \\ &= -K\ln|\mathbf{K}_\mathbf{x}(\mathbf{\Theta})| - KN\ln\pi - \sum_{k=1}^{K}\left(\mathbf{x}_k^H - \mathbf{m}_\mathbf{x}^H(\mathbf{\Theta})\right)\mathbf{K}_\mathbf{x}^{-1}(\mathbf{\Theta})\left(\mathbf{x}_k - \mathbf{m}_\mathbf{x}(\mathbf{\Theta})\right)\end{aligned} \qquad \text{(A-3)}$$

The elements of Fisher Information Matrix are

$$J_{ij} = E\left\{\frac{\partial L_{\mathbf{x}}(\mathbf{\Theta})}{\partial\Theta_i}\frac{\partial L_{\mathbf{x}}(\mathbf{\Theta})}{\partial\Theta_j}\right\}$$

$$= -E\left\{\frac{\partial^2 L_{\mathbf{x}}(\mathbf{\Theta})}{\partial\Theta_i\partial\Theta_j}\right\}$$

(A-4)

The second derivative of (A-3) can be found by using the following properties,

$$\frac{\partial\ln|\mathbf{X}|}{\partial\Theta_i} = \text{tr}\left[\mathbf{X}^{-1}\frac{\partial\mathbf{X}}{\partial\Theta_i}\right],$$

(A-5)

$$\frac{\partial\mathbf{X}^{-1}}{\partial\Theta_i} = -\mathbf{X}^{-1}\frac{\partial\mathbf{X}}{\partial\Theta_i}\mathbf{X}^{-1}$$

(A-6)

and

$$\frac{\partial^2\ln|\mathbf{X}|}{\partial\Theta_i\partial\Theta_j} = \text{tr}\left[-\mathbf{X}^{-1}\frac{\partial\mathbf{X}}{\partial\Theta_i}\mathbf{X}^{-1}\frac{\partial\mathbf{X}}{\partial\Theta_j} + \mathbf{X}^{-1}\frac{\partial^2\mathbf{X}}{\partial\Theta_i\partial\Theta_j}\right].$$

(A-7)

Hence the first and second derivative will be,

$$\frac{\partial L_{\mathbf{x}}(\mathbf{\Theta})}{\partial\Theta_i} = -K\text{tr}\left[\mathbf{K}_{\mathbf{x}}^{-1}(\mathbf{\Theta})\frac{\partial\mathbf{K}_{\mathbf{x}}(\mathbf{\Theta})}{\partial\Theta_i}\right]$$

$$-\sum_{k=1}^{K}\frac{\partial\left(\mathbf{x}_k^H - \mathbf{m}_{\mathbf{x}}^H(\mathbf{\Theta})\right)}{\partial\Theta_i}\mathbf{K}_{\mathbf{x}}^{-1}(\mathbf{\Theta})\left(\mathbf{x}_k - \mathbf{m}_{\mathbf{x}}(\mathbf{\Theta})\right)$$

$$+\left(\mathbf{x}_k^H - \mathbf{m}_{\mathbf{x}}^H(\mathbf{\Theta})\right)\frac{\partial\mathbf{K}_{\mathbf{x}}^{-1}(\mathbf{\Theta})}{\partial\Theta_i}\left(\mathbf{x}_k - \mathbf{m}_{\mathbf{x}}(\mathbf{\Theta})\right)$$

$$+\left(\mathbf{x}_k^H - \mathbf{m}_{\mathbf{x}}^H(\mathbf{\Theta})\right)\mathbf{K}_{\mathbf{x}}^{-1}(\mathbf{\Theta})\frac{\partial\left(\mathbf{x}_k - \mathbf{m}_{\mathbf{x}}(\mathbf{\Theta})\right)}{\partial\Theta_i}$$

,

(A-8)

$$\frac{\partial^2 L_\mathbf{x}(\mathbf{\Theta})}{\partial\Theta_i\partial\Theta_j} = K\mathrm{tr}\left[-\mathbf{K}_\mathbf{x}^{-1}(\mathbf{\Theta})\frac{\partial\mathbf{K}_\mathbf{x}(\mathbf{\Theta})}{\partial\Theta_i}\mathbf{K}_\mathbf{x}^{-1}(\mathbf{\Theta})\frac{\partial\mathbf{K}_\mathbf{x}(\mathbf{\Theta})}{\partial\Theta_j} + \mathbf{K}_\mathbf{x}^{-1}(\mathbf{\Theta})\frac{\partial^2\mathbf{K}_\mathbf{x}(\mathbf{\Theta})}{\partial\Theta_i\partial\Theta_j}\right]$$

$$-\sum_{k=1}^{K}\left(\mathbf{x}_k^H - \mathbf{m}_\mathbf{x}^H(\mathbf{\Theta})\right)\left[-\mathbf{K}_\mathbf{x}^{-1}(\mathbf{\Theta})\frac{\partial\mathbf{K}_\mathbf{x}(\mathbf{\Theta})}{\partial\Theta_i}\mathbf{K}_\mathbf{x}^{-1}(\mathbf{\Theta})\frac{\partial\mathbf{K}_\mathbf{x}(\mathbf{\Theta})}{\partial\Theta_j} + \mathbf{K}_\mathbf{x}^{-1}(\mathbf{\Theta})\frac{\partial^2\mathbf{K}_\mathbf{x}(\mathbf{\Theta})}{\partial\Theta_i\partial\Theta_j}\right.$$

$$\left.+ \mathbf{K}_\mathbf{x}^{-1}(\mathbf{\Theta})\frac{\partial\mathbf{K}_\mathbf{x}(\mathbf{\Theta})}{\partial\Theta_i}\mathbf{K}_\mathbf{x}^{-1}(\mathbf{\Theta})\frac{\partial\mathbf{K}_\mathbf{x}(\mathbf{\Theta})}{\partial\Theta_j}\mathbf{K}_\mathbf{x}^{-1}(\mathbf{\Theta})\right]\left(\mathbf{x}_k - \mathbf{m}_\mathbf{x}(\mathbf{\Theta})\right)$$

$$-2\mathrm{Re}\left\{\frac{\partial^2\mathbf{m}_\mathbf{x}^H(\mathbf{\Theta})}{\partial\Theta_i\partial\Theta_j}\mathbf{K}_\mathbf{x}^{-1}(\mathbf{\Theta})\left(\mathbf{x}_k - \mathbf{m}_\mathbf{x}(\mathbf{\Theta})\right)\right.$$

$$+ \frac{\partial\mathbf{m}_\mathbf{x}^H(\mathbf{\Theta})}{\partial\Theta_i}\mathbf{K}_\mathbf{x}^{-1}(\mathbf{\Theta})\frac{\partial\mathbf{K}_\mathbf{x}(\mathbf{\Theta})}{\partial\Theta_j}\mathbf{K}_\mathbf{x}^{-1}(\mathbf{\Theta})\left(\mathbf{x}_k - \mathbf{m}_\mathbf{x}(\mathbf{\Theta})\right)$$

$$+ \frac{\partial\mathbf{m}_\mathbf{x}^H(\mathbf{\Theta})}{\partial\Theta_j}\mathbf{K}_\mathbf{x}^{-1}(\mathbf{\Theta})\frac{\partial\mathbf{K}_\mathbf{x}(\mathbf{\Theta})}{\partial\Theta_i}\mathbf{K}_\mathbf{x}^{-1}(\mathbf{\Theta})\left(\mathbf{x}_k - \mathbf{m}_\mathbf{x}(\mathbf{\Theta})\right)$$

$$+ \left.\frac{\partial\mathbf{m}_\mathbf{x}^H(\mathbf{\Theta})}{\partial\Theta_i}\mathbf{K}_\mathbf{x}^{-1}(\mathbf{\Theta})\frac{\partial\mathbf{m}_\mathbf{x}^H(\mathbf{\Theta})}{\partial\Theta_j}\right\} \tag{A-9}$$

In order to take the expectation of the first term in the following is used,

$$E\left\{\sum_{k=1}^{K}\left(\mathbf{x}_k^H - \mathbf{m}_\mathbf{x}^H(\mathbf{\Theta})\right)(\cdots)\left(\mathbf{x}_k - \mathbf{m}_\mathbf{x}(\mathbf{\Theta})\right)\right\} =$$

$$\sum_{k=1}^{K}\mathrm{tr}\left[(\cdots)\left(\mathbf{x}_k - \mathbf{m}_\mathbf{x}(\mathbf{\Theta})\right)\left(\mathbf{x}_k^H - \mathbf{m}_\mathbf{x}^H(\mathbf{\Theta})\right)\right] = K\mathrm{tr}\left[(\cdots)\mathbf{K}_\mathbf{x}(\mathbf{\Theta})\right] \tag{A-10}$$

Hence the expectation will be,

$$E\left\{\frac{\partial^2 L_\mathbf{x}(\mathbf{\Theta})}{\partial\Theta_i\partial\Theta_j}\right\} = tr\left[-\mathbf{K}_\mathbf{x}^{-1}(\mathbf{\Theta})\frac{\partial\mathbf{K}_\mathbf{x}(\mathbf{\Theta})}{\partial\Theta_i}\mathbf{K}_\mathbf{x}^{-1}(\mathbf{\Theta})\frac{\partial\mathbf{K}_\mathbf{x}(\mathbf{\Theta})}{\partial\Theta_j} + \mathbf{K}_\mathbf{x}^{-1}(\mathbf{\Theta})\frac{\partial^2\mathbf{K}_\mathbf{x}(\mathbf{\Theta})}{\partial\Theta_i\partial\Theta_j}\right.$$

$$+ \mathbf{K}_\mathbf{x}^{-1}(\mathbf{\Theta})\frac{\partial\mathbf{K}_\mathbf{x}(\mathbf{\Theta})}{\partial\Theta_i}\mathbf{K}_\mathbf{x}^{-1}(\mathbf{\Theta})\frac{\partial\mathbf{K}_\mathbf{x}(\mathbf{\Theta})}{\partial\Theta_j} - \mathbf{K}_\mathbf{x}^{-1}(\mathbf{\Theta})\frac{\partial^2\mathbf{K}_\mathbf{x}(\mathbf{\Theta})}{\partial\Theta_i\partial\Theta_j} \tag{A-11}$$

$$\left.- \mathbf{K}_\mathbf{x}^{-1}(\mathbf{\Theta})\frac{\partial\mathbf{K}_\mathbf{x}(\mathbf{\Theta})}{\partial\Theta_i}\mathbf{K}_\mathbf{x}^{-1}(\mathbf{\Theta})\frac{\partial\mathbf{K}_\mathbf{x}(\mathbf{\Theta})}{\partial\Theta_j}\right] - 2\mathrm{Re}\left\{\sum_{k=1}^{K}\frac{\partial\mathbf{m}_\mathbf{x}^H(\mathbf{\Theta})}{\partial\Theta_i}\mathbf{K}_\mathbf{x}^{-1}(\mathbf{\Theta})\frac{\partial\mathbf{m}_\mathbf{x}^H(\mathbf{\Theta})}{\partial\Theta_j}\right\}$$

After the cancellations we finally have the following result:

$$J_{ij} = -E\left\{\frac{\partial^2 L_{\mathbf{x}}(\mathbf{\Theta})}{\partial\Theta_i\partial\Theta_j}\right\}$$

$$= K\mathrm{tr}\left[\mathbf{K}_x^{-1}\frac{\partial\mathbf{K}_x}{\partial\Theta_i}\mathbf{K}_x^{-1}\frac{\partial\mathbf{K}_x}{\partial\Theta_j}\right] + 2K\,\mathrm{Re}\left\{\frac{\partial\mathbf{m}^H}{\partial\Theta_i}\mathbf{K}_x^{-1}\frac{\partial\mathbf{m}}{\partial\Theta_j}\right\}^{\cdot} \qquad \text{(A-12)}$$

CURRICULUM VITAE

PERSONEL INFORMATION

Surname, Name : Toygar Birinci

Nationality : Turkish (TC)

Date and Place of Birth : 1974, İzmir

Phone : +90-312-2252297

Email : birinci@aselsan.com.tr

EDUCATION

Degree	Institution	Year of Graduation
MS	Middle East Technical University - EEE	1999
BS	Bilkent University- EEE	1995
High School	İzmir Atatürk Lisesi	1990

WORK EXPERIENCE

Year	Place	Enrollment
2002-Present	ASELSAN Inc.	Systems Engineer
2000-2002	ASELSAN Inc.	Project Engineer
1995-2000	ASELSAN Inc.	Software Engineer

PUBLICATIONS

1. T. Birinci and Y. Tanık, "Optimization of Non-Uniform Planar Array Geometry for Direction of Arrival Estimation", in EUSIPCO 2005, Antalya, Turkey, 2005